University of Kentucky
UKnowledge

Theses and Dissertations--Biomedical Engineering

Biomedical Engineering

2014

STABILIZATION OF EXTENDED DIFFUSE OPTICAL SPECTROSCOPY MEASUREMENTS ON IN VIVO HUMAN SKELETAL MUSCLE DURING DYNAMIC EXERCISE

Brad A. Henry
University of Kentucky, bahe224@g.uky.edu

Recommended Citation
Henry, Brad A., "STABILIZATION OF EXTENDED DIFFUSE OPTICAL SPECTROSCOPY MEASUREMENTS ON IN VIVO HUMAN SKELETAL MUSCLE DURING DYNAMIC EXERCISE" (2014). *Theses and Dissertations--Biomedical Engineering*. 22.
http://uknowledge.uky.edu/cbme_etds/22

This Master's Thesis is brought to you for free and open access by the Biomedical Engineering at UKnowledge. It has been accepted for inclusion in Theses and Dissertations--Biomedical Engineering by an authorized administrator of UKnowledge. For more information, please contact UKnowledge@lsv.uky.edu.

STUDENT AGREEMENT:

I represent that my thesis or dissertation and abstract are my original work. Proper attribution has been given to all outside sources. I understand that I am solely responsible for obtaining any needed copyright permissions. I have obtained needed written permission statement(s) from the owner(s) of each third-party copyrighted matter to be included in my work, allowing electronic distribution (if such use is not permitted by the fair use doctrine) which will be submitted to UKnowledge as Additional File.

I hereby grant to The University of Kentucky and its agents the irrevocable, non-exclusive, and royalty-free license to archive and make accessible my work in whole or in part in all forms of media, now or hereafter known. I agree that the document mentioned above may be made available immediately for worldwide access unless an embargo applies.

I retain all other ownership rights to the copyright of my work. I also retain the right to use in future works (such as articles or books) all or part of my work. I understand that I am free to register the copyright to my work.

REVIEW, APPROVAL AND ACCEPTANCE

The document mentioned above has been reviewed and accepted by the student's advisor, on behalf of the advisory committee, and by the Director of Graduate Studies (DGS), on behalf of the program; we verify that this is the final, approved version of the student's thesis including all changes required by the advisory committee. The undersigned agree to abide by the statements above.

Brad A. Henry, Student

Dr. Guoqiang Yu, Major Professor

Dr. Abhijit Patwardhan, Director of Graduate Studies

STABILIZATION OF EXTENDED DIFFUSE OPTICAL SPECTROSCOPY MEASUREMENTS ON IN VIVO HUMAN SKELETAL MUSCLE DURING DYNAMIC EXERCISE

THESIS

A thesis submitted in partial fulfillment of the requirements for the degree Master of Science in Biomedical Engineering in the College of Engineering at the University of Kentucky

By

Brad Henry

Lexington, Kentucky

Director: Dr. Guoqiang Yu, Associate Professor of Biomedical Engineering
Lexington, Kentucky

2014

Copyright © Brad Henry 2014

ABSTRACT OF THESIS

STABILIZATION OF EXTENDED DIFFUSE OPTICAL SPECTROSCOPY MEASUREMENTS ON IN VIVO HUMAN SKELETAL MUSCLE DURING DYNAMIC EXERCISE

This research investigates various applications of diffuse correlation spectroscopy (DCS) on in-vivo human muscle tissue, both at rest and during dynamic exercise. Previously suspected muscle tissue relative blood flow (rBF) baseline shift during extended measurement with DCS and DCS-Near infrared spectroscopy (NIRS) hybrid optical systems are verified, quantified, and resolved by redesign of optical probe and alteration in optical probe attachment methodology during 40 minute supine bed rest baseline measurements.

We then translate previously developed occlusion techniques, whereby rBF and relative oxygen consumption $r\dot{V}O_2$ are calibrated to initial resting absolute values by use of a venous occlusion (VO) and arterial occlusion (AO) protocol, respectively, to the lower leg (gastrocnemius) and these blood flows are cross validated at rest by strain gauge venous plethysmography (SGVP). Methods used to continuously observe 0.5Hz, 30% maximum voluntary isometric contraction (MVIC) plantar flexion exercise via dynamometer are adapted for our hybrid DCS-Imagent diffuse optical flow-oximeter in the medial gastrocnemius. We obtain healthy control muscle tissue hemodynamic profiles for key parameters BF, $\dot{V}O_2$, oxygen saturation (StO_2), deoxyhemoglobin, oxyhemoglobin, and total hemoglobin concentrations ([Hb], [HbO_2], and THC respectively), as well as systemic mean arterial pressure (MAP) and pulse rate (PR), at rest, during VO/AO, during dynamic exercise and during 15 minute recovery periods.

Next, we began investigation of muscle tissue hemodynamic disease states by performing a feasibility pilot study using limited numbers of controls and

peripheral arterial disease (PAD) patients using the translated methods/techniques to determine the ability of our technology to assess differences in these populations.

KEYWORDS: Diffuse correlation spectroscopy; near-infrared spectroscopy; blood flow; oxygen consumption rate; skeletal muscle;

Brad Henry

9/22/2014

STABILIZATION OF EXTENDED DIFFUSE OPTICAL SPECTROSCOPY MEASUREMENTS ON IN VIVO HUMAN SKELETAL MUSCLE DURING DYNAMIC EXERCISE

By

Brad Henry

Dr. Guoqiang Yu
Director of Thesis

Dr. Abhijit Patwardhan
Director of Graduate Studies

9/22/2014

ACKNOWLEDGEMENTS

Here I would like to show my appreciation for the people who have been of the utmost importance to the work codified here. Firstly I would like to thank my advisor and lab supervisor Dr. Guoqiang Yu. He recruited me to UK thanks to my background in physics and, I hope, he found that my analytical skills coupled with my biology/physiology strengths were of use after all. If not for his dogged insistence that more could be done and that the work we were doing was valuable I might have been discouraged during the many hours of baseline data collection and validation experiments. Such things do not lend themselves to excitation but he managed to motivate despite this. I owe these two years to him and appreciate the experience in what is, in my own opinion of course, a most worthy lab in the a worthy department.

Next I would show my appreciation for my predecessor, Katelyn Gurley. Without her guidance and assistance I would have found the experience of graduate school to be quite overwhelming and would almost certainly have taken up hoboing as a preferable alternative lifestyle. Her advices in matters of the lab, and in methods of escaping said lab, were of great import. Finally, I would like to thank her for filling the, at times incredibly tedious, hours with talks ranging from the philosophical to the utmost practical and with a wry wit interspersed.

In a very close third I must express my utmost regard for Dr. Yu Shang. In a lab of the size of this one, he found time to not only be of great help with the learning of how to operate the equipment of the lab, writing code, data analysis, and experimental design/data collection for me but for the rest of the lab. Truly I

could not have done the work that I have without his aid. In addition to the challenges of the lab during this past year he and his wife had their first child and the challenges that come with newborns, but he was still available to resolve all manner of question and confusion that accompanied this research. At the end of things, a co-authorship and my gratitude seem a shallow thanks, but they are all I have and are so given in hopes that they may somewhat repay you for all your help.

Next I would extend my thanks to the remaining members of the lab. Lian He was quite interesting to converse with regarding research and topics of various kinds. I spent not enough time extracurricular with her and wish that I'd made it a point to do so as she knows how to have fun. Ran Cheng's experience in the lab and knowledge of the ins and outs of research made a great deal of the work not nearly as frustrating as it could have been. His thoroughness in analysis and in the subtleties of optical spectroscopy, both hardware and software, were both amazing. I will miss the lunches and chats with he and his wife, they are both quality people. Dr. Yu Lin may have the best sense of humor in the lab. I will keep many of his stories and one liners in memory and I hope that border security will be a bit less harsh on his travels in the future else his vacations may stretch to tedium. Of our more recent additions, Dr. Chong Huang was predominantly engaged in working on the noncontact system but still found time to assist me in several aspects of my project, for which I am grateful. I would also like to thank Mingjun Zhao for her utmost interest and rapid progress in the aspects of the lab with which I am familiar. Discussing topics with her and having an extra set of

hands allowed both Dr. Yu Shang and I to be more productive and greatly enhanced the quality of this project. I'd like to thank all of you for your time, patience, and engaging discourse and wish you all the very best. I can honestly say that you're a fine lot and I wouldn't have traded you for any other lab mates around.

Additionally I'd like to thank Dr. Timothy Uhl. Without his contribution of equipment, lab time (which came entirely at the expense of his own department), and advice this research could not have been completed. I leaned rather heavily on his knowledge of limb mechanics and the subtleties of posture about which I had no previous knowledge. I do appreciate his patience with my tendencies for disorganization and sometimes lack of consideration for the difficulty my research added to his life, he was more kind than I had any right to expect. I also thank my other collaborators Dr. Sibu Saha, and Dr. Eleftarios Xenos for their help in advancing PAD research.

Lastly thank you to my committee, who had the patience to wade through this thesis and provide quality feedback despite being quite busy themselves. I'm appreciative for your efforts on my behalf and for your utmost professionalism throughout my interactions with you.

Table of Contents

LIST OF TABLES

LIST OF FIGURES

CHAPTER 1: INTRODUCTION AND BACKGROUND

1.1 Microvascular Hemodynamics and Metabolism in Muscle

The delivery of metabolic nutrients, oxygen, and removal of waste molecules is of paramount importance for the maintenance of healthy tissue. As such, the network of vessels, and the regulation of flow through those vessels have reached a phenomenally sensitive status with respect to nervous, mechanical, and metabolic stimulation. The small vessels (arterioles, capillaries, and venules) are of a particular interest since it is in this part of the vasculature that large scale exchange of O_2 molecules occurs and where many of the regulatory systems take their effect, as in the resistive elements of the pre-capillary arterioles. By observing the hemodynamics, that is the blood flow, oxygenation status, and tissue oxygen consumption rate parameters, of a tissue one can better understand the extent to which the microvasculature is functioning and therefore how well the homeostatic environment of the tissue is responding to functional demands. Of particular interest is the study of the hemodynamics of the skeletal muscle.

Skeletal muscle, by virtue of both its sheer mass of body composition (40-50% by mass)[1] and its necessity to everyday life, is a system whose function is critical to maintaining a healthy, active lifestyle and whose function has been strongly correlated to survival/life expectancy in various disease conditions[2]. Skeletal muscle is involved in every voluntary motion and in the function of the muscles that operate the chest cavity during breathing. Disorders in skeletal muscle function, whether by metabolic impairment, insufficient perfusion, or contractile malfunction range in severity from decreased activity, pain and limited

mobility, such as in peripheral arterial disease (PAD), to loss of limb and tissue ulcers, as experienced in diabetes and bedridden patients, to terminal wasting diseases, as in muscular dystrophy and age related sarcopenia[2]. It is estimated that about 8 million cases of PAD currently exist in the U.S. alone and that 12-20% of people over the age of 60 suffer from the disease[3]. These numbers are expected to swell with the increasingly aged population and the highly prevalent risk factors (smoking, obesity, diabetes, and high cholesterol) that contribute to the disease. The costs associated with patient care for PAD and other muscle wasting diseases will likewise rise substantially[4].

In addition to the various disease states which affect muscle, the function of muscle is of great interest to sports and exercise medicine. It can be difficult to assess functionality in terms other than gross power output or morphology. The perfusion and oxygenation of muscle tissue has direct implications on the ability of that muscle to perform[5]. Different activities and types of exercise/athletics exert different forms of hemodynamic response and these can be characterized to improve the responsiveness of a training regimen or to tailor a training toward a specific functional state (high endurance via sustained oxygen saturation vs. hypertrophic increases in muscle mass for power lifting)[6].

Despite the imminent importance of the skeletal muscle system and the volume of disease populations suffering from muscular disorders, there are relatively few ways to noninvasively assess the performance of muscle tissue *in vivo*, especially with respect to local blood perfusion and tissue oxygenation[7].

1.2 Tissue Blood Oxygenation Measurement

Traditional measurement techniques for determining the oxygenation of blood/tissue and thus the metabolic activity of the tissue relied on indirect methods such as Douglas bag spirometry or respiratory gas analysis, which measure oxygen concentration decreases/carbon dioxide increases in expired air[8]. This technique only measured the global metabolic rate and would only be used to indicate net gas exchange at time points for only as many gas bags as are feasibly available to be implemented as a single measurement may be taken with a particular bag and thus serial measurements require multiple bags, thus greatly limiting sampling rates and specificity of the measurement. Spirometry is then unable to localize oxygen consumption rate measurements in active muscles and cannot then be used in a diagnostic or evaluative manner for specific organ systems. More recently, blood oxygen and chemical analysis have been used to sample tissue metabolism but this involves invasive catheterization of the vessels and lacks an ability to make continuous measurements[9]. These techniques also share the weakness of being unable to localize the oxygen consumption rate to a specific muscle compartment since the vessels catheterized are typically large arteries and veins at opposing ends of the limb. Functional MRI (fMRI) has also been used to track changes in blood oxygenation in the tissue microvasculature[10]. The functional MRI imaging allows continuous and noninvasive monitoring of tissue oxygenation with high spatial resolution in deep tissues. Temporal resolution of such measurements is limited with BOLD (blood oxygen level dependent) measurements requiring as much as 12-18 seconds to

produce a measurement [11, 12]. fMRI and other radio-imaging techniques will be discussed further in Chapter 1.4 as they are also used to assess tissue blood flow. Optical methods of measuring local tissue oxygenation have been developed that use near infrared (NIR) light to measure the concentration of oxygen binding chromophores; the specifics of which are discussed more thoroughly in Chapter 1.3.

1.3 Near-infrared Spectroscopy (NIRS) for Tissue Blood Oxygenation Measurement

Over the last few decades, near-infrared (NIR) tissue oximetry has gained wide acceptance and been implemented in a broad range of applications, both clinically and in academia[12-20]. The noninvasive and exquisitely sensitive detection of tissue oxygenation, using relatively inexpensive and portable equipment with fast acquisition times has revolutionized deep tissue metabolic observation. NIR is made possible by the existence of a low absorbance band (700 to 900 nm) of light in tissue. Within this band, the dominant absorbers in tissue are oxy-hemoglobin, deoxy-hemoglobin, fat, and water (Figure 1).

Of the aforementioned absorbers, the primary two to change dynamically are the oxygen binding blood metalloproteins: oxy- and deoxy-hemoglobin, denoted HbO_2 and Hb respectively. Thus the majority of light absorption changes in this band are attributable to the blood chromophores and these two are clearly spectrally distinguishable (Figure 1)[15, 21].

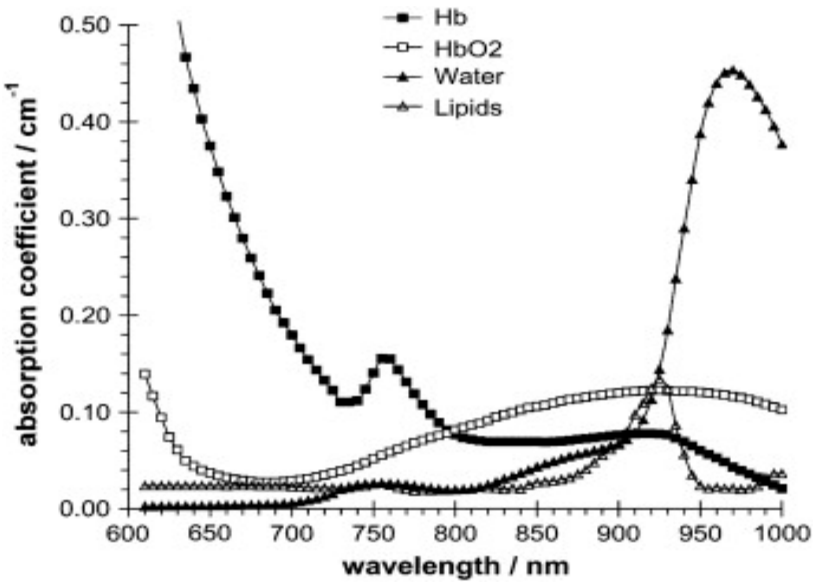

Figure 1. Absorption Spectra and the NIR Optical Window

The aborbances of HbO_2 and Hb are very similar at 800 nm thus this wavelength should be avoided when using NIR light to detect tissue absorption. Other absorbers such as water and lipid (fat) have minimal absorption between 700 and 900 nm thus sources in this range should have maximal penetration depths.

As NIR photons move through tissue, they are scattered at a much greater rate than they are absorbed creating a diffusive profile of movement through the tissue medium in which some photons are eventually diffused back to the tissue surface interface. This process is very complex and has been given a thorough treatment elsewhere, readers are invited to examine literature[15, 22]. The degree to which a media will absorb light is characterized by its absorption coefficient (μ_a), and the degree to which photons tend to scatter is likewise characterized by its reduced scattering coefficient (μ_s'), both with the unit of per centimeter (cm^{-1}). In NIRS it has been established that by illuminating tissue with two or more wavelengths of light in the NIR optical window band, measuring the changes in detected light intensity a certain distance away from the source, and knowing the

extinction coefficients of the involved absorbers, the changes in absorber concentration can be quantified[12, 15, 17, 22-24]. This relationship, including a modification that adjusts for multiple scattering events, is known as the modified Beer-Lambert Law[15, 21] and will be discussed in detail later. The use of different source illumination modalities, as well as the detection of intensity changes at multiple source-detector (S-D) separations allows for the calculation of absolute absorbers' concentrations (e.g., [HbO_2] and [Hb]) in tissue[25]). These absolute measurements may then be combined to derive total hemoglobin concentration (THC= [HbO_2] + [Hb]), and tissue blood oxygen saturation (StO_2 = [HbO_2]/THC ×100%).

The three categories of NIR oximeter are continuous wave (CW), frequency domain (FD), and time domain (TD) systems whose categorization can be made by illumination pattern (Figure 2).

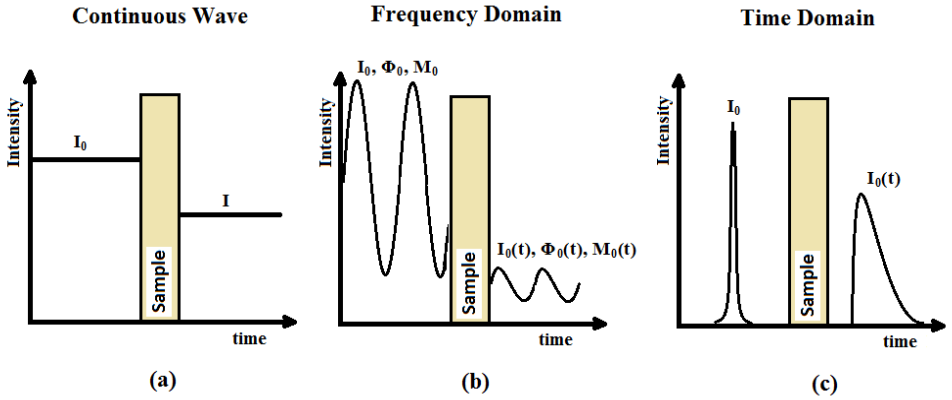

Figure 2. NIRS Illumination Modalities

The CW system (panel a) employs a continuous source illumination in which the intensity changes can be used to calculate absorber concentration changes. FD system (panel b) modulates the line with sine waves and the changes in signal amplitude and phase allow for calculation of absolute μ_a and μ_s. These are then used to calculate absolute concentrations of absorber molecules[24]. The TD system (panel c) injects a defined short pulse of light into the tissue and detects the change in amplitude of the pulse as well as its shape. These two qualities can be used to determine the values of the absolute chromophore concentrations[19].

CW oximeter is the simplest to operate and analyze, as well as the most inexpensive, but can only yield relative changes in hemoglobin concentrations. The other two systems can produce absolute absorber concentrations but are more expensive with an additional layer of data analysis. The TD system, requiring a larger amount of time to measure intensity pulse width, thus has a lower sampling time than the other two systems. Our lab makes use of a commercial FD-NIRS oximeter (Imagent, ISS Inc., IL), whose details will be discussed in Chapter 2.1, to detect absolute values of [Hb] and [HbO_2] as it has the capability of detecting absolute tissue oxygenation with temporal resolutions ranging from 0.5 to 100 Hz, depending on noise tolerances.

1.4 Tissue Blood Flow Measurements

Using NIRS to measure blood flow is a relatively recent addition to the repertoire of noninvasive optical measurements. Previous flow measurements relied on invasive catheterization of the large vessels with pressure transducers. In addition to the invasiveness of this technique, it limits measurement to the vessels smaller than the catheter. More advanced local clearance techniques such as 133-Xe washouts and Indocyanine green dyes (ICG) make use of indicator dyes and their clearance rates to quantify blood flow through the microvascular beds. However, these techniques are still invasive and some may also employ radioactive materials. Furthermore, due to recycling of the dye, continuous or quickly repeated measurements are impossible[26].

Noninvasive measurements of flow historically include strain gauge venous plethysmography (SGVP), a technique in which pressure in excess of diastolic (venous return) pressure is applied to the limb, preventing blood from leaving the compartment. A strain gauge is used to measure the rate of change in limb circumference and thereby calculate the volume of inflowing blood. This measurement is, by its nature, disturbing to flow and cannot be performed in rapid succession[12, 26, 27]. This measurement method is also only useful for assessing whole limb flow and so cannot be used to distinguish local working muscle group blood flow from passive muscle flow. SGVP will be discussed more thoroughly in Chapter 4 and the Appendix where it was used as part of a protocol, for comparison/validation purposes.

More advanced noninvasive flowmetry has been developed using magnetic imaging techniques or PET. fMRI and PET stand out as effective methods for assessing the combined parameters of tissue oxygenation, blood flow, or phosphate metabolites. Temporal resolution for these is fair (~0.1 Hz for arterial spin labeled fMRI and 0.025 Hz for PET), though lacking when compared to other techniques such as Doppler Ultrasound, Laser Doppler, and NIR diffuse correlation spectroscopy (DCS)[11, 28]. The spatial resolution to both is fine, ranging from 100-250 μm for fMRI and 1.5 mm for PET[11, 29]. Whether the temporal sensitivity loss is worth the spatial gain is dependent on the purpose of the study. The major disadvantages of fMRI and related imaging technologies have always been the cost, the degree of difficulty in analysis of acquired signals, and the requirement that patients be confined to an MRI tube which severely limits the potential exercising applications of the technology. Additionally, PET is still reliant on the use of radioactive elements. Some of these methods, ASL MRI at least, may have limited use in low blood flow scenarios which makes it non optimal for assessing resting or recovery values of blood flow[28].

Doppler ultrasound (DU) has proven to be a reliable technique for assessing large vessel flow with a high temporal resolution and deep tissue penetration. As its name implies, ultrasound relies of the insonation of the tissue with high frequency sound waves[26]. However, the technology is limited in exercise protocols by the necessity of maintaining a set insonation angle and good insonator/receiver contact. The major weakness inherent to DU flowmetry is in

that only larger blood vessels may be observed. This means that only the supply vessel flow and not the exchange vessel flows can be observed.

Overall, each of these flowmetries has advantages or disadvantages in terms of cost, sensitivity, or ease of operation. However, none of them meet the demand of making noninvasive, continuous and dynamic measurements, with high sensitivity, high temporal resolution, in deep tissue microvasculature. Recently developed NIR DCS-based technologies showed the potential to meet these requirements (see Chapter 1.5)[12, 15, 30-32].

1.5 NIR Diffuse Correlation Spectroscopy (DCS) for Microvascular Blood Flow Measurement

NIR Diffuse correlation spectroscopy (DCS) is a method of assessing microvascular perfusion that has been developed over the last twenty years. DCS incorporates the same NIR light band as NIRS but applies this photon illumination and detection scheme to observe a distinctly different system. Instead of observing chromophore concentrations, this system monitors light speckle fluctuation at the tissue surface. Speckles are discrete regions of photon intensity generated by the effects of moving scatterers in highly scattering media on photons traveling through it, and which can be produced by illuminating tissue with a long coherence CW laser[15, 22]. The presence of scattering bodies under motion, which for biological tissues is predominantly limited to erythrocytes in the blood, causes these speckles to fluctuate rapidly. The multiple scattering of photons by moving bodies, each of which imparts a random vector and phase shift to the photons producing, when summed, a temporally fluctuating interference

pattern at the interface[15, 22]. By measuring the intensity changes of a single speckle using a single mode optical fiber connected to a single photon counting photodetector and correlating them using an autocorrelator, these changes can be quantified to assess the average flow of moving scatterers (red blood cells) within the photon path and used as an index of blood flow. By normalizing the blood flow index to its initial resting baseline value, the relative blood flow (rBF) can be obtained[15, 20, 33]. The theoretical specifics of how speckle intensity fluctuations are used to calculate blood flow index and rBF will be left to the discussion of methods in Chapter 2.

The advantage of this system is that it possesses a high temporal resolution (up to 100 Hz), a reliable tissue penetration depth of up to ~1.5 cm (deep enough to observe superficial muscle), noninvasiveness, portability, and low running costs of optical spectroscopy[34]. The ability to noninvasively measure microvascular blood flow with high temporal resolution is unique to the DCS and makes it of particular use in clinical application to evaluating deep tissue perfusion. This technology has been validated against several accepted techniques including Xe-CT, arterial-spin-labeled MRI, Doppler ultrasound, power Doppler ultrasound, and fluorescent microspheres[16, 28, 35-40]. The tissues observed, as previously mentioned, also range broadly and include human/mouse brains, head/neck tumors, breast, and skeletal muscle[16, 28, 31, 36-43]. The recent innovation of a novel gating algorithm in our laboratory has allowed the use of DCS with minimal motion artifacts, such as those prevalent during muscle contractions in previous studies[16, 31, 44]. Also, a commercial tissue oximeter has been

employed in conjunction with DCS to create a hybrid diffuse optical flow-oximeter (see Chapter 1.6)[8, 15, 31, 32].

1.6 Hybrid Diffuse Optical Spectroscopies for Measurements of Both Tissue Blood Flow and Oxygenation

In the past our lab had developed two types of hybrid instruments for simultaneous microvascular blood flow and oxygenation measurements: a dual-wavelength DCS (CW)[45-52] flow-oximeter and a combined DCS/FD-NIRS (Imagent) flow-oximeter[31, 32, 41, 53]. By using a second wavelength long coherence source laser and alternately illuminating the tissue with 2 wavelengths it is possible to simultaneously collect both relative changes in tissue oxygenation (Δ[Hb], Δ[HbO_2], and ΔTHC), as discussed in Chapter 1.3, and rBF as discussed in Chapter 1.5[15]. CW-DCS flow-oximetry is relatively inexpensive and allows for continuous quantification of the real time changes in microvascular hemodynamics with a locality, sensitivity, and temporal resolution unavailable to other systems.

Combination of an FD-NIRS and DCS requires the integration of two separate sets of hardware and their associated operating software. This additional layer of complexity is largely offset by the gain of absolute tissue absorption and reduced scattering coefficients, which were previously assumed for the sake of DCS measurements. Most importantly, this system has the advantage of determining [HbO_2], [Hb], THC, and StO_2 in absolute units. These are necessary to perform occlusion calibrations for initial values of absolute tissue blood flow (BF) in units

of ml blood*100ml tissue^{-1}*min^{-1} and the derived oxygen consumption rate ($\dot{V}O_2$) in units of mlO_2*100g^{-1}*min^{-1}[31, 53].

This recently adopted hybrid FD-NIRS/DCS optical system, combined with finger plethysmography measurements of mean arterial pressure (MAP) and pulse rate, allows for the simultaneous collection of a suite of hemodynamic parameters which include relative/absolute blood flow (rBF/BF), relative/absolute oxygen consumption rate ($r\dot{V}O_2/\dot{V}O_2$), [Hb], [HbO_2], THC, StO_2, MAP, and pulse rate. All of these measurements are made continuously, noninvasively, and rapidly making hybrid diffuse optical measurements of unique benefit in evaluating tissue microvascular hemodynamics and metabolism.

1.7 Baseline Stability of DCS Contact Blood Flow Measurement

In previous studies performed on muscle tissue, we noted that blood flow index (αD_B) exhibited an unexpected increase during prolonged measurements. Previous investigations revealed that no such trend in blood flow was observed during contact probe cerebral hemodynamics measurements[41] nor were they observed during preliminary measurements on gastrocnemius tissue using a noncontact probe (unpublished data). This eliminates immediately DCS hardware drift and effects of the source on the tissue since both the noncontact and contact probe use the same instrument. Given that muscle tissue and cerebral tissue have vastly different conditions (fixed skull geometry for the cerebral tissue, pliable muscle tissue with possible contractile motion/geometry artifact in the muscle, different autoregulatory innervations, etc.), it is possible that the tissues might

have differential responses associated with the measurement. We thus hypothesize that only factors related to the unique combination of muscle tissue and use of contact probe to measure it can be attributed to the baseline BF shift. Details for solving the problem of baseline BF shift can be found in Chapter 3.

1.8 Measurement of Hemodynamic and Metabolic Profiles During Exercise in Gastrocnemius Muscle

Eventually our research aims to examine patient populations which have diseases of muscle hemodynamics and metabolism. Many of these diseases preferentially affect the lower limbs. This study then aimed at applying absolute calibration of continuous, relative, optical measurements during exercise to the lower limb (gastrocnemius). Calibration of relative measurements consists of performing a series of occlusions in order to obtain initial resting baseline values for BF and $\dot{V}O_2$ that have been met with success in previous studies by this lab[32]. For the purposes of transferring the dynamic measurement methods in forearm, as described by Gurley et al [32] during handgrip exercise, to the lower limb, we decided to employ a plantar flexion exercise protocol with a fixed percentage (30%) maximum voluntary isometric contraction (MVIC) in healthy subjects. This protocol would allow us to establish a complete hemodynamic/metabolic profile of typical responses to exercise in the lower limb. The protocol, detailed in Chapter 4.1 and 4.2, closely mirrored a study performed by Bauer et. al., giving this protocol some precedent in physiological literature[54]. Strain gauge venous occlusions were used to concurrently measure absolute limb BF in the gastrocnemius at resting baseline and post exercise in

order to assess the validity of our BF calibration and to examine the whole limb BF response to exercise in comparison to local tissue.

1.9 Pilot Study on Peripheral Arterial Disease (PAD)

Our major purpose in transferring continuous absolute measurement methods applied previously in the forearm to the gastrocnemius is to initiate investigation into the hemodynamic effects of PAD on lower limb muscles. PAD is a vascular insufficiency in the lower limbs that results in an ever increasing difficulty in supplying the tissue with oxygen, particularly noticed during every day events such as walking or working on ones feet. The disease is commonly found in patients who suffer from hypertension, diabetes mellitus, atherosclerosis, and smokers[55]. As the vascular integrity of the patients deteriorates, the symptoms of PAD worsen until the ischemia becomes severe enough to induce necrosis. In this case the lower limbs, most often starting at the feet, begin to ulcerate producing wounds prone to infection and highly resistant to healing[3, 55-57]. The muscle locality and compromise of both flow and oxygenation due to this disorder seemingly make hybrid flow-oximetry an ideal system with which to observe such a disorder.

1.10 Thesis Organization

This thesis is organized as follows. Chapter 2 introduces the methods and theory behind NIRS oximetry and DCS flowmetry, which are the predominant systems employed in this work. The methods for calibrating relative blood flow using venous occlusion and relative oxygen consumption using arterial occlusion

are also described. Lastly a brief discussion of data processing and statistical methods is made.

Blood flow measurement stability on in-vivo muscle must first be established to confirm/remediate possible baseline blood flow elevations. Thus a series of baseline DCS contact measurements are made to assess the long term stability of in-vivo relative flow, which are presented in Chapter 3.

The diffuse optical techniques used to calibrate local absolute baseline values for blood flow and oxygen consumption rate and for continuous monitoring related hemodynamic responses during exercise have thus far only been applied to examine hemodynamics of the forearm flexor muscles. This muscle group is of limited interest in the investigation of some perfusion disorders in lower limb and the broadening of ranges of muscle groups which we may assess during exercise is important for bringing this technology to clinical relevance. Chapter 4 then describes a study performed to translate absolute calibration of relative hemodynamics and continuous exercise methods to the gastrocnemius.

The ultimate goal of this research is to use hybrid diffuse optics clinically, applying them to patient populations (e.g., PAD) for eventual diagnoses and treatment monitoring. To this end, the final study of this thesis, Chapter 5, is a small pilot study designed to determine whether or not our methods and instrumentation is feasible to be used in patients with PAD at rest and during exercise.

At the end, Chapter 6 discusses the difficulties and methodological considerations that were involved with each of the studies herein, and summarizes results, conclusions and future perspectives.

CHAPTER 2: DIFFUSE OPTICAL METHODS, INSTRUMENTATION AND DATA PROCESSING

This chapter is devoted to discussion of the theories of diffuse optical flowmetry and oximetry and instrumentation used to make microvascular hemodynamic/metabolic measurement (Chapter 2.1 and 2.2). It also introduces the methodology and theory of using venous and arterial occlusions to measure absolute tissue blood flow and oxygen consumption rate respectively (Chapter 2.3 and 2.4). These values are used to calibrate relative optical measurements. Lastly a brief discussion of gating algorithm to reduce motion artifacts and data analysis methods will be made (Chapter 2.5).

2.1 FD-NIRS Oximetry

Absolute tissue oxygenation measurements are made using a commercial 4-wavelength FD-NIRS instrument (Imagent, ISS Inc., IL). The Imagent spatially resolved spectroscopy employs four, 110 MHz modulated sources at 690, 750, 780 and 830 nm to probe tissue absorbance. The source light is injected via multimode source fiber optic cables (diameter = 400 μm) at 4 S-D separations (2.0, 2.5, 3.0 and 3.5 cm) for all wavelengths. After diffusing through the tissue, the light is collected via large diameter multimode fibers (diameter = 2.5 mm) and detected by a photomultiplier tube (PMT) which converts the detected photons into a voltage signal.

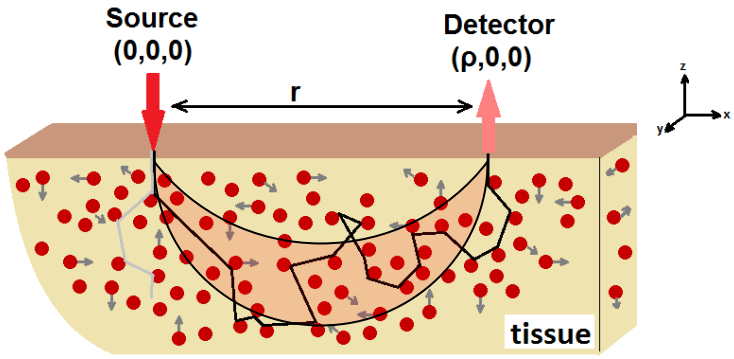

Figure 3. Probe Geometry and Photon Path

The path of photon diffusion is characterized by an inverted "banana" shape region from the source to the detector, distance denoted ρ. Note the random scatter vectors and semi-infinite geometry. Semi infinite refers to the existence of a single flat boundary condition in which photons only undergo transitional effects at the source/detector interface. Additionally assumed is the homogeneity of this medium, which is a somewhat generous approximation of tissue.

Since the light is frequency modulated, the detected intensity has a modulated light amplitude (AC signal), an average light intensity (DC signal), and a difference in time or phase (φ).

The method of calculating the absolute scattering and absorbing coefficients of the tissue are based upon a photon diffusion equation [15, 30]. The equation, and details related to its derivation and solution may be found in the immediately preceding citations. The results are that a linear relationship exists between the natural log of the AC signal, the natural log of the DC signal, and φ at different S-D separations (r). These linear relations can be fit and their slopes (denoted S_{dc}, S_{ac}, $S_{\varphi)}$ can be used to calculate the absolute μ_a and μ_s' via the following equations[58]:

$$\ln\left(dc \cdot r^2\right) = rS_{dc}\left(\mu_a, \mu_s'\right) + In_{dc}\left(D, K_{dc}\right) \qquad (1)$$

$$S_{dc} = -\left(\frac{\mu_a}{D}\right)^{1/2} \tag{2}$$

$$\ln\left(ac \cdot r^2\right) = rS_{ac}\left(\mu_a, \mu_s', \omega, v\right) + In_{ac}\left(D, K_{ac}\right) \tag{3}$$

$$S_{ac} = -\left(\frac{\mu_a}{D}\right)^{1/2}\left[\left(1+\left(\frac{\omega}{v\mu_a}\right)^2\right)^{1/2}+1\right]^{1/2} \tag{4}$$

$$\varphi = rS_{\varphi}\left(\mu_a, \mu_s', \omega, v\right) + In_{\varphi}\left(K_{\varphi}\right) \tag{5}$$

$$S_{\varphi} = \left(\frac{\mu_a}{2D}\right)^{1/2}\left[\left(1+\left(\frac{\omega}{v\mu_a}\right)^2\right)^{1/2}-1\right]^{1/2} \tag{6}$$

Here, μ_a is absorption coefficient, μ_s' is reduced scattering coefficient, D is the photon diffusion constant ($\upsilon/3\mu_s$'), υ is the speed of light in the media, r is the S-D separation, ω is the modulation frequency, and K_x represents constants associated with the illumination/detection hardware. Specifically, these constants depend on detector sensitivity and modulation frequency (K_{AC}), source intensity (K_{DC}), and phase differences (K_{φ}) between source and external phase contributions (outside noise). To reduce noise from the environment and since only two slopes are required to calculate the optical properties (μ_a and μ_s') at each wavelength, it is preferable to use the ac and phase slopes[58].

The absorption coefficient can be related to chromophore contributions at a particular wavelength wherein the total absorbance is a sum of contributing absorbers 1 to i[15]:

$$\mu_a(\lambda) = \sum_i \varepsilon_i(\lambda)[i] \quad (7)$$

This equation indicates that $\mu_a(\lambda)$ is dependent on the extinction coefficient (ε_i) of the contributing chromophores multiplied by their concentrations [i]. By knowing the $\mu_a(\lambda)$ at two wavelengths (from the slope acquisitions Eq(1) to Eq(6)) and the extinction coefficients for the two chromophores at both wavelengths, the two unknown concentrations of absorbers ([Hb] and [HbO_2]) can be reconstructed.

Examination of in-vivo measurements of tissue oxygenation found that the phase components of spatially resolved spectroscopy at multiple separations introduced noise that was confounding to the precise short time changes in hemoglobin concentrations necessary for calibration of BF[20]. To retain the advantage of FD-NIRS absolute measurements but eliminate this noise, we obtained absolute baseline measurements of [Hb], [HbO_2], THC, and StO_2 using the spatially resolved spectroscopy capability during an initial baseline. These absolute baselines were used to calibrate the relative hemoglobin concentrations Δ[Hb], Δ[HbO_2], and ΔTHC obtained using modified Beer-Lambert calculations of single separation (2.5 cm) detected intensities from 690 and 830 nm sources[15, 20]. Specifically, the calculation of relative chromophore concentrations involves the following procedure:

First the differential pathlength factor (DPF) or distance traveled by photons in a scattering media with a fixed S-D separation must be calculated. It should be noted that the DPF listed here is an empirically determined value which is based

on the relationship between changes in absorption coefficient, reduced scattering coefficient, and S-D separation (r):

$$DPF(\lambda) = \frac{\sqrt{3\mu_s'(\lambda)}\sqrt{3\mu_a(\lambda)\mu_s'(\lambda)}\cdot r}{2\sqrt{3\mu_a(\lambda)}\sqrt{3\mu_a(\lambda)\mu_s'(\lambda)}+1\cdot r} \quad (8)$$

The advantage here of using a spatially resolved FD-NIRS instrument is that the baseline μ_s' and μ_a is measured directly for the calculation of DPF.

Next, "A (λ)" refers to the optical density or the logarithmic change in detected intensity due to changes in absorber concentration compared to the initial baseline intensity and is calculated by[15]:

$$A(\lambda) = \log\frac{I}{I_0} = \Delta\mu_a(\lambda)DPF(\lambda)r \quad (9)$$

By measuring the optical density (A) at two wavelengths, substituting Eq. 7 for the changes in absorption coefficient concentration, and knowing the extinction coefficients of the absorbers it is possible to solve for the changes in the two chromophore concentrations as shown here:

$$\Delta[Hb] = \frac{\varepsilon_{HbO_2}(\lambda_2)\frac{A(\lambda_1)}{DPF(\lambda_1)} - \varepsilon_{HbO_2}(\lambda_1)\frac{A(\lambda_2)}{DPF(\lambda_2)}}{\varepsilon_{Hb}(\lambda_1)\varepsilon_{HbO_2}(\lambda_2) - \varepsilon_{Hb}(\lambda_2)\varepsilon_{HbO_2}(\lambda_1)r} \quad (10)$$

$$\Delta[HbO_2] = \frac{\varepsilon_{HbO_2}(\lambda_1)\frac{A(\lambda_2)}{DPF(\lambda_2)} - \varepsilon_{HbO_2}(\lambda_2)\frac{A(\lambda_1)}{DPF(\lambda_1)}}{\varepsilon_{Hb}(\lambda_1)\varepsilon_{HbO_2}(\lambda_2) - \varepsilon_{Hb}(\lambda_2)\varepsilon_{HbO_2}(\lambda_1)r} \quad (11)$$

Relative changes in hemoglobin concentration (Eq. 10 and 11) are calibrated to absolute units by addition of absolute baseline values of the respective chromophore concentrations obtained by the spatially resolved spectroscopy method.

2.2 Diffuse Correlation Spectroscopy (DCS) Flowmetry

DCS measurements of a microvascular flow index are described in detail in many previous publications[22, 35] and so will be discussed here more briefly. The technology has its roots in the physical modeling of light correlation dynamics through turbid media. By illuminating the tissue with a long coherence, CW-NIR source (785, 830, or 854 nm, Crystalaser Inc. NV, USA) a temporally varying speckle pattern may be generated at the tissue surface. This speckle fluctuation is detected by a single-mode fiber connected to a single photon counting avalanche photodiode (APD, PerkinElmer Inc., Canada). By using 4 bundled fibers bundled into a single tip, 4 channels of speckle intensity data can be collected simultaneously from a single location. The data are sent to a 4-channel autocorrelator board (Correlator.com, NJ, USA), producing normalized intensity autocorrelation functions (g_2), which are averaged to improve signal-to-noise ratio (SNR). The intensity autocorrelation function is then related to the normalized electric field autocorrelation function (g_1) through the Siegart relation:

$$g_2(\vec{r}, \tau) = 1 + \beta |g_1(\vec{r}, \tau)|^2 \quad (12)$$

where g_2, again, is the normalized intensity autocorrelation function, g_1 is the normalized electric field autocorrelation function, τ is the delay time, $\vec{r}$ is the position vector associated with the photon path, and β is the coherence factor. β is

related to the coherence length, optical system stability, and is inversely proportional to the number of speckles observed[15, 20, 30, 33, 59]. The reason for introduction of the normalized electric field autocorrelation function g_1, is that the relation of dynamic scatterer motions (erythrocytes) in turbid media (tissues) to correlation diffusion are actually derived in terms of the un-normalized electric field autocorrelation function G_1. For a thorough treatment of the derivation and solution of the equations that model these processes the reader is encouraged to attend the following sources[15, 22, 30]. To abbreviate this more rigorous process, it will do here to say that the electric field correlation dynamics, from a CW-long coherence source, in a homogenous turbid medium is of the following form[15, 22]:

$$\left(D\nabla^2 - v\mu_a - \frac{1}{3}v\mu_s{}'k_0\alpha\langle\Delta r^2(\tau)\rangle\right) G_1(\vec{r},\tau) = -vS(\vec{r}) \qquad (13$$

Equation 13 is the so-called correlation diffusion equation where α is the ratio of dynamic to total (static + dynamic) scatterers, $k_0 = 2\pi n/\lambda$ is the photon wave number (n is refractive index), and $S(\vec{r})$ is the source light distribution term[15, 30]. Critical to this equation is the term $\alpha\langle\Delta r^2(\tau)\rangle$ (α multiplied by the mean squared displacement of dynamic scatterers), which introduces the relation of photon correlation decay to the ratio and mean squared displacement of moving scatterers. It should be noted that α and $\langle\Delta r^2(\tau)\rangle$ are inseparable in this treatment. The mean squared displacement of moving scatterers is parameterized by a diffusion model via:

$$\langle\Delta r^2(\tau)\rangle = 6D_B(\tau) \qquad (14)$$

Of particular importance is the relationship between $\langle \Delta r^2(\tau) \rangle$ and the Brownian diffusion coefficient D_B given by Eq.14. Flow through capillary networks is tortuous and, in a spatial average, without specific direction, thus movement of erythrocytes can be approximated by diffusion. For more discussion of D_B and the justifications for its use in biological tissue see references[22, 45]. After substitution, a blood flow index αD_B can be obtained. Equation 14 is supported by experimental fit to diffuse models and Monte Carlo simulation[15, 30, 45, 60]. The advantage of this model of autocorrelation function diffusion in tissue is that the mathematics of the equation is well defined, similar to the photon diffusion equation[15, 30]. For a fixed semi-infinite geometry (See Figure 3) alongside a few assumptions, this equation can be solved to generate an analytical solution[22, 35]:

$$G_1(\rho,\tau) = \frac{\nu S_0}{4\pi D}\left(\frac{e^{-k(\tau)r_1}}{r_1} - \frac{e^{-k(\tau)r_2}}{r_2}\right) \tag{15}$$

which can then be normalized to the form

$$g_1(r,\tau) = \left(\frac{e^{-k(\tau)r_1}}{r_1} - \frac{e^{-k(\tau)r_2}}{r_2}\right) \bullet \left(\frac{e^{-k_0 r_1}}{r_1} - \frac{e^{-k_0 r_2}}{r_2}\right)^{-1} \tag{16}$$

where $r_1 = \sqrt{\rho^2 + z_o^2}$, $r_2 = \sqrt{\rho^2 + (z_0 + 2z_b)^2}$, $k_0 = \sqrt{3\mu_a \mu_s'}$, $z_0 = 1/(\mu_s' + \mu_a)$, $z_b = 2(1+R_{eff})/3\mu_s'(1-R_{eff})$, $R_{eff} = 1.440n^{-2} + 0.710n^{-1} + 0.0636n + 0.668$, n = 1.33 for tissues, and $k(\tau)^2 = 3\mu_s'\mu_a + \mu_s'^2 k_0^2 6\alpha D_B$. The position vectors r_1 and r_2 refer to the S-D geometry with ρ being the S-D separation and values of z being related to the boundary condition of light moving through mismatched indices of

air and tissue (R_{eff}) at the surface interface of the source ([0, 0, 0]) and detector ([ρ, 0, 0]). For a given measurement of g_2, and the subsequent calculation of g_1, the only unknowns in this solution are the optical properties of the medium and the flow index αD_B [cm^2/s]. This unit is not typical of flow and results from the spatial averaging of moving scatterers within the tissue volume and the source-detector geometry[15, 30].

By assuming or measuring the optical properties of the media (e.g., using Imagent), the solution listed in Eq. 15 can be normalized and then employed to calculate flow index αD_B by least mean square error fitting of the measured g_1 curve with the modeling g_1 curve as described by Eq. 16. The process is diagramed in Figure 4. While each intensity autocorrelation curve only takes a few fractions of a second to obtain, many of these correlation curves are averaged to reach adequate SNR. In effect these correlation averaging times are the limiting factor for DCS temporal sampling rates. In this study we used ~300 ms to produce a single blood flow index. This index can then be used to calculate relative blood flow (rBF) by normalizing $\alpha D_B(t)$ to a passive, unperturbed baseline via:

$$rBF = [\alpha D_B(t)/\alpha D_B(t = 0)] \times 100\% \quad (17)$$

This relative measure of blood flow can be calibrated through a well accepted protocol combining the measurement of THC increases during a venous occlusion protocol as will be discussed in detail in Chapter 2.3[13, 14, 20, 61].

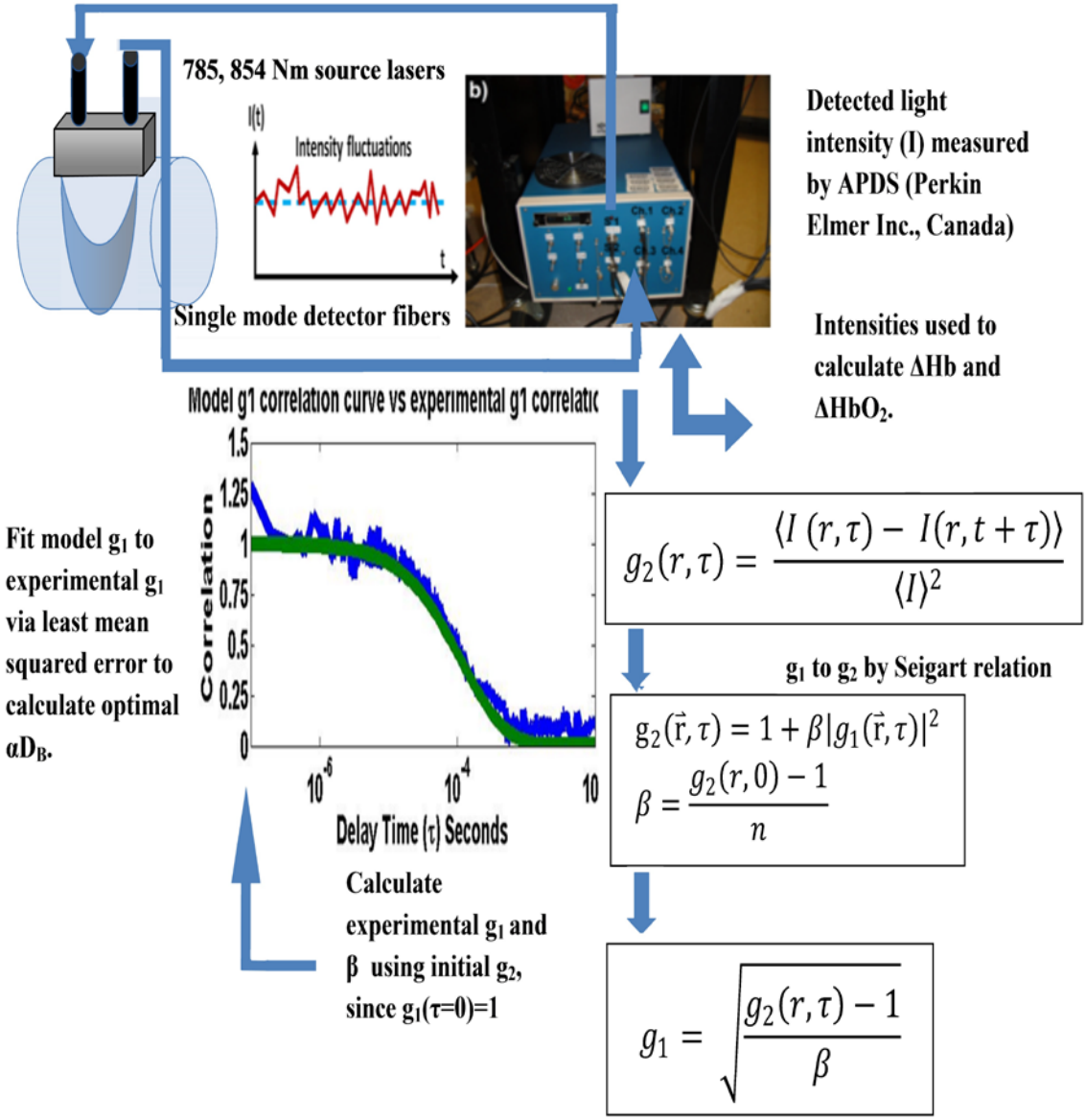

Figure 4. Data Collection and Analysis Regime for DCS

Detected speckle intensities are collected and autocorrelated to produce intensity autocorrelation curves g_2. This data is then related to the electric field autocorrelation function and fitted against a model solution to compute the flow index αD_B. Analysis is performed via MATLAB code and the fitting between calculated G_1 and theoretical solution G_1 curves is done by fminsearch function for multiparameter least mean squares. The initial value for αD_B is set as 1E-8 and then the values of αD_B are varied until a minimum error is reached within a certain number of iterations. This method can be used for simultaneous fitting of coherence factor β and αD_B since the two parameters have no cross talk, as investigated in detail elsewhere[62].

2.3 Calibration of Relative Blood Flow (rBF)

As has been mentioned earlier, the result of DCS flow index measurements requires a calibration to provide an absolute flow value in standard unit (ml/100ml/min). This calibration is provided by the well accepted method of performing a venous occlusion (VO) and calculating the arterial inflow via a change in blood volume within the compartment[14, 26, 27, 55, 61]. VO is accomplished by use of a pressure cuff acting as a tourniquet[13, 14, 61]. Inflating the cuff to super-diastolic pressures of 50-60 mmHg results in the inability of blood to leave the venous compartment. Strain gauge plethysmography, as earlier described, measures gross change in limb volume globally. NIRS however measures the change of THC (proportional to blood volume) for a discrete volume of tissue[14, 26, 27, 63, 64]. The equation to calculate BF is given as:

$$\mathrm{BF} = \frac{1}{\mathrm{C}} \cdot \frac{d[\mathrm{T}HC]}{dt} \tag{18}$$

Thus the NIRS measurement during VO provides a rate of change for the concentration of hemoglobin in μM/kg/min, which can then be converted to blood flow by the application of Eq. 18. The example measurement of THC using Imagent and THC fitting during multiple VOs is illustrated below in Figure 5.

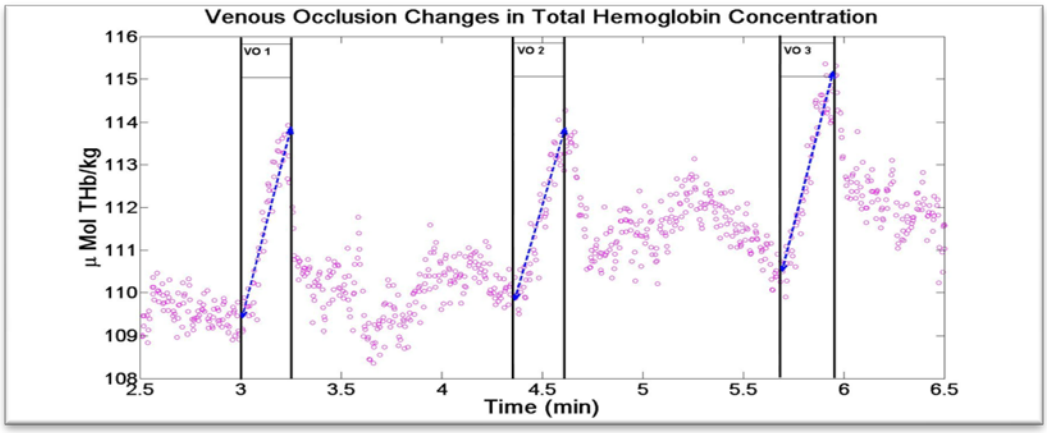

Figure 5. Venous Occlusion Protocol and THC Slope Fitting

Each occlusion was performed for 10 seconds as the linear increase in THC is transient. This slope was fitted using MATLAB polyfit function for the THC (note that THC and THb are interchangeable) between the two marked (vertical line) data points. The average of these three slope values was used to calibrate rBF measurements.

The conversion to ml blood/100ml/min is performed by dividing concentration by the concentration of hemoglobin in blood (14.1 g/dL) and multiplying by the molecular weight of hemoglobin (64.458 g/mol)[17, 31]. You then perform some minor unit conversions to take into account the μMol to mol ratio (divide by 10^6) and convert to per minutes (multiply by 60) along with converting from deciliters to 100ml and g/kg to resolve the g/kg muscle ratio (multiply by 10,000). Nioka et al provides an abbreviated approximation of 1 μM/kg/sec to 3 ml/100ml tissue/min[17]. This approximation is very close to Gurley's calculated value of 2.74 ml blood/100ml tissue/min per 1 μM/kg/sec [20].

2.4 Calibration of Relative oxygen Consumption Rate ($r\dot{V}O_2$)

In addition to flow, oxygen consumption rate is one of the metabolic parameters of greatest interest to physiologists and clinicians trying to determine the health/level of activity of tissue. The metabolic activity of a tissue can be used to diagnose its functional condition and to discern a pathological loss of said

function. Derivation of oxygen consumption rate requires both the arteriovenous difference in O_2 concentration and blood flow information of the tissue via the Fick principle[31, 45, 65]:

$$\dot{V}O_2 = BF \times ([O_2]_a - [O_2]_v) \quad (19)$$

The arterial blood has an assumed constant oxygen saturation (SaO_2) of >98%. This blood is then understood to deliver some amount of oxygen into the tissue and then mixed with the blood occupying the venous compartment. StO_2 may be measured by NIRS and from these we can calculate the oxygen extraction fraction (OEF) as the arteriovenous difference comparing tissue StO_2 during arterial occlusion to the initial SaO_2:

$$OEF = ([O_2]_a - [O_2]_v)/[O_2]_a \quad (20)$$

This equation can then be considered in terms of StO_2 saturation, which should decrease due to oxygen consumption during arterial occlusion.

$$OEF = (SaO_2 - StO_2)/(\gamma \times SaO_2) \quad (21)$$

By approximating > 98% SaO_2 as 1 and the term γ (the percentage of blood volume contained by the venous compartment) as a constant, we may calculate the relative OEF as

$$rOEF = (1 - StO_2)/(1 - StO_{2baseline}) \quad (22)$$

The relative oxygen consumption rate may then be calculated using only optical information obtained by the hybrid optical instrument:

$$r\dot{V}O_2 = rBF \times rOEF \quad (23)$$

This relative value is useful but the absolute values are desired, as is the case for blood flow, in order to compare the potentially meaningful baseline, maximum, and minimum values to other measurements obtained using different equipment, or to determine physiologically relevant differences between patient/subject populations.

The calibration of absolute $\dot{V}O_2$, similarly to that of BF, is done using a brief occlusion of the limb. In the case of $\dot{V}O_2$ however, it is necessary to increase the pressure of occlusion to super-systolic (at least systolic + 50 mmHg) levels for a total arterial occlusion (AO). As a matter of course we prefer to use 225 to 250 mmHg to ensure halt of blood flow, inasmuch as this is possible. The DCS rBF measurement is useful in this to verify the extent of flow reduction due to AO. The rate of change from oxy-hemoglobin to deoxy-hemoglobin should then be due to the tissue consumption of oxygen (see Figure 6). Thus $\dot{V}O_2$ can be estimated by fitting the slope of the difference between $[HbO_2]$ and [Hb]. The calibration of the baseline $\dot{V}O_2$ only requires a single minute of AO, which has minimal impact on system hemodynamics (See Figure 6).

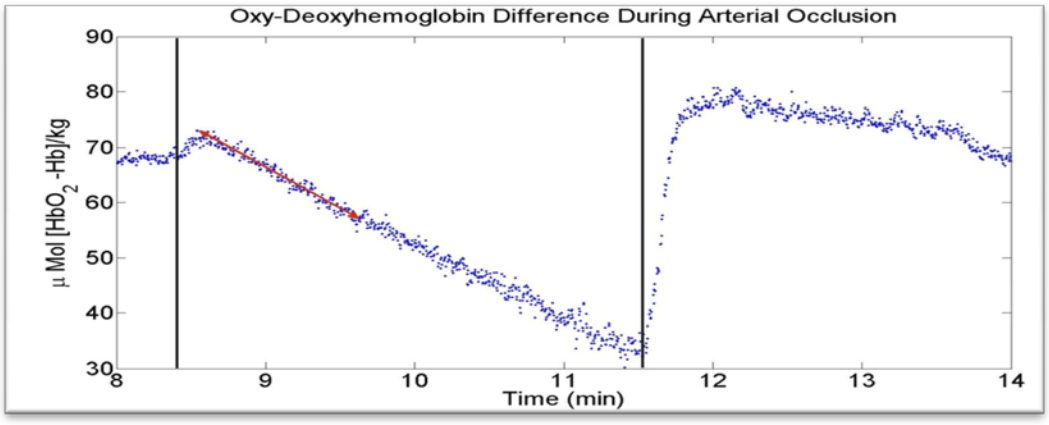

Figure 6. Arterial Occlusion via HbO_2 and Hb Difference Fitting

At the onset of occlusion, a transient initial increase occurred due to the slow (3-5 seconds) filling of the cuff which induced sub arterial occlusion pressures and a very temporary venous occlusion. The first minute of desaturation was fitted to determine the rate of change for calibration. The occlusion was continued for another 2 minutes to observe flow/hemoglobin concentration changes and the subsequent hyperemic/reperfusion response following the end of occlusion. These parameters can verify the successfulness of the arterial occlusion and reinforce experimental confidence in calibration values.

The change in hemoglobin concentration results in a unit of μM/kg/min and may be converted to mlO_2/100g tissue/min by knowing the molar ratio of 4 Mol O_2 to 1 Mol Hb, the molecular weight of oxygen (32 g/mol), the density of O_2 (1.429g/L), and the density of muscle (1.04 kg/L)[18, 31]. As with the calibration for flow there exists an approximate conversion factor of 1 μM ($[HbO_2]$–[Hb])/ kg/sec which is approximately equal to 0.54 ml O_2/100g/min[17].

2.5 Gating algorithm, Data Processing and Statistical Analysis

Data collection during exercise protocols is restricted to only periods of rest between contractions by a gating algorithm. The gating algorithm, described more fully in previous publications from this lab, uses analog output from the dynamometer foot plate, with signal intensity dependence on footplate position, to limit data collection to the time period between contractions[20]. When the foot

plate is at rest position the dynamometer analog signal is below a certain threshold and data collection is permitted. When the foot plate is moved through the contraction range, the amplitude of the signal passes a threshold (set very close to the resting position amplitude) and signals the DCS to halt data collection. Without the DCS sending a TTL signal to the Imagent the FD-NIRS remains on standby, following the return of dynamometer output to below threshold levels the DCS/ISS data collection cycle resumes. By default a single data point from each device is collected and then the cycle is halted to ensure that the next contraction does not induce artifact, thus data collection only resumes upon receipt of the return to rest trigger.

The processing and examination of data often requires the use of filters in order to clearly display trends and behaviors. The only filter employed during the extent of this research was a simple convolution (moving average) filter with a window size of 10 or 20 data points, depending on the sampling rate. This filter was chosen because it has a much less intrusive effect on data behavior, particularly during the rapid onset and end exercise periods of these protocols than does a Butterworth or equivalent filter. The convolution filter manages to obtain the central tendency while still retaining the instability of the original data set.

Student t-tests were used to analyze difference in time point means for all tables and values in this thesis. The means used for these statistical analyses are from overlaying time series and taking the mean of the entire time series thus great importance was placed on the proper timing and synchronization of multiple

systems of data collection. On some occasions, where a precise overlapping of data is not possible, the region of interest is selected manually for each period and subject, so that the period involved can be precisely controlled/matched between subjects. An example of this is given for the strain gauge data sets which could not, due to technical reasons (the two were measured on separate computers without TTL links), be aligned exactly with DCS data frames and so venous occlusion periods were selected manually for calculation based upon the time point where volume began to increase and ended where the linear behavior ended.

CHAPTER 3: BASELINE HEMODYNAMIC ASSESSMENT AND STABILIZATION

Blood flow baseline study protocols were begun by observing baseline stability using DCS optical probe on calf muscles in the lower limb (Protocol #1, see Chapter 3.1.1). After a review of literature and previous research in our lab narrowed likely effects to be due to contact probes on muscle tissue, whereupon a redesign of the optical probe pad (see Chapter 3.1.2) and attachment methodology (see Chapter 3.1.3). Among these factors, local heating could possibly play a role for the contact measurements since the probe pad covers the skin and is made up of highly insulating materials. Furthermore, the contact probe is covered by layers of surgical tape and compression bandage which also insulate the limb. If a local heating were taking place it would possibly increase skin and muscle blood flow[66-68]. Another possible flow modulator would be the application of circumferential pressure due to the use of elastic bandage and wrapping tape around the limb[56, 69-73]. Such wrapping was desired to secure the optical probe due to the use of thick silicon rubber pads and bundled fibers and resulted in a somewhat heavy optical probe. Taping and wrapping the probe were the default methods of attaching DCS optical probes to tissue in all previous studies.

A second baseline measurement, from the same subjects and in the same calf muscle indicated success in removing the predominant factor related to increased blood flow (Protocol #2, see Chapter 3.1.4).

A confirmation protocol was then performed in the forearm flexor muscles (Protocol #3, see Chapter 3.1.5), as the effect had been previously observed in

both lower and upper limbs and a body of data existed against which we could compare. This confirmation demonstrated a great increase in measurement stability for the redesigned probe and showed that increases in rBF were, most likely, due to predominantly local factors. Lastly the baseline study was concluded by performing a repeat of the forearm flexor experiment using a subset of those subjects and removing elastic bandaging from the protocol. Lack of increase in the measured rBF for both arms suggested that elastic bandaging is most likely to be solely responsible for previous baseline shifts whereas probe pad contact is not a factor.

3.1 DCS Baseline Study Experimental Protocols

3.1.1 Protocol #1: Gastrocnemius Baseline Stability Evaluation

Before determining potential flow modulators and their effects it was necessary to confirm the baseline shift through an extended *in vivo* resting protocol in the muscle tissue of interest, the gastrocnemius. Examination of resting muscle blood flow shift with DCS had never been done, making this a novel measurement.

For the first experiment, 6 subjects (3 males and 3 females) were recruited and their consent obtained via University of Kentucky Institutional Review Board (IRB) approved forms. Subjects were instructed to lie supine and relax for at least 5 minutes prior to collection of data to allow flow to stabilize. The DCS optical probe was secured to the limb as described in previous publications[15, 16, 28, 31, 44]. Briefly, the attachment protocol was to disinfect and clean the probe pad

and probe site with alcohol prep. The probe was then placed in contact with the subject's medial gastrocnemius (location determined as the region of greatest contraction during a plantar flexion) and lightly held by cotton surgical tape and more firmly secured by use of an elastic bandage (ACE^{Tm}) as illustrated in Figure 9. In this way external room light was reduced and probe position secured, even during subject movements. It was deemed appropriate, as room lights were dimmed to assist in preventing signal contamination, to engage subjects during the experiment to prevent them from dosing or entering pre sleep states of consciousness which can have substantial effects on pulse rate and blood pressure[74, 75]. These conversations were of a generally neutral nature to keep physio-emotional responses at a minimum whilst holding subject attention. Retaining subject consciousness proved to be non trivial as we noted a distinct tendency toward sleep due to the combination of low light, and highly static supine bed rest for extended periods.

Baseline measurement duration was set at 40 minutes and the subjects instructed to remain as still as possible, since DCS signals and the hemodynamics of musculature in general are exquisitely sensitive to motion. Duration of baseline measurement was extended to 40 minutes for two main reasons: first, baseline shifts appeared to be a result of prolonged drift that was observed in protocols lasting up to 40 minutes (with similar durations planned for future studies) and therefore the presence/extent of any shift should be verified under similar time courses. Second, no such extended evaluation of resting muscle blood flow had been performed so determining the stability of passive muscle

flow was relevant to understanding how meaningful a baseline measurement could be in the first place.

A CW-DCS flow-oximeter system (see Figure 7), detailed in Chapter 1.6, was used in this study. The CW-DCS flow-oximeter makes use of two wavelengths (785 and 854 nm) of long coherence laser light for the source and uses 4 bundled detector fibers at a single S-D separation of 2.5 cm as illustrated in Figure 7b. This relatively large separation used was to ensure that the optical path was predominantly inside muscle tissue and to minimize surface layer artifact. This assumption is generally safe as all of our subjects had adipose tissue thicknesses (ATT) of less than 8 mm over the gastrocnemius muscles[10, 72, 90].

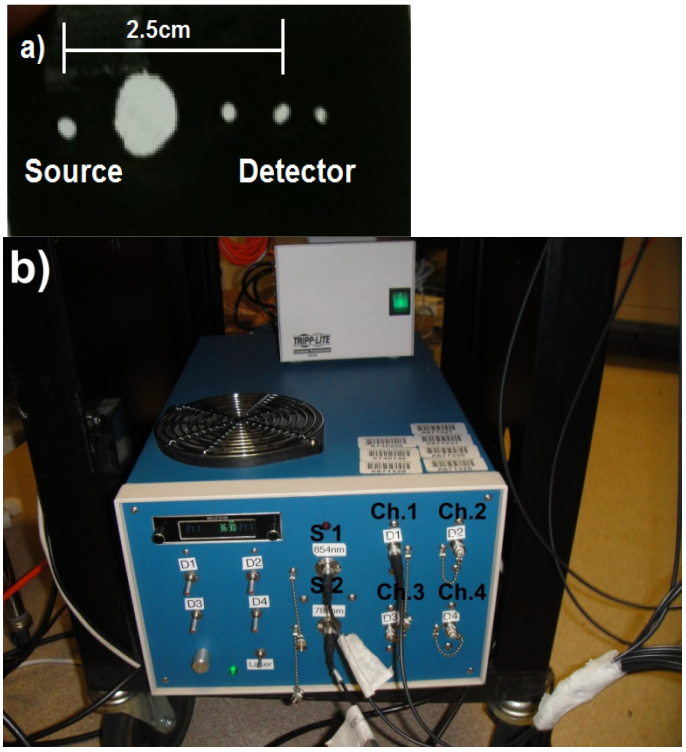

Figure 7. Fiber-Optic Probe and DCS Flow-Oximeter

The probe pad (a) consists of a simple foam block of dimensions 6×3×1 cm. The foam is black and therefore an excellent isolator of probe signal from room light. The material is lightweight and of intermediate stiffness, resisting curvature around the limb but conforming after application of tape. Probe fibers are held firmly in perpendicular to the skin (not shown). Multiple holes exist for adjustment of S-D separation. The DCS flow-oximeter (b) employs the 2 source, 4 channel detector layout. Black coating is necessary for fiber optics to reduce external noise. The 4 measured autocorrelation curves for each source are averaged to produce a single relative flow calculation.

The bundled detector fibers allowed for a higher data quality (SNR) compared to a single fiber since the flow and oxygenation values can be measured in quadrature for a single location simultaneously and averaged. This eliminated some of the random noise and allowed for better quality data even in subjects with low intensity signal (highly absorbing tissues). A sampling rate of 0.5 Hz was used with one second of autocorrelation averaging for each source wavelength. Flow values at both wavelengths were then averaged. After this averaging of

flow between sources and calculation of relative hemoglobin concentration changes from their intensities, a 10-point window convolution filter was applied to further reduce high frequency noise and produce a smooth curve that shows the central tendency of the raw data. Only raw data were used for statistical analysis however, as filtering/sampling and other such data processing methods can have effects on statistical power[76].

In addition to end point mean comparisons, extended baseline data stability was evaluated with linear regression. It was determined empirically that most baseline shifts tended to be pronounced after 20-40 minutes. Observed short duration bidirectional fluctuations (occurring over 2-3 minutes and being 10-20% rBF in magnitude) made mean comparisons non-optimal for assessing baseline stability. This is because the peak of a short duration fluctuation at time point could be present during the initial 2-minute mean period with the trough of a fluctuation occurring during the end time period (or vice versa). This could render the time point means statistically different while overall behavior suggested no real variation over the long term. Rather than imposing harsh filters to remove these physiological variations, a linear regression model to assess long term baseline stability was used. Typical variation, i.e. standard deviation, of raw data ranges between 15% and 30%, meaning at any time point a particular datum could be, at worst, between 70% and 130% baseline. A linear model for stability entailed applying a linear fit to the data and evaluating a slope of greater than or equal to 0.7 (rBF/min) as a baseline shifted measurement. For a justification of the model and slope threshold of 0.7, see the discussion in Chapter 3.3.1.

3.1.2 Optical Probe Design Adjustments

Following the results of the first in-vivo DCS stability evaluation, we determined that some aspect of the measurement was causing rBF to drift upward (as shown in Chapter 3.1.1). This necessitated an investigation into possible causes via a search of literature involving limb blood flow modulators. As mentioned in Chapter 1, the two major suspected flow modulators were temperature and pressure. Without the use of precise and somewhat invasive probes, temperature and pressure data within the muscle were unavailable to us. The lack of suitable measurement equipment for intramuscular/surface pressure meant that we lacked a definitive way to measure either parameter, although the use of the elastic bandage and tape virtually guaranteed that there were pressures being applied to the limb, and that those pressures were probably sufficient to affect local blood flow[56, 69-73]. Without hard data on either temperature or pressure we decided that the probe/attachment protocol should be designed to minimize the contributions from both parameters. Toward that end, the first line of research was to design a probe pad which would be structurally robust as to maintain source detector separations, provide a stable platform for optical fiber insertion and constancy of optical geometry, and be easily and reliably attached to the limb for repeatable measurements with the knowledge that such qualities must be evident even during possibly strenuous exercise protocols. These necessary qualities were of foremost importance as these are the conditions for getting adequate signals and quality data with the minimization of probe pad area (for

less insulation) and adhesive use, not to mention the removal of elastic bandage, being crucial to eliminate possible flow perturbation.

It was determined that, based on several iterations of probe pad design, leaving the area between the source and detector uncovered might reduce the temperature effects as probe pad/tape insulation were minimized. By using a three sided frame shape it was hoped that the attachment would be of sufficient integrity as to be useful during exercise protocols but without the degree of taping/pressure application as were present in the original probe (see Figure 8). Stability of probe position and optical fiber geometry was achieved with the use of braided wire struts. This design could maintain source detector separation but the strut, while strong in the requisite source to detector axis, was flexible enough to bend plastically so that no additional force pulling the fiber tips away from the skin was present allowing the probe to match even the relatively severe curvatures of the forearm.

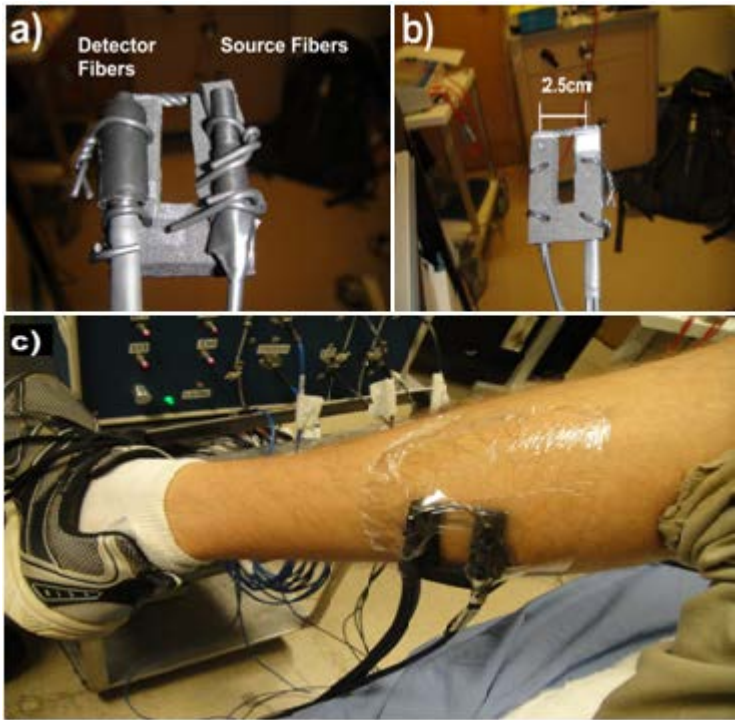

Figure 8. Redesigned Probe Pad and Attachment to Limb

(a) The fiber-optic probe held in place by the twist wires shown fiber tip length differences can be adjusted to fit with spacers made of the same foam as the probe pad. (b) Probe pad shape allows for a single S-D separation fiber arrangement. A separate probe pad would be necessary for each distance as necessary to measure a particular depth. Wires secure the probe pad and fibers to preserve the original orientation throughout the experiment. Tissue interface side illustrates the diffuser, which covers the source fibers as discussed, and the detector fibers held flush to the probe surface. (c) Shows the entire probe as it would be attached during protocols. The tegaderm film has been vented over the open region of the pad to allow heat convection. Not shown is that the fibers would be secured to remove their weight from the tissue surface and reduce amount/strength of adhesive used to secure the probe.

An additional challenge arose in the form of isolated incidents of source laser burning on the skin, despite the low power emission. Such burning was hypothesized to be due to slight imperfections of the source fibers. In order to be assured that no subjects would be burned, an optical diffuser was constructed from Teflon. This polymer has a very low attenuation of NIR light and so does not dramatically weaken the signal intensity of the source light but does broaden the spot size of the source. The diffuser was created by shaving a thin block of

Teflon until it was sufficiently thin. This thin (< 0.25 mm, as measured by digital caliper) layer of Teflon prevents source fiber/tissue surface interactions without significantly attenuating light nor decorrelating the light as the intensity and flow signal are not apparently affected. More information about Teflon diffusers and their effects on DCS may be found in the following citation [22]. The probe pad now had all the qualities we were looking for in a DCS standalone system. Attention now was turned to the problem of how to attach the probe securely without applying excessive pressure.

3.1.3 Optical Probe Attachment Revision

After some investigation it was decided that a better alternative for surgical tape adhesive was Tegaderm thin film dressing (3M^{Tm}) which allowed heat to escape from the skin, had slightly better tack, and allowed the fiber/probe contact to be visually observed during the experiment (refer to Figure 8c). The Tegaderm adhesive proved effective and could be cut to allow a window over the source detector area to vent air. Attachment of the optical probe to the limb by use of a 4x6 inch piece of Tegaderm thin film with a vent over the middle of the detection path allows better convection of trapped heat away from the skin and no elastic bandage was employed to minimize pressure application to the muscle tissue. The weakness of this set up is that it is more prone to room light contamination and so care must be taken to turn off room lights. Surgical tape may be used in lieu of Tegaderm but should not be wrapped around the limb. Experimentally, a 7 inch strip laid along the tibial axis and a 4 inch strip circumferentially proved to be sufficient to hold the probe, as detected intensities were stable and no direct

source to detector signal contamination could be discerned. Room lighting was turned off for all baseline measurements and did not play constitute an optical signal variable for this study but bears consideration for future experiments or clinical applications where room lights may be required.

3.1.4 Protocol #2: *In-Vivo* DCS Gastrocnemius Baseline Stabilization

Probe/protocol redesign to remove DCS flow baseline shift was confirmed by performing a 40-minute supine baseline test in 6 young healthy controls. The redesigned optical probe (detailed in Chapter 3.1.2) was secured to the medial gastrocnemius using surgical tape adhesive (as described in Chapter 3.1.3). The same DCS flow-oximeter system was employed as described in Chapter 3.1.2 (Figure 8b) but with the probe design employed in Figure 9. Other than probe pad and attachment no changes in procedure or data collection methodology were made. Long term stability of data was evaluated by use of a linear regression and slope examination. The slope threshold of 0.7 (refer to Chapter 3.1.1) serves as a rubric for making judgments, in addition to end point mean comparisons, on baseline stability.

3.1.5 Protocol #3: *In-Vivo* Forearm Baseline Stabilization and Examination of Baseline Shift Origin

Following gastrocnemius measurements, we performed confirmation tests in the forearm flexor muscles, in deference to the familiarity of our lab with measuring this muscle group and fairly large subject populations of responses against which to compare. We also attempted to identify the predominant factor

causing baseline shifts using a subset of the forearm flexor subjects. This baseline experimental protocol was designed using a concurrent forearm flexor measurement protocol in which the right arm rBF was observed using the redesigned probe/protocol and the left arm rBF using the original probe/protocol (Figure 9). To ensure that the measurement was truly concurrent we used two detector channels per probe with our 4-Channel 2-wavelength DCS flow oximeter. This reduced the number of detector signals averaged, which led to lower SNR, but guaranteed synchronicity in data collection and improved sampling rates. In addition to the optical probes, a finger plethysmograph (Portapres, FMS Inc., Netherlands) was used to observe systemic pulse rate and blood pressure to determine global hemodynamic influence on local measurements.

Ten young healthy control subjects were measured in supine for 40 minutes, as detailed before. Probe position was kept consistent between subjects by placing the probe over the region of maximum contraction of the forearm flexors as determined by having subjects clench their fists. The entire protocol layout can be seen in Figure 10.

After the completion of the 10 subject measurements, a subset (n = 4) of these subjects repeated the measurement (on a different day but under identical conditions) with the exception that the original protocol arm (left) did not employ elastic bandage. This was done to examine whether removing the pressure component of the original probe would reduce baseline shift, allowing us to judge

whether or not probe pad insulation or pressure application was dominant in inducing flow alterations (Figure 10).

Figure 9. Original Optical Probe Position and Attachment

Attachment was performed as depicted with tape to initially hold the probe (left), elastic bandage to secure this position, and surgical tape to maintain elastic bandage pressure (right). The location was based upon the maximum contraction response for clenched hands/flexed wrists. For gastrocnemius measurements the probe was positioned based upon the greatest contraction during plantar flexion in the medial gastrocnemius.

Figure 10. Concurrent Baseline Protocol Set-up

Subjects are positioned on a bed with head and forearms comfortably resting on padding/pillows. Forearms are slightly elevated to reduce venous pooling associated with extended stationary positions. Placing the hand at heart level also is required for accurate finger plethysmography pressure and pulse rate data. Room lights are turned off and the subject is asked to remain at resting supine for 5 minutes prior to start of data collection. 1) refers to the original probe and attachment protocol on the left arm, 2) refers to the newly designed probe/protocol employed on the right arm, and 3) indicates the finger plethysmography instrument.

3.2 DCS Baseline Study Results

3.2.1 Protocol #1: *In-vivo* DCS Baseline Gastrocnemius Stability Evaluation

Relative blood flow significantly ($p < 0.05$) increased throughout the protocol (refer to Chapter 3.1.1 for protocol details) from the first two minutes of baseline to the final two minutes of the experiment for all but one subject (see Table 1). The group mean of the final 2-minute value was 163.5 ± 5.9%, which represented a tendency towards flow increase (see Table 1, Figure 11). The significance of difference was determined via Student t-tests for the two groups (initial 2 minutes of data vs. final 2 minutes). Subject 6 data was discarded as the detected light intensity was only 10-15 KHz and the resulting calculated relative flow, while in rough agreement with other subjects' trends, was laden with noise (standard deviations of greater than 90%). Only one subject (Subject 1) had a trend uncharacteristic of the others. The change for this subject was also significant but somewhat anomalous in that the trend was for decrease. The net result is that the group mean response is higher than baseline after 40-minute supine bed rest.

Table 1. Baseline Measurement Means and Fitting Slope

Subject	Initial mean rBF (2 minutes)	Final mean rBF (2 minutes)	Linear Fit Slope
1	100.0±23.6	87.9±52.6	-0.21
2	108.0±22.8	208.2±32.7*	3.41
3	105.1±9.4	217.8±15.4*	4.56
4	102.0±22.3	168.9±27.5*	2.39
5	99.6±6.0	122.8±14.1*	0.62
6	N/A	N/A	N/A
Group Mean	102.9±3.9	161.1±5.9*	1.39

Significance between data sets is denoted with an *.

A linear fit of time series data showed a baseline shift that was in a distinctly positive direction (Figure 11). While responses varied substantially between subjects the increasing trend is consistent. For subjects with obvious elevations in baseline, the statistical mean tests are sufficient to describe data, however, given the somewhat large standard deviations associated with individual subjects for particular time points, as discussed in Chapter 3.1.1, data stability in non-obvious cases would be difficult to evaluate without resorting to unrealistically large averaging times (5-10 minutes) and would still be greatly influenced by outliers while linear models would be more insulated against such disturbances.

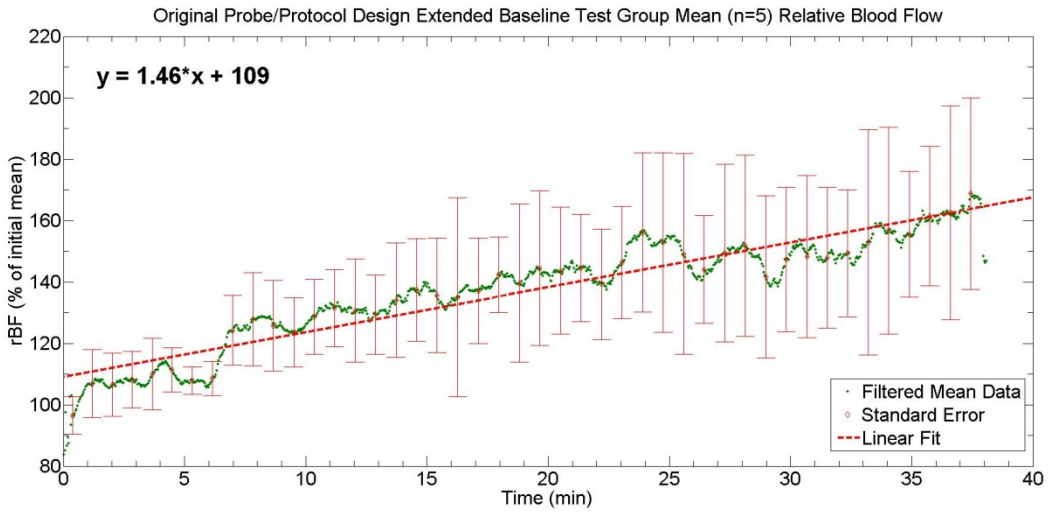

Figure 11. Group Mean (n = 5) Relative Flow with Linear Fit

Filtered mean data (green dots) demonstrate the central tendency of the data via a 10 point convolution filter while standard error (red bars) demonstrates difference between subjects and clearly shows an increase in flow during the baseline.

End value data for the old probe were significantly ($p < 0.05$) greater than baseline, and were increasing at a substantially greater (slope = 1.46) rate than the

0.7 model threshold for sustained elevation (Figure 11). For more explanation of the linear fit slope threshold see the discussion in Chapter 3.3.1.

3.2.2 Protocol: #2: *In-Vivo* DCS Gastrocnemius Baseline Stabilization

The typical flow response for these same 6 subjects (see Chapter 3.2.1) oscillated around the baseline value (Figure 12) throughout the protocol with the revised probe (See Chapter 3.1.4) but some subjects exhibited a marked decrease (15-20%) in flow (Figure 13).

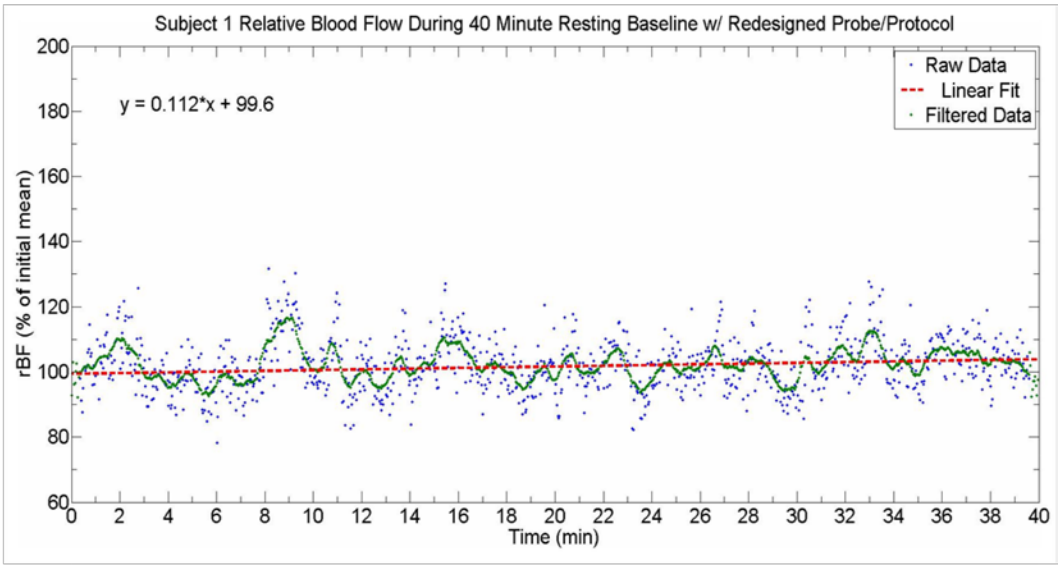

Figure 12. Typical Subject Response with Redesigned Probe: Stable Blood Flow

The most typical response to baseline protocol with the revised probe is a general stability around 100% with a minimal difference between end and beginning relative blood flow. The blood flow naturally fluctuates around this baseline value highlighting the variable nature of microvascular flow. A linear fit of the data shows an intercept close to 100% supporting the stability of the data and the slope = 0.112 is much less than the empirical 0.7 threshold for a shift.

The decreases in flow (Figure 13) observed are likely attributed to the effect of prolonged bed rest, for a justification of this decrease see Chapter 3.3.3. Systemic indicators such as pulse and mean arterial pressure were considered to be

important to facilitate a better understanding of these trends and were measured in later studies.

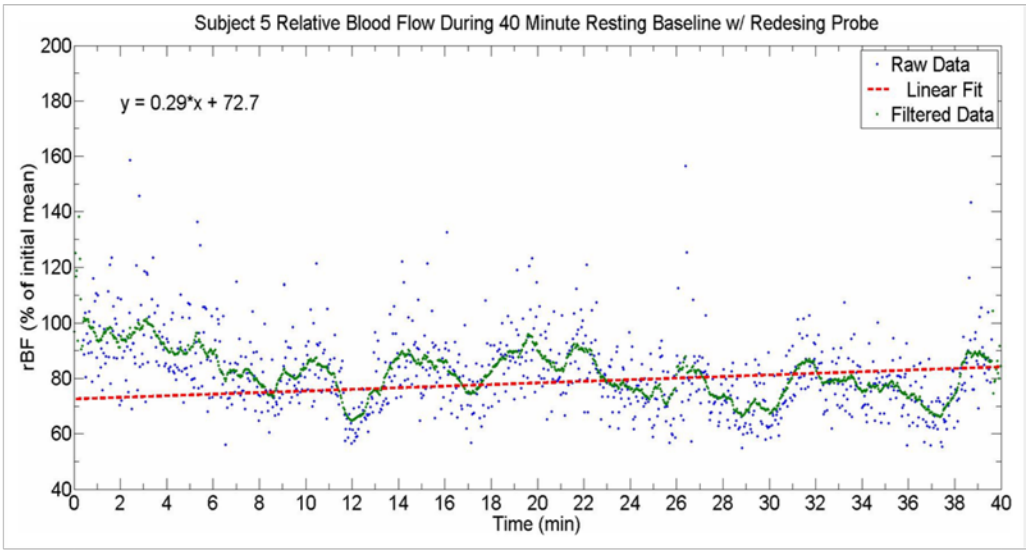

Figure 13. Typical Subject Response with Redesigned Probe: Decreased Blood Flow

The second typical response is that of a slight decrease (20%) from baseline. The linear fit of data has a positive slope but has a substantially lower intercept which is indicative of the stability of the latter part of the data following an initial 10 minutes period of decrease. This highlights the weakness of using a linear model to describe nonlinear systems and would also indicate that the some subjects can experience a slightly stressed state for longer than 10 minutes even at rest and following at least 5 minutes of supine experimental set up.

Group mean response was an oscillatory and slightly decreasing time course with end mean values comparable to the initial baseline value (Figure 14). Despite the degree of variation of blood flow in time for each subject, the mean of each subject showed remarkable stability which supports our hypothesis that the removal of insulation and pressure application from probe design stabilizes the system (Figure 14).

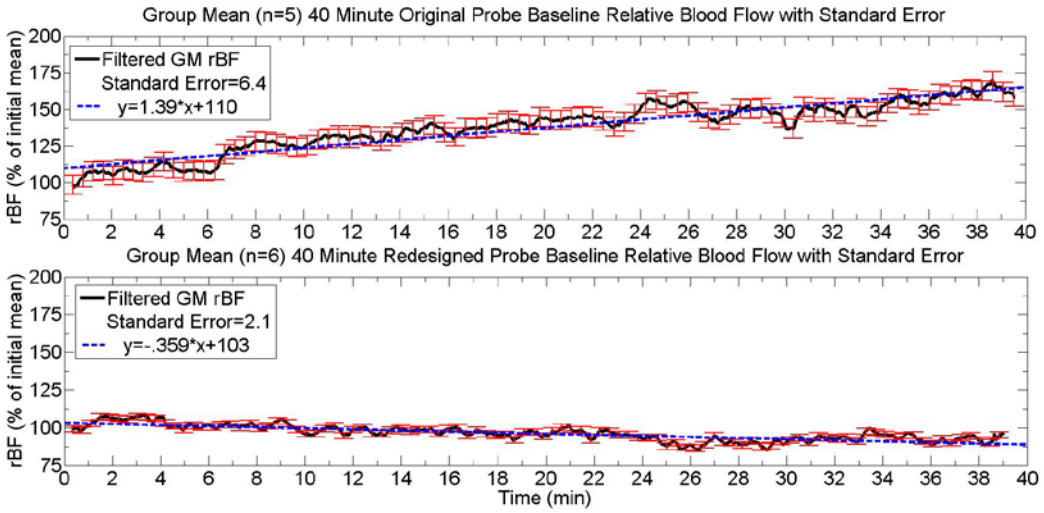

Figure 14. Group Mean Comparison of Original (n = 5) and Redesign (n = 6) Gastrocnemius Baselines

The redesigned probe (bottom) has a final mean value (final 3 minutes) of 93.3% of baseline compared to the initial (3 minutes again) value of 102.5 and a linear fit slope of -0.356 which is less than the 0.7 value attributed to describe a baseline shift. This is compared to the initial (3 min) mean of 102.9 and final (3 min) mean of 163.5 for the previous probe (top) and its obvious shift of 1.46, which is double the empirical threshold of 0.7.

Statistical analysis of these data sets showed that the initial values of the group means for either probe (first 2 minutes) was not significantly different meaning that both studies had a stable initial relative blood flow and that the difference between end values would then reflect the long term effects of the probes/protocol on relative blood flow. The same analysis, applied to the final 2 minutes of each group mean time course, showed significant difference between the two with the redesigned probe having a value significantly ($p < 0.05$) lower than both the initial 2 minutes of the measurement and the final 2 minutes of the original probe baseline. The redesigned probe data stability (as assessed by linear fit), is much increased compared to the previous probe design with a reduced slope and magnitude of difference in end points.

These results support the hypothesis that the baseline shift was induced by our measurement protocol and that the redesign (see Chapter 3.1.2 and 3.1.3) of said protocol was successful in reducing the effect.

Table 2 summarizes the individual and group mean initial and final 2-minute time period means as well as which ones are significant and the linear fit slope of each.

Table 2. Probe Redesign Summary for Gastrocnemius Baseline

Subject	Revised Probe Initial mean rBF (2 minutes)	Revised Probe Final mean rBF (2 minutes)	Linear Fit Slope
1	102.3±6.5	101.7±5.5	0.11
2	103.5±7.5	101.5±8.1	-0.17
3	106.1±12.8	65.7±15.0*	-0.55
4	104.2±22.6	102.8±16.4	0.13
5	97.8±14.3	85.6±13.3*	-0.39
6	100.9±7.1	102.8±10.6	0.20
Group Mean	102.5±2.5	93.3±1.7*	-0.36

The smaller changes in baseline over the 40 minute duration and the linear fit slope of values (magnitude as well as direction) demonstrate a marked improvement of measurement stability in vivo for the redesigned protocol. Standard deviations are less than those of the previous probe which suggests an improvement in the S/N ratio for these data sets.

3.2.3 Protocol #3: *In-Vivo* DCS Forearm Baseline Stabilization and Examination of Baseline Shift Origin

The use of relatively larger subject population (n = 10) and concurrent measurements enabled us to determine a significant difference ($p < 0.05$) between local hemodynamics in both limbs during the 40-minute baseline protocol in forearms (see Chapter 3.1.5). All subjects had significant changes in blood flow compared to the baseline but only 3 had that change in the increasing direction.

The remainder exhibited a decrease in final 2-minute rBF that ranged from 10 to 40%.

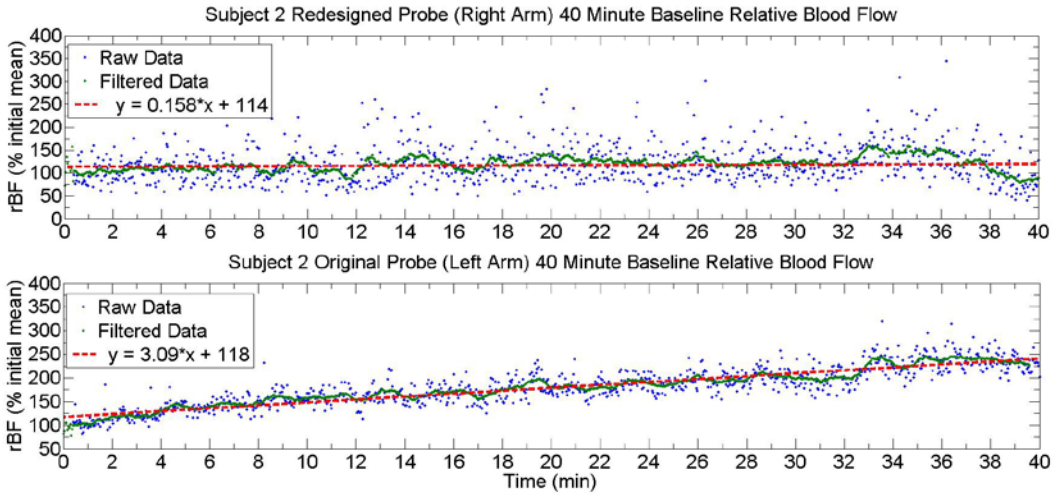

Figure 15. Typical Subject Contra-Lateral Relative Flow

Most subjects showed a significant decrease in rBF with a linear fit far below the 0.7 threshold for the right arm with redesigned probe (top panel). This is compared to the obviously increasing flow (mean 200%) in left arm with original probe (bottom panel), and a linear fit triple that of the threshold (mean slope: 2.26).

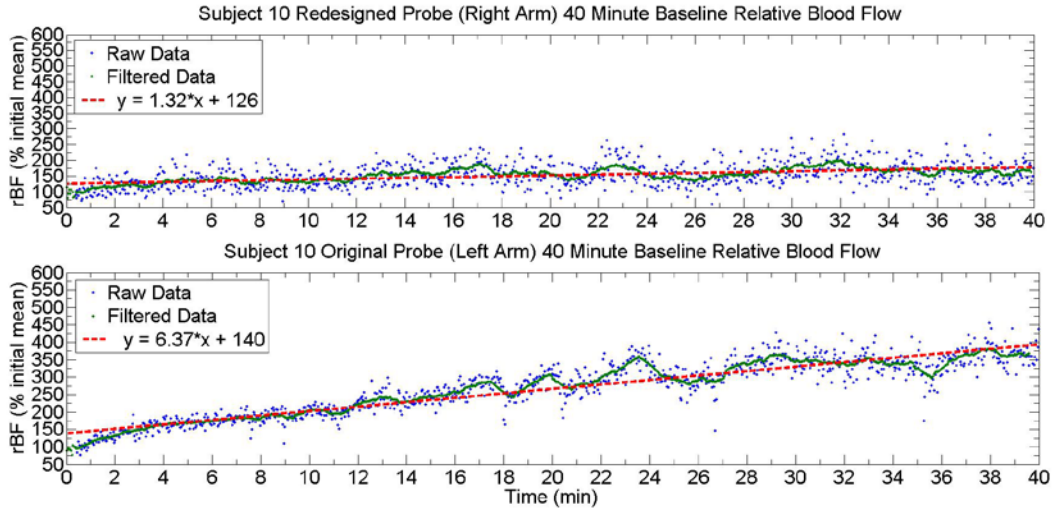

Figure 16. Atypical Subject Contra-Lateral Relative Flow

Of the three subjects this one had the most extreme increased blood flow with values approaching those expected during exercise. The left arm blood flow (original probe) increases to 370% of baseline while the redesigned probe has a still significant 163% increase. Such dramatic increases may be due to the involvement of systemic parameters.

The two distinct response trends are best shown in Figures 15 and 16, the atypical response (Figure 16) is characterized by a very large increase in blood flow over the duration of measurement, increasing to 370% of the initial value in the previous protocol arm and 160% in the redesigned probe arm. The expected response (Figure 15) showed an increase in the old probe arm from 100 to 200% of baseline and a decrease in the new probe arm of 100 to 75% of baseline. Trends of increase in previous probe arm rBF and a much reduced increase in redesigned probe arm, with the same systemic cardiovascular environment, indicate that the baseline shift had been dramatically reduced and was caused by local factors. Linear fits for each subject are characteristic for baseline shifts in all previous probe arms but not for new probe arms, except for those atypical response subjects (Table 3).

Table 3. Summary of Relative Flow Data Baseline Means for Contra-Lateral Forearm Measurement

Subject	Previous Probe Initial mean rBF (2 minutes)	Previous Probe Final mean rBF (2 minutes)	Linear Fit Slope
1	96.8±24.6	142.1±27.8*	1.18
2	105.1±16.7	232.2±17.8*	3.09
3	108.1±14.7	145.5±23.4*	1.06
4	95.5±42.3	124.2±15.4*	0.72
5	106.0±13.1	149.5±34.2*	1.10
6	102.2±30.9	224.4±21.6*	3.12
7	95.4±15.1	134.3±13.1*	1.04
8	100.1±11.1	195.4±25.5*	2.28
9	97.0±13.1	174.3±20.7*	2.16
10	111.2±16.4	367.3±29.6*	6.37
Group Mean	101.7±1.8	193.6±5.6*	2.26
Subject	**Revised Probe Initial mean rBF (2 minutes)**	**Revised Probe Final mean rBF (2 minutes)**	**Linear Fit Slope**
1	98.6±15.7	94.2±22.6	-0.30
2	102.9±25.9	89.2±34.9	0.16
3	102.9±8.0	92.6±14.1*	-0.03
4	100.2±24.2	80.2±19.1*	-0.84
5	101.2±11.6	89.3±12.5	-0.36
6	110.4±18.3	184.0±21.2*	1.11
7	98.4±12.9	69.2±10.9*	-1.13
8	99.0±16.2	60.8±11.1*	-0.99
9	105.6±22.2	228.3±46.7*	3.37
10	106.9±22.8	163.8±31.6*	1.32
Group Mean	102.1±1.8	119.1±3.4*	0.28

Significant change in baseline flow ($p < 0.05$) is noted for all subjects and group means and this difference applies both to final 2 minutes vs. initial 2 minutes and to difference between final 2minutes for each probe. Note the larger standard deviations for these data as only two detectors were averaged, which supports the use of a multiple detector bundle fiber device for better data quality.

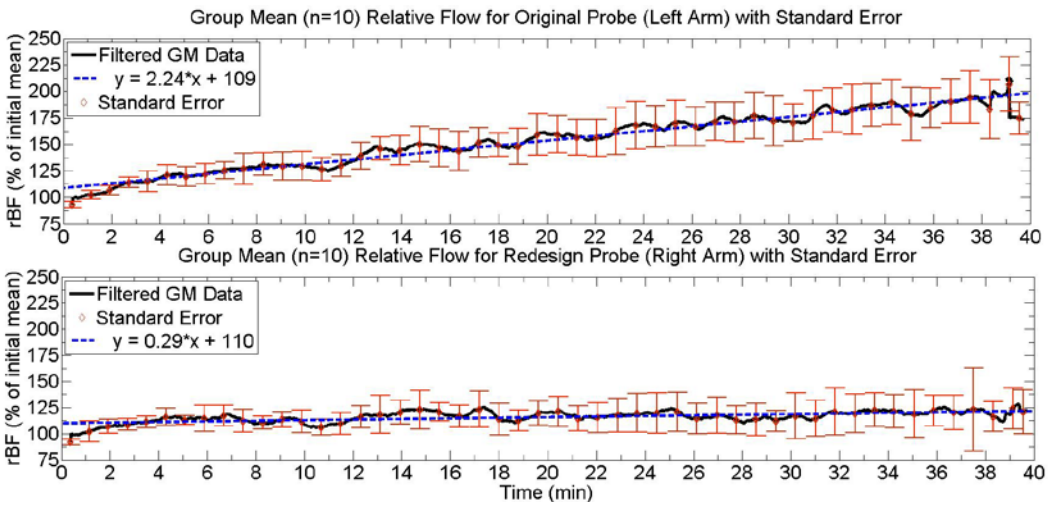

Figure 17. Group Mean (n = 10) Contra-Lateral rBF with Linear Fitting and Standard Error

The original probe design shows a steadily increasing trend that is consistent with gastrocnemius baseline measurements but generally higher (slope = 2.24 in arm compared to slope = 1.39 in leg) with an overall increase of 199.1% (arm) compared to 163% in leg. The redesigned probe shows a behavior consistent with leg measurements. Redesign (small linear fit) but has a still significant increase due mostly to a short onset increase. This increase is almost certainly due to the large, rapid increase observed in the 3 anomalous subjects, as depicted in Figure 17, which would have skewed the mean upwards initially but was offset by general trends of decrease for later time periods. Even so, the end result is a minor (117.9%) elevation over 40 minutes and a linear fit which suggests stable baseline.

Group mean time series show greatly reduced baseline drift in redesigned arm with a linear fit of 0.29 and final value of 119% of baseline while relative flow in the previous probe site rises dramatically to a mean 193% of baseline and has a mean linear fit of 2.24 (Figure 17). Statistically the two arms had a non significant difference in initial 2 minutes of baseline flow ($p > 0.05$) and a significant difference in final baseline flow both between probes and initial 2 minutes values for each probe.

Systemic data trends show that subject systemic parameters may have played a role in anomalous flow responses as both MAP and pulse rate increased for the

subjects experiencing greatest contra-lateral flow increase (Table 3 and 4, Figure 17 and 19).

Table 4. Forearm Study Summary of Systemic Parameter Means

Subject	Subject Initial 2 mins MAP (mmHg)	Subject Final 2 mins MAP (mmHg)	Subject Initial 2 mins Pulse Rate	Subject Final 2 mins Pulse Rate
1	64.0±4.7	64.8±4.7*	60.5±10.0	54.9±2.0*
2	73.0±4.2	88.0±5.2*	77.2±6.2	62.5±4.9*
3	99.2±6.5	~103	82.9±5.1	84.0±3.9
4	~62	63.0±3.6	82.8±3.9	72.2±6.1*
5	69.5±3.3	81.5±2.0*	60.4±4.1	58.5±4.1
6	69.3±9.1	76.1±6.3*	71.2±9.8	61.7±5.2*
7	59.0±2.9	73.3±4.1*	64.6±5.2	60.5±3.1*
8	76.0±2.9	88.0±2.2*	59.0±2.8	56.4±2.7
9	84.9±9.0	107.9±6.3*	71.6±6.7	70.8±7.1
10	65.3±3.4	87.5±5.7*	65.3±7.4	75.2±4.6*
Group Mean	73.3±0.7	82.1±0.6*	69.7±0.8	65.7±0.5*

Significant difference from initial baseline (denoted *) to end baseline is found in most subjects but MAP and pulse rate often differ in direction. Pulse rate decreases, as expected in resting subjects, and MAP increases although it is not well understood why. Some literature indicates that compression of the limbs can induce reflexive MAP increase[77]. ~ indicate finger plethysmograph recording errors which produced gaps in data collection for these regions, the mean was taken from available data within this time period.

Group MAP response shows an increase from 73.3 to 82.1 mmHg while pulse rate decreases from 69.7 to 65.7 BPM. Group mean values for both MAP and pulse rate have significant changes in final vs. initial two minute mean values with MAP increasing and pulse rate decreasing. These changes are consistent with a body of literature that indicates increased vagal tone during supine postures can produce increased blood pressure and decreased pulse rate[78-80].

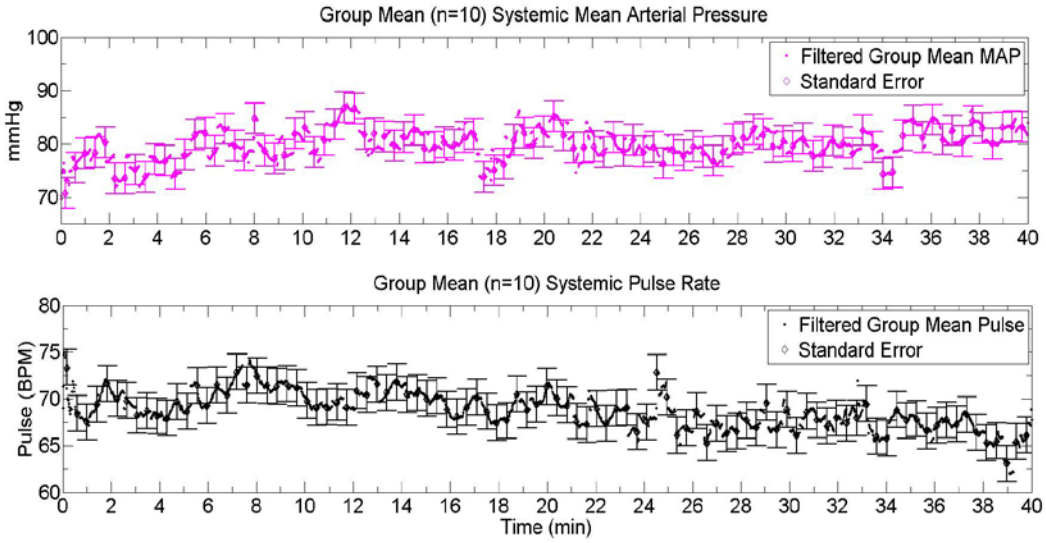

Figure 18. Group Mean (n = 10) Time Series for Systemic Parameters

Despite a high degree of variation within each time series the overall behavior of systemic group means is somewhat stable with a slight but significant ($p < 0.05$) decrease in pulse rate and a similar magnitude significant increase in MAP.

Results from 4 subjects, elastic-free, sub groups show similarly stable blood flow response with an absence of linear fits that meet the standard of baseline shift occurrence (Table 5, Figure 19). Initial two minutes of baseline rBF held at 102.1% and 101.2% for both arms (the former being original probe, the latter being the redesigned probe) and both demonstrated a significant ($p < 0.05$) decrease to 89.7% and 93.8% of baseline respectively. Mean linear fits of rBF are likewise indicative of stability with slope values of -0.32 and -0.29 for previous and redesigned probe (Table 5). Changes in systemic parameters indicate that overall pulse rate is decreasing during the protocol while MAP increases. These effects seem consistent with previous 10 subject forearm observations and produce a non-increasing, more stable rBF (Tables 4 and 6, Figures 17-19).

Table 5. Summary of 4-Subject Sub-Group Relative Flow without Compression Bandage

Subject	Original Probe Initial mean rBF (2 minutes)	Original Probe Final mean rBF (2 minutes)	Linear Fit Slope
1	105.8±14.9	124.5±24.5*	0.53
2	103.8±28.9	68.8±14.8*	-0.98
3	97.6±11.9	78.6±14.9*	-0.57
4	98.7±10.3	87.0±7.6*	-0.31
Group Mean	101.5±4.6	89.7±5.4*	-0.32
Subject	**Redesigned Probe Initial mean rBF (2minutes)**	**Redesigned Probe Final mean rBF (2minutes)**	**Linear Fit Slope**
1	98.9±31.8	104.6±50.5	-0.30
2	106.2±38.1	107.2±23.6	0.14
3	95.1±11.3	73.4±10.2*	-0.10
4	103.5±13.9	89.9±15.8*	-0.65
Group Mean	100.9±5.7	93.8±7.5*	-0.29

No subject had initial 2 minutes flow significantly different ($p > 0.05$) than 100%. Most but not all had significantly ($p < 0.05$) lower final 2 minute rBF and multiple mean comparison. All linear fits had slope < 0.7 and this applied to magnitude as for all but one subject.

Table 6. Sub-Group Systemic Parameter Mean Summary

Subject	Subject Initial 2 mins MAP (mmHg)	Subject Final 2 mins MAP (mmHg)	Subject Initial 2 mins Pulse Rate	Subject Final 2 mins Pulse Rate
1	83.1±9.5	78.7±5.6*	78.6±8.4	62.1±10.0*
2	58.6±3.3	76.8±2.5*	64.5±4.5	71.9±5.7*
3	89.1±4.7	113.5±5.3*	67.0±8.2	71.1±8.7*
4	89.7±5.6	80.7±5.5*	58.9±4.7	55.6±5.3*
Group Mean	80.2±1.3	87.4±1.4*	67.3±1.4	65.2±2.3*

Responses vary highly in both magnitude and direction. This inconsistency indicates that there is no dominant probe related effect on either pulse rate or MAP. All changes from baseline are significant ($p < 0.05$) but this is not very informative given the sample size.

These two forearm muscle hemodynamic measurements show distinctly different trends of response (Figures 17 and 19) with the most obvious effect being seen on local rBF endpoints (Table 3 and 5). The changes in cardiovasculature during the measurement were consistent with those of the 10 subject trial with a slight increase of MAP being observed and this increase in pressure may be attributed to the supine posture rather than compressive vascular reflex, given the absence of the elastic bandage[77-80]. Pulse rate appears to be largely slowed during baseline study (given the significant decrease for most subjects and group means) which is supportive of the assumption that all subjects were measured at rest.

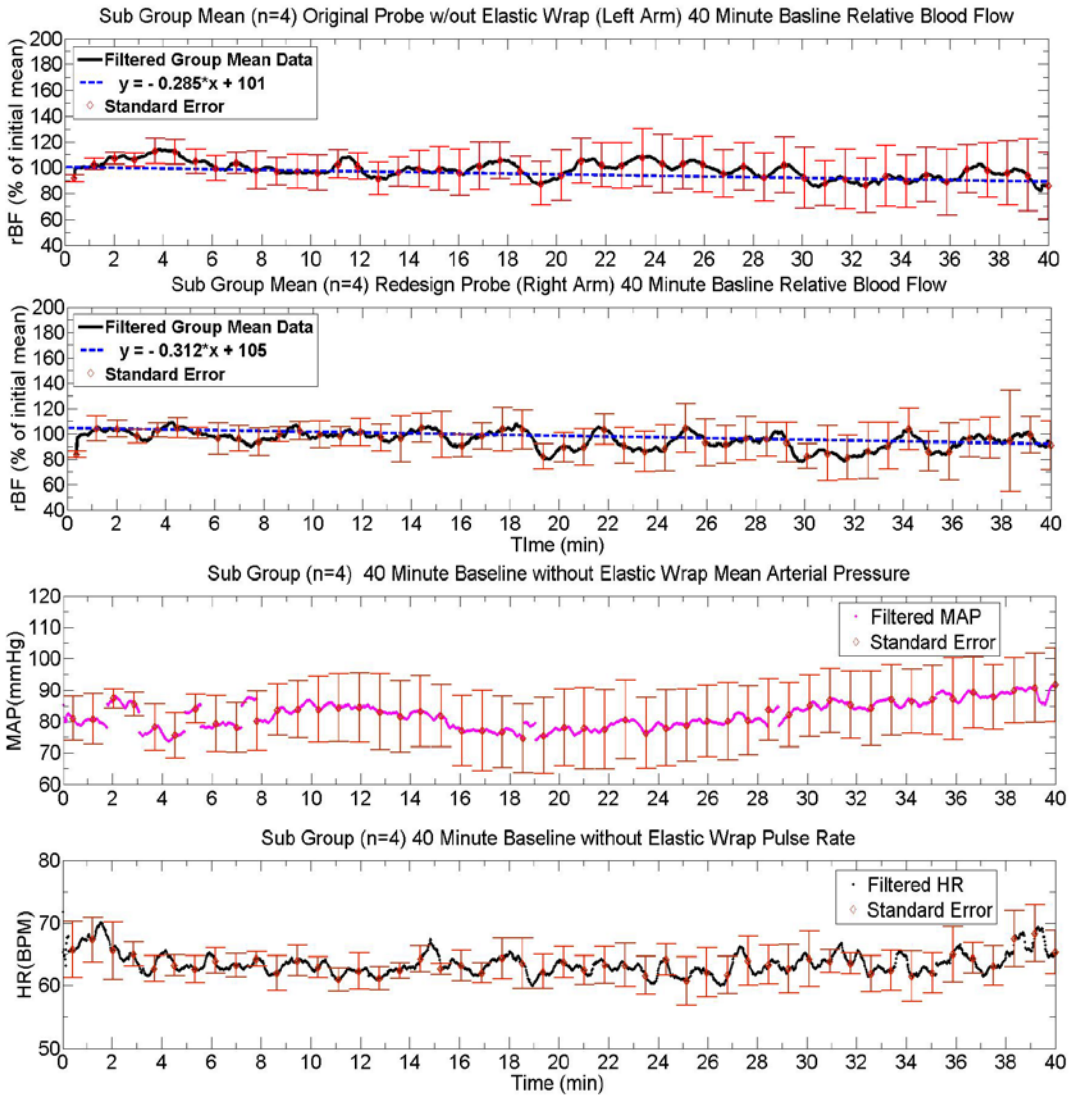

Figure 19. Sub-Group Mean (n = 4) Contra-Lateral rBF with Linear Fitting and Baseline Systemic Parameters

With the removal of the elastic wrap both probes had significant ($p < 0.05$) decrease in final 2 minutes rBF compared to initial 2 minutes but neither baseline or end final rBF was significantly ($p > 0.05$) different from each other. The linear fit of both time series showed a tendency to decrease and the magnitude of the shift was much less than our threshold of 0.7. Pulse rate is for the most part stable around its initial value without trend in any direction. MAP shows markedly more change in response but overall the extent of this increase remains fairly small (though statistically significant). Greatly indicative of predominant elastic bandage effect on local microvascular blood flow. Systemic parameters appear to be more independent of compressive effects.

3.3 DCS Baseline Study Discussion

3.3.1 Protocol #1: *In-vivo* DCS Gastrocnemius Baseline Stability Evaluation

Initial *in-vivo* contact probe data clearly showed that some aspect of the measurement was inducing a slow hemodynamic response in the limb (see Table 1). Relative changes in hemoglobin were of no consequence with few consistent trends, as would be expected in a resting baseline measurement. Subjects possessed a slight increase in total hemoglobin (not shown) but, again, this change was subtle and consistent with the more interesting changes in relative blood flow. The absence of global systematic measurements (blood pressure and pulse rate) in this protocol meant that baseline status had to be assumed and 5 minutes bed rest prior to the beginning of the protocol was deemed sufficient but confirmation via a finger plethysmograph was desired to confirm systemic status.

Linear fits were performed to characterize the global data trends for a more useful examination of rBF changes over time. An empirically set threshold of slope ≥ 0.7 was chosen to linearly model a significant baseline shift. Such a threshold, not based on physiological theory and predicated solely on examination of data, is justified as during our initial 40-minute baseline study it was found that end point rBF data standard deviations (calculated for each subject from Table 1, Chapter 3.2.1) averaged 28.4%. Against a theoretical final mean of 100% (ideally stable), the z score for our measured final mean (161.1%) was 2.15 meaning that it was more than 2σ or possessed a less than 5% rate of occurring due to chance. A 1σ threshold for increase over 40-minutes indicates that an observed mean

increase could occur up to 128.4% approximately 1 in 3 times. A linear fit slope ≤ 0.7 would have the effect that an increase in rBF (128% over 40 minutes with intercept = 100%) would fall within a single standard deviation of the expected 100% final stable baseline mean, but larger slopes would not. That is to say, starting at 100% theoretically stable rBF, the increase due to variance (within a single standard deviation) over a period of 40 minutes can be up to 128%, given a 0.7%/min slope. Stated as an equation, stability was determined thusly: 128% = m %/min · 40 minutes + 100%; m = 0.7 (%/min)

Thus a linear fit of less than this would show that the overall tendency for change is small (less than a standard deviation) and well within reason given our data variation, a larger fit shows a drift that is larger than variance would predict, and increasingly unlikely to be due to chance. Such an evaluation also minimizes the influence of short duration (2-3 minutes), low magnitude (10-20%), fluctuations as well as of high frequency noise observed on end point mean comparison Intercepts of the linear fit were not considered important, as long as they remained close enough (within 15%) to the initial baseline value of 100% that this value could be assumed to be the stable end baseline value. Sudden initial or final changes could potentially deviate intercepts sufficiently as to make the simple linear model of stability/shift inaccurate but it was determined to be sound enough to make a viable determination of baseline data behavior and was used for all baseline analysis.

Short duration rBF fluctuations are hypothesized to be related to many possible factors. e.g., subtle motion artifacts, postural contractions of nearby

muscle groups, changes in breathing pattern, pulse rate, arterio-venous tone, blood pressure, etc. that are difficult to accurately observe/monitor. Concurrent monitoring with EMG may be useful to distinguish the local muscle activity and assess the degree to which small muscle motions may affect blood flow but was unavailable to our lab for this study.

3.3.2 Protocol #2: *In-Vivo* DCS Gastrocnemius Baseline Stabilization

The measurement philosophy for this optical research is to avoid invasive methods to make hemodynamic or intramuscular condition measurements. Such noninvasive oriented research is optimal for developing methods directly applicable to the clinical environment given that all invasive procedures carry an increased risk of infection. This does mean that we must assume intramuscular conditions (relying upon literature for these assumptions), if they cannot be observed without the use of invasive procedures. This means that the methodology employed to mitigate possible contact probe effects was to reduce overall probe area, while retaining previously mentioned structural elements and signal stability, and reduce the amount of circumferential pressure applied to the limb, in an attempt to avoid intramuscular pressure increases and temperature elevation without being able to measure either parameter.

Several iterations of probe design were attempted and tested before the final design was adopted. Attachment protocol iterations found that acrylic liquid adhesives and similar substances were non optimal since most adhesives strong enough to maintain stable probe position proved difficult and uncomfortable to

remove as well as having some risk of skin irritation. In the end, the reduction of probe pad weight and securing of fibers allowed the use of the thin film adhesive Tegaderm which effectively reduced circumferential pressure application and insulation of the measurement region. While not optimized for multiple separations or adaptation of Imagent probe, the probe/protocol redesign successfully reduced the degree of probe influence on resting baseline blood flow over long duration measurements (see results in 3.2.2). Responses varied between relative stability and slight, but significant, decrease in end-point mean comparisons. All measurements, as well as the linear regression model of those measurements, showed a recovery of stable baseline measurements (see Table 2). The effectiveness of the linear regression model designed for assessing baseline stability was demonstrated to be effective at determining between overall stable and drifting blood flow trends for this study. This protocol was successful in reducing baseline shifts by use of the redesigned probe and new installation, but did not contain a means for identifying the dominant flow modulator responsible for this behavior. As such, another protocol was necessary to isolate the dominant variable influencing microvascular tissue hemodynamics. The next study (Protocol #3) used a relatively larger sample size to add statistical power, measured the forearm flexor muscles to confirm the phenomenon and its remediation in a separate and previously affected muscle group, and differentially measured attachment protocols and probe pad differences between limbs in a subset of the sample population.

3.3.3 Protocol #3: *In-Vivo* DCS Forearm Baseline Stabilization and Examination of Baseline Shift Origin

At rest, in the supine position, there is a tendency for blood pressure (systolic and therefore MAP) to rise and pulse rate to decrease[78-80]. Resting muscle is absent working muscle related metabolic/mechanical vasodilatory signaling. Given the lack of parasympathetic innervations of the muscular microvasculature, the aforementioned MAP increases and myogenic response of feed arteries produce an overall higher vascular resistance[81]. The decreased perfusion pressure of the lower limbs in supine, coupled with increase in vascular resistance and lack of vasodilatory stimulation, is seemingly able to produce a decrease in muscular perfusion, thus the decreased muscle blood flow (rBF) trend during these extended baseline measurements. This result is independent of the optical probe set up and is a consequence of systemic/local hemodynamic response to supine posture. Since no literature has been found which reports continuous, extended, resting baseline microvascular flow, this data, while in agreement with basic physiological principles, may be somewhat novel.

Removal of the elastic bandage removed subsequent baseline shift from the 4 subject subgroup regardless of which probe pad was used (see Table 5). This lends support to the hypothesis that application of circumferential pressure on the tissue to hold the probe pad in place is the predominant hemodynamic modulator inducing a significant elevation in subject local relative blood flow. The increase of MAP and blood flow in most subjects using the previous probe/protocol can be majorly attributed to the compression bandage having a local and systemic effects

which is linked to mechanically induced arterial vasodilation and autonomic response[70, 71, 77-79, 82]. The decreases in rBF observed (both in gastrocnemius and forearm flexors) during baseline measurements with revised probe and protocol are likely a result of the prolonged supine posture[78-80].

Group mean data for the forearm studies (Protocol #3) agree with the findings from previous gastrocnemius study (Protocols # 1 and 2) confirming that the original probe design induces a baseline shift while the redesigned probe/protocol does not.

Linear regression models successfully differentiate between short duration increases and true tendencies to increase over the duration of the measurement. The redesigned probe/protocol while significantly different from baseline ($p < 0.05$) at 102.1% to 119.1% only had a mean linear slope of 0.28, due to a sudden initial increase in rBF that is subsequently stable. This mean behavior is attributable to the effects of 3 atypically increasing subject responses offsetting with the more normal decreasing response in the long term, resulting in an initial increase followed by stability. These atypical responses are discussed further below.

There were found to be 3 subjects whose rBF increased in both arms regardless of probe/protocol and each of these was associated with the largest increases in rBF for the previous probe design (see Table 3). While unexpected, the data was accepted as reliable and a result of local/systemic hemodynamic factors rather than some outside source of noise. This stance is adopted as the

intensity and signal contact data were of good quality and no systematic or protocol deviations were noted in any of these subjects.

Atypical subject responses are included in the group mean which helps to explain the observed behavior therein. Most subjects had a final 2 minutes MAP value either non-significantly or 5-10 mmHg higher than initial 2 minute means. Subjects 9 and 10 exhibited drastic flow increases in both limbs and MAP increases of 23.0 mmHg and 22.2 mmHg respectively which would amount to a large increase in perfusion pressure at the microvascular level and at least suggests a non-stable baseline global hemodynamic environment. Reasons for the atypical increases could be attributable to some systemic upregulation (see the MAP increases for those subjects) or local activity but are not certainly known. Future studies must be cautious in applying protocols with attention to detail to prevent unknown variables from inducing potentially large changes in the sensitive microvascular hemodynamics.

In summary, despite the anomalous data, the general trend for the 10 subject group is in agreement with the previous gastrocnemius study (Chapter 3.2.1 and Chapter 3.2.2) in that previous probe/protocol application induced significant increases in resting baseline rBF while the redesigned probe/protocol greatly stabilized the measurement over the duration of the protocol. By concurrently measuring forearms with different optical probes, this study gives us reason to believe that local hemodynamic parameters are predominantly at the heart of the baseline shift and are likely related to vascular tone changes in the underlying muscle at the probe site[66-70]. This stance is further supported by highly

divergent local responses given the same global increases in MAP and decreases in pulse rate, expected of prolonged supine bed rest (see Table 4).

3.4 DCS Baseline Study Conclusions

Following the completion of analysis on both leg and forearm studies, it can be ascertained that the original contact probe and attachment protocol were inducing a significant flow perturbation, likely by way of inducing local vasodilation via elastic bandaging[16, 31, 69, 72, 73, 77]. Without being able to measure the intramuscular conditions regarding heat and pressure we attempted to design around evaluation of both parameters and obtained a final design that was efficient in terms of probe weight, easy to use, possessed of rigidity, durability, and fiber optic support. This redesign subsequently appeared to stabilize *in vivo* measurements. Study in both the gastrocnemius and forearm found the newly designed probe/protocol reduced the contact measurement hemodynamic effects which was significant with regards to local blood flow shift. An additional advantage to the major findings is that the probe pad was not the dominant factor in measurement induced hemodynamic shifts and we can therefore apply the hybrid DCS/Imagent probe (Illustrated in Figure 20) to measure absolute quantities for both flow and oxygen consumption rate, following the appropriate calibration protocols[31, 32].

Having satisfied our 3 major aims for this blood flow baseline shift study, i.e., verifying the presence of a gradual increase in rBF in healthy controls, stabilizing the measurement through probe redesign and protocol adjustments, and

ascertaining the origin of the baseline shift, we were now able to make continuous measurements in vivo with confidence that the measurement procedure itself was as minimally intrusive to the observation as possible.

CHAPTER 4: TRANSLATION OF ABSOLUTE HEMODYNAMIC/METABOLIC MEASUREMENT METHODS TO THE GASTROCNEMIUS DURING DYNAMIC EXERCISE

Our lab had previously investigated hemodynamics of the lower limbs using DCS/NIRS oximetry and validated this data against other technologies[16, 28]. However, these methods involved previously described optical probe attachment which was demonstrated to induce instabilities in rBF which we believe to have been addressed using current methods. In addition to this, our recent use of calibration techniques and dynamometer controlled exercise protocols[31, 53] had not been tailored to the lower limb, nor had we developed a protocol for exercise that would be easily comparable to literature. This research then focused on addressing these by developing an exercise and calibration protocol for use in the lower limb that would be comparable in duration/intensity to those of literature and, optimally, can be done by both healthy controls and PAD patients [13, 18, 19, 31, 54, 83, 84]. The success (or failure) to produce consistent and comparable responses would determine if these techniques were sound and would offer a platform to extend measurement to patient populations.

4.1 Gastrocnemius Translation Experimental Protocols

The primary motivation for using such an exercise protocol was in developing a protocol that could examine working muscle tissue hemodynamics and also be used to compare between healthy controls and PAD patients. By applying our recently developed calibration and measurement methods to the lower limb, this study would provide us a set of hemodynamic responses in young healthy

controls, using a protocol adapted to our equipment, as was the case in previous forearm studies[20]. The successful transference of our calibration and measurement techniques in the lower limb would then be our basis for comparison in future studies, perhaps in healthy control populations age-matched to standard PAD populations.

Secondary to the above motivation was the desire to cross-validate our resting baseline BF measurements using strain gauge plethysmography (SGVP) during our previously described microvascular flow calibration measurements. Such investigation marks a unique aspect of this study, as we had not previously concurrently validated our absolute measurements, but only compared the results of NIRS blood flow calibrations with literature. By concurrently measuring resting blood flow with both methods during the same venous occlusions we could remove procedural, temporal, and subject population variables from consideration and directly validate our optical methods. Methods employed here would make one of the few studies to comprehensively document muscle microvascular blood flow, limb blood flow, muscle blood oxygen saturation, as well as the derived metabolic parameter of oxygen consumption rate, continuously during dynamic exercise.

4.1.1 Subjects and Measurement Setup

10 subjects (2 females, 8males) were recruited and were all generally young with a mean age of 28 ± 2.8 yrs and without any known medical conditions. None were taking medication for any cardiovascular disorder. Subjects were all

active, engaging in activity multiple times per week but none were involved in regularly strenuous exercise regimens and none had participated in any exercise the day of the measurement. Subjects were recruited on a voluntary basis from a pool of healthy individuals and agreed to be measured via signed University of Kentucky Internal Review Board (IRB) approved consent forms.

The subjects were positioned in supine with head supported by a pillow and right arm supported at heart level, for the measurement of systemic pressure/pulse via finger cuff plethysmography. A finger plethysmograph (the same used in Chapter 3.3) was secured to the middle digit and used to monitor mean arterial pressure and pulse rate during the exercise protocol. Supine posture was used to more directly compare our data to other studies that, predominantly, used supine postures[13, 31, 54, 65]. Velcro straps secured the foot to the plate and the elevation of the dynamometer head was then raised to slightly above heart level. An inflatable thigh cuff (Zimmer ATS 1000, Indiana) was secured around the thigh above the knee firmly but without squeezing the leg. This cuff was then primed with a brief inflation. This served to set the tourniquet, fixing its position and decreasing the time to inflation during later occlusions.

Tissue hemodynamics were collected by using the FD-NIRS/DCS hybrid optical device. As described in Chapter 2.1 a commercial Imagent NIRS oximeter was used to acquire tissue oxygenation data and DCS was used to obtain rBF, from which the derived parameter (relative changes in oxygen consumption rate) could be calculated. The hybrid DCS/Imagent flow oximeter probe (Figure 20) was attached to the medial gastrocnemius of the test leg, after sterilizing both the

probe site and probe pad with alcohol preps. Adipose tissue thickness (ATT) was measured at the probe site before attaching the probe using a manual caliper (Lange 85300, Texas) three times consecutively and the result averaged to produce a determination of the optical barrier.

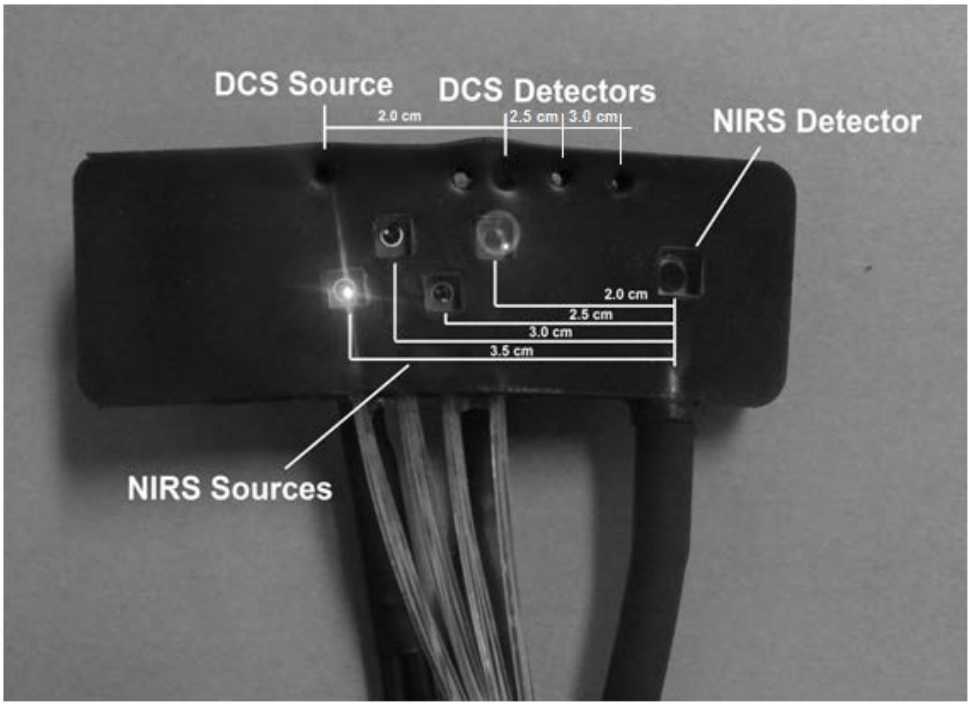

Figure 20. Hybrid Optical Probe

The hybrid optical probe consisting of a modified Imagent ISS optical probe. The silicone block had holes punched to accommodate the bundled 2-wavelength (785 and 853 nm) DCS source fibers and the 5 bundled single mode DCS detector fibers. This silicone rubber is 1cm thick and black which makes it an excellent shield to external noise, as well as having sufficient pliability to conform to the curves of human limbs and thus make good contact.

The optical probe pad was secured to the medial gastrocnemius with clear thin film adhesive dressing (Tegaderm, 3M, St. Paul, Minnesota) or two 6 inch strips of surgical tape one placed along axis of the muscle and the other in the circumferential direction (with care not to compress the muscle only to apply enough force to secure the optical probe). The strain gauge was placed just above the probe pad, underneath the tape layer and in the “shadow” of the pad such that

tape did not grab the strain gauge or pull on it which would induce artifact; this was easily verifiable by observing the strain gauge signal during final application of tape. Signal sensitivity of the strain gauge plethysmograph (Hokanson E-4 Strain Gauge Plethysmograph, Bellevue WA) was set to 1%. The device was then electronically calibrated and zeroed to the subject's resting limb circumference. Strain gauge signals were recorded via a visual basic program and written to a text file with the computer time stamped to assist in alignment of data with DCS data. Sampling of analog signals from an AD board was set at 1 KHz and 200 data points were then averaged to produce a final sampling rate of 5 Hz. This data was read into MATLAB for processing along with the DCS/Imagent data. Once the probe was secured, the optical fibers were taped to the bed to remove their weight from the probe and reduce negative pressure on the muscle belly. The signal was then tested and the probe pad readjusted, if necessary, in order to maximize signal integrity. Upon completion of the instrumentation set up (~5 minutes) a calibration protocol was performed. The entire experimental layout is demonstrated in Figure 21.

Figure 21. Equipment and Exercise Protocol Set-up

(1) DCS/ISS Hybrid Equipment; separate control computers connected via TTL link and receive analog position input from dynamometer to gate data collection during exercise. Total sampling rate (consisting of alternating between DCS acquisition and Imagent acquisition) is 1 Hz. (2) Optical probe sited over medial gastrocnemius at location of the muscle belly. (3) Occlusion cuff secured above the thigh for inducing venous occlusion and arterial occlusion for calibrations. (4) Strain gauge and control computer run independently and concurrently during both calibration and exercise protocols. Sampling rate set at 100 Hz with an average of 50 data points per recorded data point for overall data collection of 0.5 Hz. (5) Dynamometer is used to control exercise workload and frequency via setting 30% MVIC resistance and passive return to rest. A visual metronome is used to regulate subject timing.

4.1.2 Calibration Protocols for Absolute Hemodynamic Measurements

The calibration protocol consisted initially of a 3minute resting baseline measurement. Following that, a series of calibrating occlusions was performed. These consisted of three, 10-second, 50 mmHg, venous occlusions (VOs) with 1-minute of recovery between each occlusion. The change in THC during each VO was approximated by a linear fit and then averaged to produce the mean change in tissue compartment blood volume. This volume change, in units of μMol/kg/min, was converted to the perfusion units commonly used to describe tissue blood flow

as previously described (Chapter 2.3). These same VOs were used to compute the limb blood flow based on the increase in strain gauge resistance caused by volume increases during the occlusion. Concurrent strain gauge blood flow values were used to cross validate initial blood flow calibration. Next a single, 3-minute, 250-mmHg, arterial occlusion (AO) was performed wherein the fitted slope of the difference between [HbO_2] and [Hb] during the first minute provided the baseline muscle tissue oxygen consumption rate measurement, as described in Chapter 2.4. Following the AO, 5 minutes of recorded recovery allowed affirmation that the subjects' hemodynamics had returned to baseline values. The calibration protocols required ~15-minutes in total to complete and its organization summarized by Figure 22.

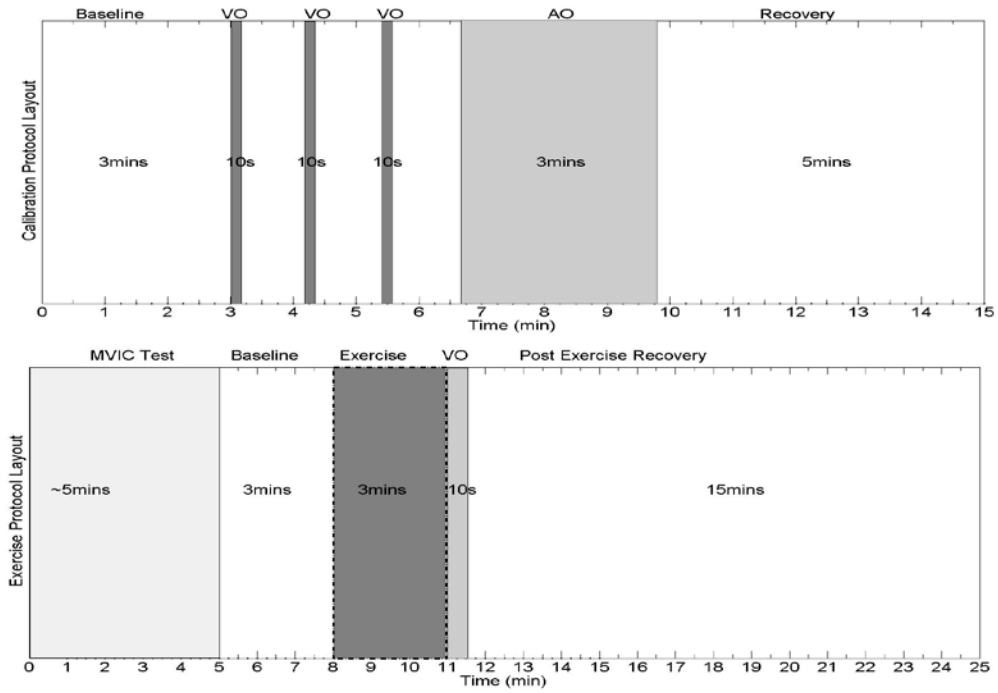

Figure 22. Absolute Hemodynamic Calibration and 30%MVIC Dynamic Plantar Flexion Protocol Layout

The above diagram summarizes duration and timing for each procedure. The black dotted box signifies the period in which the gating algorithm is active, and thus the sampling rate reduces to 0.5 Hz. Otherwise overall data sampling rates are 1 Hz as has been discussed.

The FD-NIRS Imagent collected data using a sampling rate of ~7 Hz to capture 5 data points ([Hb], [HbO_2], THC, and StO_2) per second to increase the temporal resolution of the hemoglobin concentration measurements and promote optical sensitivity to the calibration occlusions. Afterward DCS flow data (sampled for 300 ms) collected a single rBF data point. The overall sampling rate for both devices was 1 Hz. DCS and Imagent data collection was controlled by TTL signals to protect the integrity of each optical signal.

Following the calibration protocols, data collection was halted and the calibration data file saved, after which the subject's maximal voluntary isometric contraction (MVIC) load was determined. This procedure was used to normalize

exercise load to a percentage of each subject's maximal strength thus attempted to remove subject strength/fitness as a variable. The MVIC test consists of three to five, 5-second, isometric (static plate) contractions with three consecutive plateaued work outputs. The average of these values is used to determine the maximum force generation for each subject's plantar flexor muscles. The plantar flexion resistance was set as 30% of the MVIC and the subject was allowed to rest while the instrument settings and data file for the exercise protocol were prepared. Following the MVIC determination subjects were given a brief (5-6 cycles) exercise training to familiarize them with the exercise protocol to be performed. Subjects were given at least 5 minutes of recovery between MVIC test and exercise baseline measurement while investigators saved calibration data files and adjusted optical instrument data collection to exercise regime.

4.1.3 Gastrocnemius Hemodynamic Assessment During 30% MVIC Dynamic Plantar Flexion Exercise

After taking 3 minutes of baseline data to reconfirm measurement stability, subjects then performed 3 minutes of 0.5 Hz, 30% MVIC, full range of motion (15-30°) plantar flexion exercise. Exercise rhythm was preserved by use of a visual metronome and examiner prompting, in order to keep the duty cycles as consistent as possible. Each duty cycle consisted of a 0.5-second contraction, a 0.5-second relaxation to rest position, and a 1-second passive rest following the contraction/relaxation phases. Data collection was limited to this one second rest phase by the use of a gating algorithm (see Chapter 2.5). Immediately upon reaching the end of contractions, a single 50 mmHg VO was performed to assess

post exercise limb flow via SGVP. Fifteen minutes of post exercise recovery hemodynamics were measured to assess long term muscle metabolic/flow responses to rigorous exercise. Refer to Figure 22 to review the overall protocol layout.

During exercise protocols the FD-NIRS data collection regime was adjusted to 7 waveform averages per data point (300 ms total sampling time) and the measurement ratio set 1 to 1 with the DCS flow measurements. This decreased the temporal resolution of hemoglobin concentration measurements but increased sampling time for a single data point, thus increasing the signal-to-noise ratio of these measurements for more accurate determination of hemoglobin concentration and $\dot{V}O_2$ changes. DCS was set to a correlation/sampling time of 600 ms for a single data point and thus the total sampling rate for the protocol was 1 Hz, except where this 1-second of data was gated to collect between 1-second duty cycles, reducing overall sampling rate to 0.5 Hz during exercise.

File markers were used to indicate time points for the beginning and ending of exercise for offline data analysis. During the experiment, the DCS and Imagent operating programs displayed, on their respective screens, the online relative flow index, absolute hemoglobin concentrations, and tissue oxygen saturation. The calibrated blood flow and derived oxygen consumption rate were calculated via offline analysis using MATLAB processing code. Data from the Imagent, DCS, and finger plethysmography were co-registered using file marker time stamps so that all data from the three devices could be aligned precisely.

4.2 Gastrocnemius Translation and Hemodynamic Profile Results

4.2.1 Subject Demographics and Calibrated Baseline Values

Exercise strength normalization with MVIC produced comparable working loads that were a mean of 28.1 Nm. Pre-measurement ATT was normal for all subjects and did not pose substantial optical barrier. All subjects were able to complete the protocol and initial values (see Table 7) indicate healthy resting values for controls.

Table 7. Subject Demographics and Measured Resting Baseline Values

Subject Demographics and Key Protocol Values	Mean±Std
Age (yrs)	**28±3**
ATT (mm)	**6.4±1.5**
MVIC (Nm)	**93.7±26.5**
Mean Power (W)	**13.5±3.4**
Baseline StO_2 (%)	**72.6±3.0**
Baseline Optical BF (ml/100g/min)	**0.88±0.4; Optical**
Baseline SG BF (ml/100g/min)	**1.13±0.6; Strain Gage**

Individual data were shown for a single subject (Subject 4) in Figures 23-25 during calibration. Values were obtained for the resting conditions for flow and oxygen consumption rate from our calibration protocols of venous occlusions and arterial occlusion. Characteristic trends included the rBF dramatically decreasing during AO, the slight decreasing in rBF during VO, and the hyperemic overshoot

following AO of about 225%. Clear desaturation and separation of Hb/HbO_2 indicated successful $\dot{V}O_2$ calibration. THC trends closely mirrored those of the strain gauge as demonstrated in figures 25 and 26; these calculated blood flows were demonstrated to be simultaneous by time axis examination (Figures 23 and 24). All values returned to baseline levels following five minute recovery periods.

Group mean calibration was consistent with individual subject data for all parameters. Cross validation of initial absolute blood flow was successful during baselines. A correlation $R^2 = 0.51$ for mean individual absolute NIRS blood flow and SGVP blood flow was observed (Figure 26). Mean initial blood flow for muscle tissue was comparable but significantly lower than limb blood flow measured by the strain gauge (Table 8). However, limb blood flow was observed to only be an average of 1.3X greater than local blood flow in contrast to the 2-3X previously reported in literature[12, 13, 65]. Repeatability for each occlusion was good with mean strain gauge measurements having a standard error of 0.63 ml blood/100ml tissue/min and with NIRS occlusions having a standard error of 0.35 ml/100ml tissue/min (Table 8). Baseline values for NIRS blood flow measurements agreed well with literature values, finding a wide range from 0.35 to 1.36ml/100ml tissue/min (Table 8) [14, 17, 31, 61, 63, 65]. The strain gauge values were lower than most literature, ranging from 0.4 to 2.4ml/100ml tissue/min (Table 8)[27, 64, 85, 86]. $\dot{V}O_2$ measurements are likely underestimates with a mean 0.049 mlO_2/100ml/min. However the range of 0.023 to 0.127 mlO_2/100ml/min measurements agree with literature reports finding values of

around 0.02 to 0.15 mlO_2/100ml/min, with a typical mean of 0.1 mlO_2/100ml/min[12, 14, 31, 61, 63]. This might be related to the known arterial leakage that occurs even when using 50+mmHg of pressure over systolic pressure. The small influx of oxyhemoglobin depresses the decrease occurring due to occlusion and makes the [HbO_2-Hb] difference smaller, thus the underestimate.

Table 8. Subject Initial Absolute Calibration Values

	VO Calibrated Optical BF (ml/100ml/min)	VO Calibrated SG BF (ml/100ml/min)	AO Calibrated $\dot{V}O_2$ (mlO2/100g/min)
Subject 1	1.04±0.06	1.18±0.05	0.009
Subject 2	1.36±0.11	2.40±0.07	0.127
Subject 3	1.33±0.06	1.94±0.15	0.023
Subject 4	0.61±0.13	1.29±0.08	0.057
Subject 5	0.62±0.16	1.03±0.06	0.030
Subject 6	0.35±0.16	0.57±0.09	0.036
Subject 7	1.03±0.35	0.46±0.16	0.058
Subject 8	0.46±0.01	0.41±0.03	0.027
Subject 9	0.95±0.35	1.04±0.10	0.059
Subject 10	1.07±0.32	1.01±0.06	0.068
Mean±std	0.88±0.35	1.13±0.63	0.049±0.033

Each flow value is shown as the mean ± std of three VO flows. $\dot{V}O_2$ is shown as a single AO measurement only. Group means are presented as mean ± standard error.

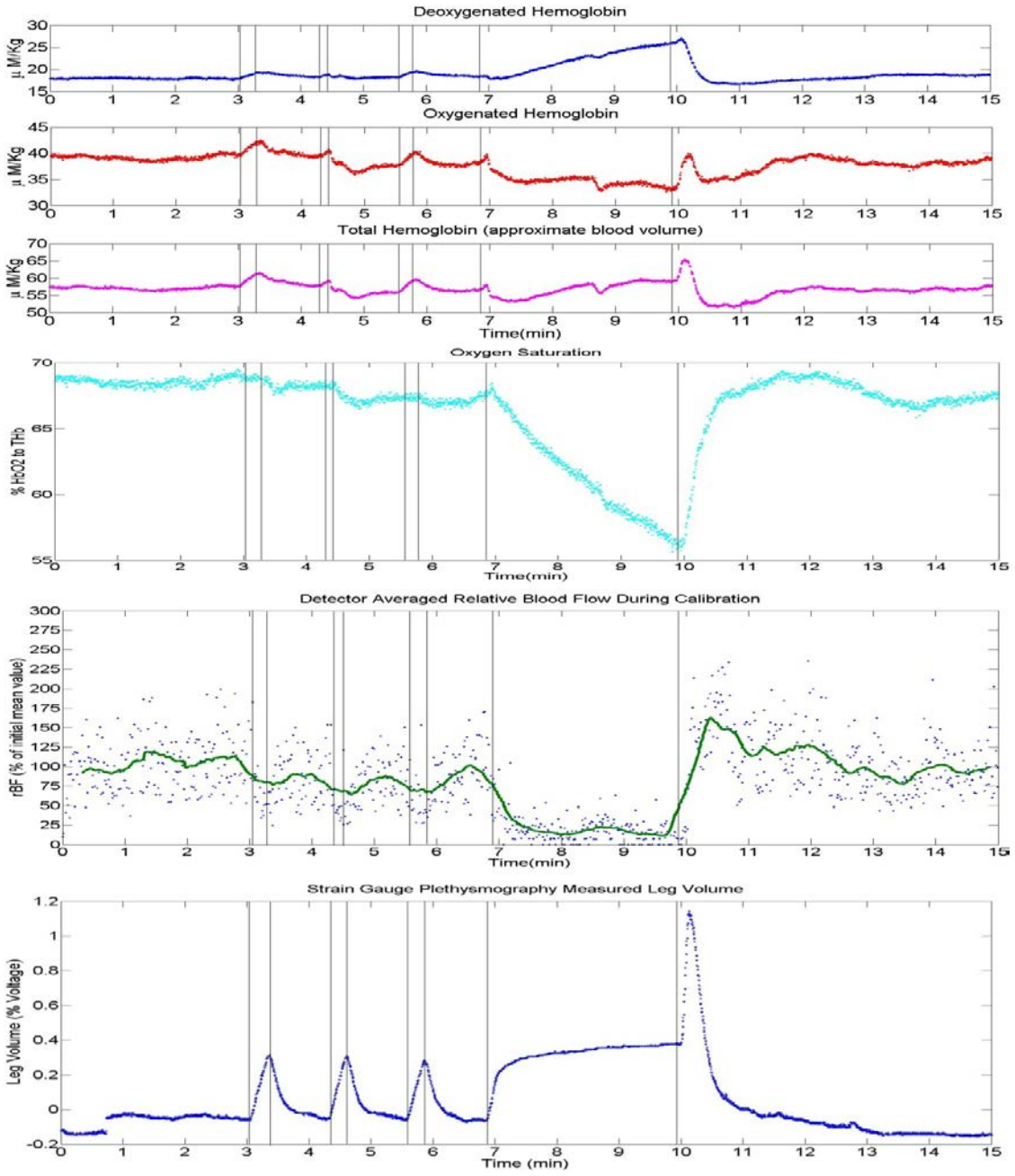

Figure 23. Sample Subject (Subject 4) Hemodynamics and Strain Gauge Data During Calibration Protocol

Descending order: Deoxy, Oxy, and total hemoglobin concentrations, StO_2, rBF (with raw data in blue, filtered in green), and strain gauge data at bottom. Hemoglobin trends, oxygen saturation, and rBF trends indicate successful occlusion; rBF decreases during VO supporting the assertion that these pressures do in fact decrease flow to the limb[27].

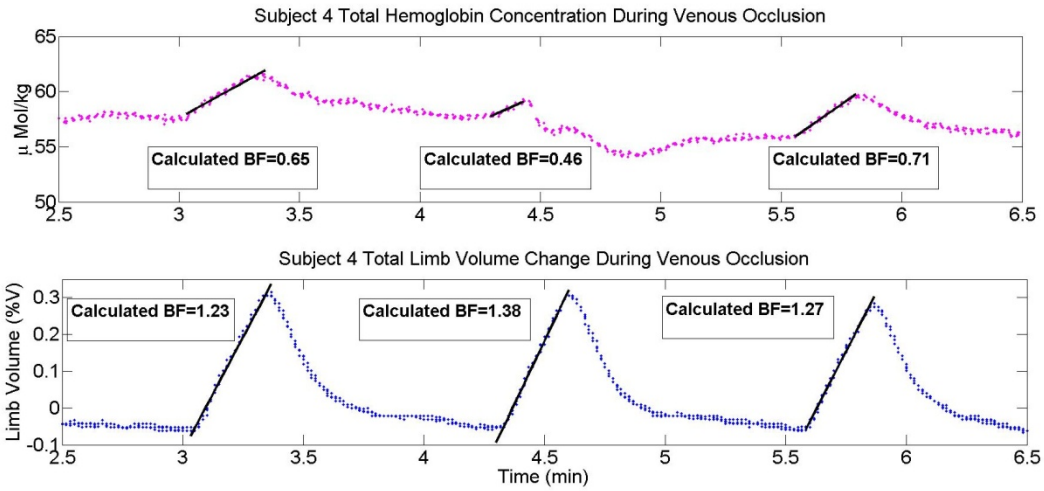

Figure 24. Zoom-in Sample Subject (Subject 4) Optical THC and Strain Gauge Data During VO

Volume changes measured by both strain gauge(bottom) and NIRS(top) concurrently, indicate that the effects of the VO upon vasculature are immediate and detectable by both systems. Correlation of individual VO volume changes between the two methods resulted in R^2 values of 0.93, 0.88 and 0.98 respectively. These correlations decreased once the conversion factors to acquire perfusion units were applied suggesting a disconnect between the set of assumptions used to calculate local tissue perfusion and limb volume changes assumed to equal flow. Black lines are the plotted linear fits of each occlusion.

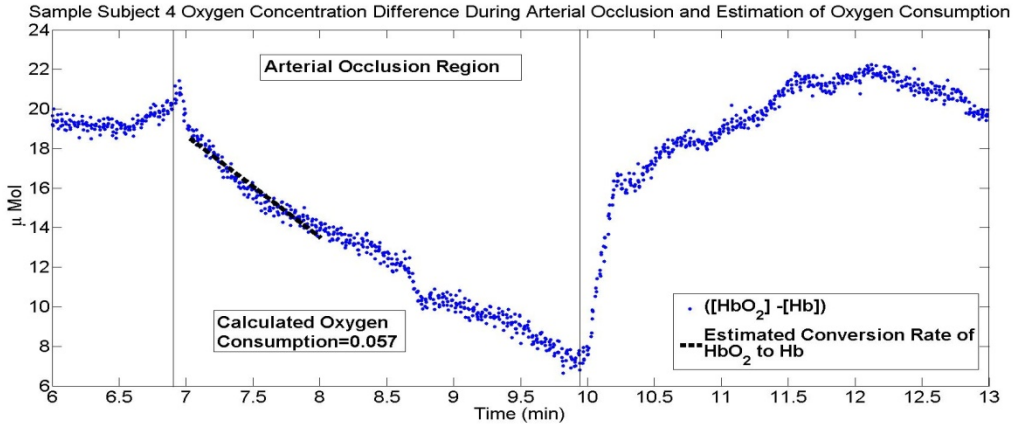

Figure 25. Zoom-in Sample Subject (Subject 4) $\dot{V}O_2$ Calculation During AO

Rapid decrease in oxygenated hemoglobin and simultaneous increase in deoxygenated hemoglobin causes the difference to approach zero during the occlusion period. This rate is estimated via MATLAB polyfit and produces a slope (shown in black dotted lines) which may be converted from units of $\mu MolO_2$/min to units of mlO_2/100g tissue/min. Note the initial increase is likely due to the cuff taking time to reach fully occlusive pressures. Only the first minute of occlusion is necessary to obtain an estimate of oxygen consumption rate, the remainder is used to assess the overall quality of the occlusion.

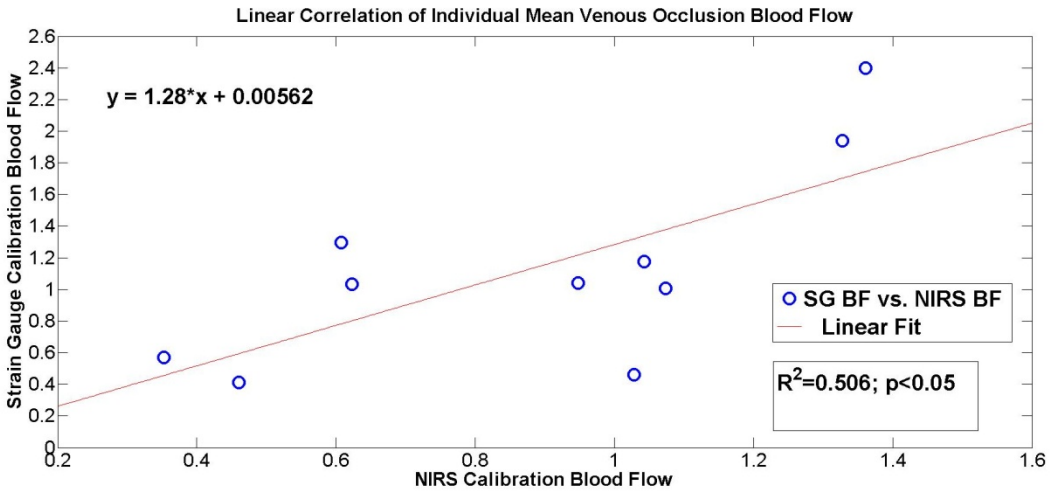

Figure 26. Correlation Curve for Baseline Absolute Blood Flow Between NIRS and Strain Gauge Plethysmography

A correlation of $R^2 = 0.51$ was obtained which indicates a sound correlation between the two parameters despite high degrees of intersubject variation and differences between limb and muscle flow (to which the remainder of variance is attributed). Strain gauge measurements are generally higher than optical methods as has been noted by most NIRS flowmetry groups. On average the difference was local blood flow measurements by the optical device was 78% lower than strain gauge measurements.

4.2.2 Gastrocnemius Hemodynamic Profiles During Exercise

Individual data for the same subject (Subject 4) are presented in Figure 27 to illustrate typical individual hemodynamic profiles during the exercise protocol. Exercise baseline data for hemodynamic parameters were stable. This subject, as is typical, shows clear initial changes due to exercise including decrease in THC caused by muscular compression of the compartment. StO_2 decreases sharply while rBF increases rapidly, contributing to the substantial $r\dot{V}O_2$ increase. At onset of exercise these values changed rapidly and a plateau was achieved within about two minutes of exercise with significant increases of ~350% rBF and ~600% $r\dot{V}O_2$. Absolute optical BF was 2.4 ml/100mltissue/min while SGVP

measurements resulted in 3.1 ml/100mltissue/min, reasons why SGVP blood flow are larger than NIRS are discussed in chapter 4.3.2 and the appendix. Neither parameter recovered completely 15 minutes post exercise, remaining significantly elevated by approximately 2 fold compared to baseline. Tissue desaturated significantly to 55% from an initial 70%, recovering to sustained super baseline levels following exercise. Subject pulse rate and MAP increased to 90 BPM and 105 mmHg respectively with end recovery pulse rate recovering completely (not significantly different from baseline) while MAP remained elevated, similarly to rBF, at 95 mmHg at the end of data collection. Strain gauge signal was stable except during exercise where noise was substantial due to muscle contractions changing limb volume (Figure 27). The post-exercise VO is observable in hemoglobin (with increases in THC) and strain gauge (increased volume) data indicating a successful occlusion.

Group mean results were similar in trend to those of individual data, as seen in Figure 28 and Table 9. All the following changes were significant ($p < 0.05$) compared to baseline. Tissue desaturated by a mean of 13.4% compared to baseline (71.1 to 57.7%) while both local hemodynamics and systemic cardiovasculature rose rapidly. All of these were indicative of substantial effort on the part of the subject population. Recovery was rapid but incomplete with all parameters except pulse rate being significantly greater than baseline, a response that has been observed elsewhere[87]. Mean BF increased from 0.91 to 1.87 ml/100mltissue/min (220%) while $\dot{V}O_2$ increased from 0.05 to 0.17 mlO_2/100gtissue/min (326%). Strain gauge mean BF increased from 1.13 to 5.13

ml/100mltissue/min (454%) with a large standard deviation of 3.15 (standard error 1.1) ml/100mltissue/min due to subjects having a range from 2.5 to 12.8 ml/100mltissue/min. This data was then regarded as unstable, as discussed in chapter 4.2.2 and the appendix. MAP and pulse rate increased from 77.9 mmHg and 63.5 BPM to 91.9 mmHg and 82.7 BPM respectively. The majority of recovery occurred within the first minute following end of exercise as can be seen by observing the end exercise, 1-minute recovery, and end-recovery values, as well as time series data (Figures 27 and 28; Table 9).

Consistency between subject responses to the protocol resulted in minimal temporal blurring of the rapid onset and end exercise trends, along with fairly small standard errors. The VO used to assess end exercise flow via strain gauge may be observed in the individual subject data (Figure 27, hemoglobin) but was not evident during the group mean response (Figure 28, hemoglobin). The interference with hemodynamics during this period was less than the variation that occurred between subjects responding to the same stimulus.

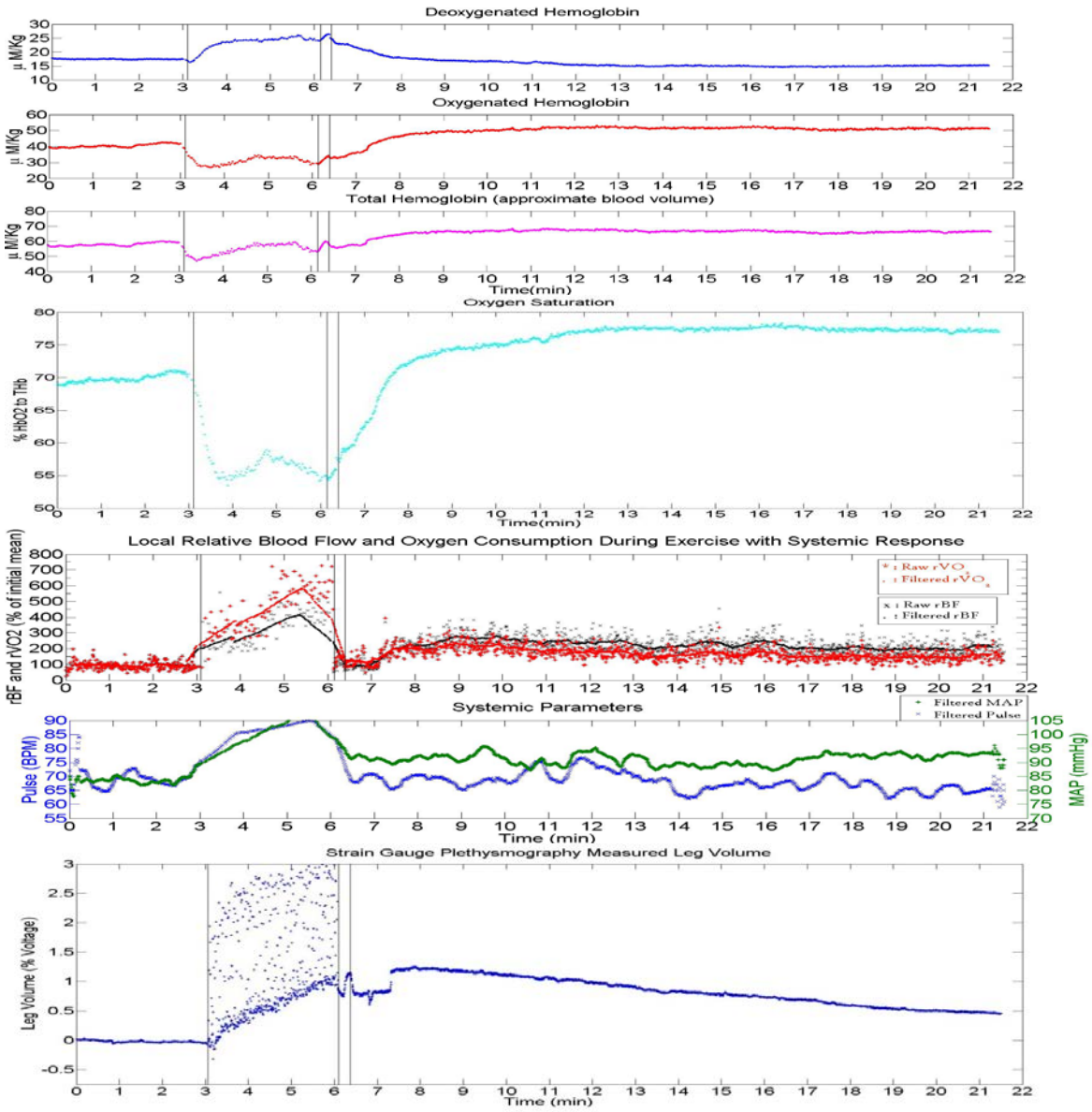

Figure 27. Sample Subject (Subject 4) Exercise Protocol Hemodynamic Response and Strain Gauge Data

Descending order: Hb, HbO_2, THC, StO_2 and coaxial rBF and $r\dot{V}O_2$, followed by systemic pulse rate and MAP, and lastly strain gauge limb volume changes. Exercise periods are marked by the first two vertical lines, the second of which also indicates the time of post exercise VO initiation. The third vertical line indicates the end of VO and beginning of recovery.

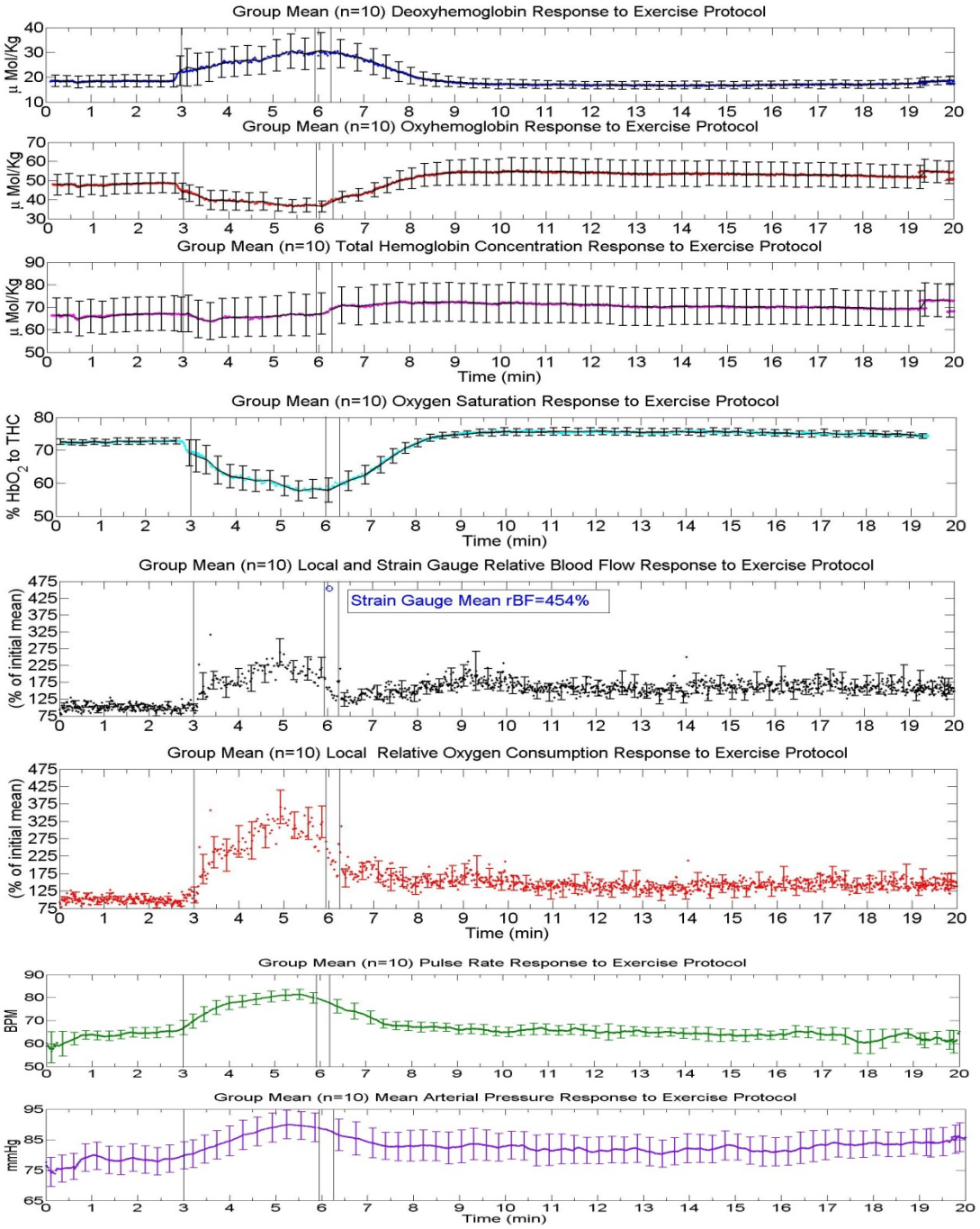

Figure 28. Group Mean (n=10) Hemodynamic Profile for Gastrocnemius Muscle During Exercise

Mean responses (with standard error bars) show clear effects of exercise, both locally and systemically. Strain gauge BF relative increases are much greater than DCS flow and have standard error of 85% which could not be shown in this figure.

Table 9. Summary Values for Blood Flow, Oxygen Consumption Rate, and Systemic Parameters

Hemodynamic Parameter	Initial Calibration	Baseline Exercise	End Exercise	1Minute Recovery	End Recovery
rBF (%)	**102.1±7.6**	**100.9±2.9**	**220.4±9.5 ***	**144.0±4.4*#**	**158.7±4.3 *# ^**
BF (ml/100ml/min)	**0.88±0.4**	**0.91±0.03**	**1.87±09 ***	**1.39±0.04*#**	**1.53±0.05*#^**
SGBF (ml/100ml/min)	**1.13±0.6**	**n/a**	**5.13±1.0***	**n/a**	**n/a**
r$\dot{V}O_2$ (%)	**99.6±1.7**	**103.7±1.5**	**326.9±15.5***	**164.6±6.8*#**	**145.1±3.8 *#^**
$\dot{V}O_2$ (mlO_2/100g/min)	**0.05±0.03**	**0.05±0.01**	**0.17±0.01 ***	**0.07±0.02 *#**	**0.08±0.01*#^**
StO_2 (%)	**71.1±0.9**	**72.6±0.1**	**57.7±1.7 ***	**68.5±0.8*#**	**74.4±0.8 *#^**
MAP (mmHg)	**n/a**	**77.9±0.5**	**91.9±5.1***	**83.2±0.2 *#**	**84.8±0.2 *#^**
Pulse Rate (BPM)	**n/a**	**63.5±0.3**	**82.7±0.2***	**69.3±0.5*#**	**62.0±0.4* # ^**

Blood flow data represents both local (rBF/BF) and strain gauge (SGBF) blood flows. Reported as mean ± standard error. * denote statistical difference ($p < 0.05$) from baseline values as determined by t-test, # represents statistical difference from end-exercise values by the same test and level of significance, and ^ denote significance between 1-minute recovery and end-recovery values.

4.3 Gastrocnemius Translation and Exercise Hemodynamics Discussion

4.3.1 Calibration of Absolute Measurement and Cross Validation with Strain Gauge

The use of VO to calibrate DCS flow indexes is based on the presumption that resting blood flow is proportional to the diffusive motion of erythrocytes in tissue. By assuming a relatively steady state resting blood flow, the initial normalized value of αD_B (100% of a 30-sec mean) is ascribed a perfusion value equal to the calculated arterial inflow via the VO protocol. For such a calibration to be trustworthy, one must have some guarantee that the measurement protocol is stable and that the vasculature is in a truly resting state. It is also important that the VO not induce large changes in local or systemic hemodynamics. This assumption is borne out experimentally with local effects observed to recover within one minute following the venous occlusion [14, 22, 28, 32].

For oxygen consumption rate calibration via arterial occlusion there are also several underlying conditions which are required for validity of the measurement. The first is that, generally speaking, since the venous compartment hold the greatest volume of blood, oxygenation values reflect a weighting toward the oxygenation of hemoglobin located in the post capillary vessels[29]. This distribution is not allowed to change or the compartment ratio of venous to arterial blood (γ, review chapter 2.4) may change and this alters the calculation of oxygen extraction. The NIRS measurement of tissue StO_2 is then safely assumed to represent muscle tissue O_2 saturation following oxygen extraction. This assumption is what allows investigators to use arterial saturation and tissue

saturation to make an artio-venous difference relation necessary for the calculation. Microvascular blood flow is not as simple as entry, residence, and outflow, however, as the system (depending on physiological necessity) is capable of shunting the capillary beds or recirculating blood. However, the spatial averaging of chromophore concentrations by NIRS results in overall tissue O_2 saturation that is insensitive to such behaviors. The second major assumption is that once the pressure cuff reaches full pressure, the blood inside the compartment is theoretically isolated and therefore THC should remain constant, while any loss of saturation is due to consumption by the tissue. In practice it is observed that this is not strictly so, but is true enough to be valid for short durations[12, 14, 20, 61, 63].

NIRS oximetry in general contains a confounding variable in muscle tissue due to the presence of the spectrally identical, single O_2 binding chromophore myoglobin. Myoglobin effects on NIRS oximetry is discussed heavily elsewhere but suffice it to say that the much higher oxygen binding affinity of myoglobin and myoglobin containing a single oxygen binding site limits the influence of myoglobin desaturation to detected signals. Only once desaturation had reached a sufficient point to decrease the tissue blood bound O_2 to myoglobin bound O_2 to somewhat extreme levels[15,23,28,29].

Calibration protocols were successful in producing venous occlusions and arterial occlusions that could be used to calibrate the relative blood flow and oxygen consumption rate measurements made during the exercise protocol. Initial blood flow measurements within each individual were consistent for each

VO but varied widely between subjects. Such variability has been noted throughout literature documenting blood flow and comes as no surprise to us[12, 63, 65, 84, 88, 89]. Despite the variations we found good agreement with literature in both reported trends and actual values of calibration blood flow as well as in other hemodynamic parameters (Figures 26 and 28, Tables 8 and 9) Initial values for hemoglobin concentration, oxygen saturation, oxygen consumption rate, blood flow, etc. were all well within normal physiological norms[12-14, 17, 31, 54, 61, 63, 83]. Cross validation of our local optical flow measurements with more global limb blood flow obtained via SGVP proved successful with there being a good correlation between mean baseline flow values obtained using the two methods (Figure 26). This agreement was lost in post exercise strain gauge measurements, due largely to the great standard deviation between subject blood flow responses to exercise with regards to both local and limb measurements of flow (Figure 28, Table 9). Thus our aim of cross validating DCS calibrated flow against strain gauge flow is met under resting conditions but not during exercise.

There exists a possible systematic underestimate of $\dot{V}O_2$ that is related to arterial leakage during arterial occlusions. Some subjects experience a small increase in THC which can be attributed to an oxyhemoglobin concentration that is not decreasing as rapidly as deoxyhemoglobin increases. Such microvascular leak would decrease the slope of ($[HbO_2]$-[Hb]) and thus the $\dot{V}O_2$ would be underestimated, (see Figures 23 and 26). The VOs measured by strain gauge and NIRS produced very similar and highly correlated changes in volume (Table 8).

Local effects due to the occlusion series were transient and fully recovered within 5 minutes of recovery and with little drift between calibration and the initial baseline for exercise (Figure 23 and Figure 27, Table 9). Minimal local hemodynamic effects following this calibration protocol are a necessity to its use since we cannot risk deviating the initial physiological conditions from baseline prior to a measurement. This is to reduce the risk of weakening our ability to distinguish exercise responses from unintended perturbation of the system during calibration and MVIC tests.

The 5-minute minimum time between calibration/MVIC protocols and beginning of baseline for exercise is used to reduce such possibility. This time was deemed satisfactory given that prior investigations used 5-minute resting periods between AO and exercise protocols or sometimes trials between exercises[17, 31, 65].

The primary objective of this study however was to transfer the techniques previously applied to the forearm to the lower limb muscles[20]. This included ensuring that skin fold thickness and penetration depth were such that we could get adequate signal. This proved to be the case with all subjects having ATTs measuring less than 8 mm, most of which were closer to 7 mm, which places the superficial muscle layer well within the ~13 mm envelope of a 2.5 cm S-D separation set up[10, 32, 72, 90].

One parameter which possessed a potent influence was subject posture. The lower perfusion pressure of the supine posture produced a substantially greater

effort for subjects than did the sitting posture which has great implications on the ability of PAD patients to perform such protocols[90]. Our original intent was to perform seated protocols but changed to supine since there is a greater pool of literature available for this posture; most notably the study performed by Bauer et al in 2007 which had both PAD and age matched controls using a very similar measurement methodology to ours consisting of measuring oxygenation with a NIRS spectrometer during supine plantar flexion exercise protocols, but with the notable exception that they measured blood flow via post exercise SGVP venous occlusions[54]. This means that the Bauer study did not measure blood flow continuously and only measured muscle tissue oxygenation (StO_2), not metabolism ($\dot{V}O_2$)[54]. Still the study served as a basis of comparison between our measurement/exercise methodology and that of already accepted techniques. However, future PAD study should use the seated posture to reduce the stress on compromised vasculature of patients and make the study more closely resemble a physiologically normal scenario (subjects will be more likely to be sitting/standing than fully reclined).

4.3.2 Hemodynamic Profiles During Exercise

Exercise results of this study proved fruitful in that the combined NIRS/DCS system, coupled with a finger plethysmograph, was able to capture a very broad range of hemodynamic parameters noninvasively and continuously during dynamic exercise. The author is aware of no other studies that demonstrate such capability and this could mark the first noninvasive examination of absolute values for all of these parameters throughout such a protocol in the

gastrocnemius. Mean subject hemodynamic and metabolic changes due to exercise parallels other similar study responses, see Table 10[13, 54, 65, 83, 84, 88]. A broad range of values exists in literature for both BF and $\dot{V}O_2$ depending largely on how BF is measured. Such variation in methodology makes direct comparison of outcomes difficult but allows us to examine trends. Of particular import is the apparent rapidity of microvascular increases in blood flow, oxygen consumption rate, tissue desaturation, as well as systemic responses. All of these parameters increase dramatically within a few seconds of exercise and a full hemodynamic plateau is reached within two minutes of 30%MVIC plantar flexions. Exercise data collection gating successfully removed motion artifacts during the protocol, preserving the quality of blood flow and metabolism optical data (see Chapter 2.5 for reminder of gating algorithm). Post exercise changes are likewise very rapid, being mostly complete within the first minute and the system seems to impose a demand for high temporal resolution measurement methods (Figures 27 and 28, Table 9).

The extent of absolute flow increase is more than 2 fold for most subjects, ranging from a 0.44 ml/100ml tissue/min minimal responder to 3.76 ml/100ml tissue/min. However, absolute resting baseline is not correlated with the magnitude of exercise as some subjects with the highest initial absolute blood flow had only mediocre relative increase (130-160%). Relative increases in $\dot{V}O_2$ are about 100% greater than those of BF and this is in line with literature reported increases of oxygen extraction for metabolically stressed muscle[16, 54, 84, 88]. Initial mean $\dot{V}O_2$ was found to be 0.06 mlO_2/100g tissue/min on average with

ranges from 0.01 to 0.14 mlO_2/100g tissue/min and typically increased much more (100%) than BF from 0.02 to 0.39 mlO_2/100g tissue/min, a pattern typical for fatiguing exercise[31, 64, 65, 88]. Oxygen saturation exhibited, for the most part, a substantial decrease, falling from initial 2-minute means of 70-75% to end exercise plateaus of 55-50%. These response time courses and extents are comparable to those of other similar studies using NIRS to measure oxygenation [54, 84, 88]. The variation of response is not unusual for exercise and accents the necessity for large subject populations in these kinds of studies.

Table 10. Comparison of Baseline and Exercise Values from Literature

Study	Methods for Measuring BF, $\dot{V}O_2$	Resting BF (ml/100ml/min)	Exercise BF (ml/100ml/min)	Resting $\dot{V}O_2$ (ml O_2/100g/min)	Exercise $\dot{V}O_2$ (ml O_2/100g/min)
Henry 2014,	**NIRS VO; SGVP, NIRS AO (n = 10)**	**0.88 ± 0.4; 1.13 ± 0.6**	**1.87 ± 09; 5.13 ± 1.0**	**0.05 ± 0.03**	**0.17 ± 0.01**
^Baur 2007 [54]	SGVP, (n=8)	~3	~26		
**Boushel 2000 [64]	SGVP, NIRS/SGVP, (n=7)	2.6 ± 0.3	44 ± 7	0.23 ± 0.07	6.6 ± 1
*Casavola 2000 [14]	NIRS VO, multiple measures on single subject	0.40 ± 0.10		0.04 ± 0.02	
*Van Beekvelt 2001 [65]	NIRS VO; SGVP, NIRS AO; NIRS SGVP, (n=26)	0.9 ± 0.45; 2.06 ± 0.70		0.11 ± 0.02; 0.15 ± 0.06	
^Kooijman 1997 [13]	NIRS VO, NIRS AO, (n=15)	0.68 (0.54-0.97)	1.36 (1.12-1.64)	0.02 (0.01-0.03)	0.04 (0.02-0.05)
^Egena 2005 [89]	SGVP, (n=12)	~3	~18		

*Data presented as mean ± std, ** data presented as mean ± std error, ^ data presented as figure (extrapolated from data but not explicitly stated in text). Due to the complexity and variety of these studies a ";" is used to indicate two methods of measuring a single parameter (reported top first bottom second) and a "," used to indicate the separation of parameters measured.

Strain gauge plethysmography BF measurements, with end exercise values ranging from 2.5 ml/100ml tissue/min (2X mean baseline) to 12.8 ml/100ml tissue/min (12X mean baseline), were of much greater variance than local optical measurements; end-exercise data show 270% (SGVP) mean standard deviation compared to 30% (DCS) mean standard deviation. The extreme variation of SGVP end-exercise values and issues related to the methodology lead us to conclude that SGVP should only be used to evaluate limb resting flow and cannot be used to accurately assess the behavior of local microvasculature. There could be a nonlinear relation between local muscle blood flow and whole limb blood flow. Indeed, the two should not be expected to have a strictly linear relation as the factors that govern microvascular flow are different in many ways than those that govern whole limb flow[13, 26, 27, 85]. Examples of this include the sympathetic vasoconstriction of vascular beds in non working muscles while working muscles vasodilate. Whole limb and working muscle blood flow may increase but microvascular flow in the non working muscles is decreased. Such difference in methodology, observed wide variances for end exercise strain gauge BF, and a lack of correlation with end exercise rBF, as well as the necessary temporal delay between end of exercise and VO, makes end exercise blood flow measurements by strain gauge non optimal.

Few studies make extended measurements of recovery periods following exercise and those that do rarely report this data as time series. Such omission makes it difficult to assess the pattern of hemodynamic recovery following

metabolic challenge. Our data show a very pronounced post exercise increase in most parameters. The only parameter to reach pre exercise values significantly was pulse rate. MAP, BF, $\dot{V}O_2$, and StO_2 all remained elevated throughout recovery (see Chapter 4.2.2). Sustained significant flow elevation post exercise is typical of rigorously exerted non athletic subjects and agrees with the results found in the few studies that included a prolonged recovery measurement of blood flow[84, 88, 91]. From this it can be definitively concluded that recovery from a strenuous exercise protocol can be quite prolonged in the muscle tissue.

These results highlight the importance of the previous baseline shift study as this time period would be highly susceptible to the influence of a gradual shift in blood flow (which would also affect the derived oxygen consumption rate). Furthermore, the increases found during the baseline study were of approximately the same magnitude and time course as the post exercise effects meaning that the two would be indistinguishable from each other had we not taken steps to alleviate the probe pad influence.

Total Hemoglobin concentration sharply decreased at the onset of contraction. This decrease seems to be more predominant in oxyhemoglobin than deoxyhemoglobin producing a steep desaturation curve that is consistent with other literature[54, 84]. If the initial contraction of the muscle causes a shift in overall hemoglobin distribution of the muscle that is not resolved before observation during the resting periods then there may be a change in γ (see chapter 2.4) for which it is necessary to account[16, 17, 54, 92]. Previously our lab had calculated that this change should be small enough to not present a

significant effect and could be ignored, with this view being also supported by literature [16, 92].

4.4 Gastrocnemius Translation Study Conclusions

Techniques developed by previous studies in the forearm were successfully translated to measurement of the lower limb, with attention to posture, contraction frequency, calibrating occlusions, and attachment of the optical probe. Success in calibration was evidenced by having obtained baseline absolute values for BF and $\dot{V}O_2$ that were comparable to those found in previous studies (see Tables 9 and 10). Cross validation of NIRS VO BF measurements at rest with SGVP was positive with SGVP BF being comparable in magnitude and correlated to optical values. This agreement was lost during exercise. Data were of good quality with fairly low variance (mean standard deviation of 30%, compared to over 200% changes in relative values for BF and $\dot{V}O_2$ at end exercise, the most unstable period) for subjects indicating that attachment protocols and data gating during exercise were functioning as intended.

Exercise protocols successfully induced physiological challenge in healthy control subjects and measurements during exercise were free of motion artifact due to implementation of a gating algorithm produced previously[20]. These exercise trends were also of similar profile to those of similar exercise studies, inasmuch as our continuous optical DCS measurements can be compared to profiles using SGVP and Doppler ultrasound to assess flow. Oxygenation data clearly agree with tissue saturation profiles in literature demonstrating the

effectiveness of this exercise protocol to induce challenge of the muscle. Systemic cardiovascular response also suggested effectiveness in challenging subjects and induction of whole body response to lower leg exercise, making this protocol a sound investigation of exercising hemodynamic response in healthy subjects.

Overall, we have generated a ready pool of data for young healthy control subjects against which we can compare future studies, satisfying both of the primary objectives of this study. Using these methods we may begin investigation into PAD subject populations.

CHAPTER 5: PAD PILOT INVESTIGATION OF HEMODYNAMIC RESPONSE IN COMPROMISED VASCULATURE

The aim of this pilot study was to explore the feasibility of the calibration and exercise methods discussed in Chapter 4 to a small population of PAD patients, as well as healthy control subjects. PAD in particular, being a perfusion disorder, stands out as being a disease about which our technology may be able to provide clinically relevant data. By using the calibration and dynamometer gated exercise protocol we may be able to assess local hemodynamic, metabolic, and systemic cardiovascular response differences in PAD patients as compared to healthy ones. But in order to pursue this research it was first necessary to test a small sample group and identify possible problems or inadequacies in our instrumentation/methodology. Toward this end we measured 2 patients, of different levels of claudication (one resting pain, one activity induced ischemia), and 3 healthy subjects using the protocol outlined in chapters 4.1.2 and 4.1.3, with the modification of using a sitting posture. This sitting posture is less hemodynamically demanding and so was judged to offer less chance of patients having an ischemic attack during the protocol and failing to complete it, or being unduly pained (which presents both ethical and physiological variability challenges).

5.1 PAD Pilot Experimental Protocols

In order to provide significant metabolic challenge to the lower extremity muscle tissue and vasculature, for the purpose of determining the functionality of such under stress, we decided to perform a sub-maximal plantar flexion exercise

protocol. The protocol was to be performed by a small pilot population of two PAD patients (recruited via collaboration with vascular surgeon Dr. Eleftherios Xenos, of the Kentucky Clinic) and three healthy control subjects. Subjects were recruited on volunteer basis gave consent, after being informed of the protocol to be performed, on approved IRB consent forms. Three control ages were 26, 35, 54years, while PAD patients were of similar ages, at 62 and 64. Patient ages were comparable to the ages (64 ± 3 PAD) listed in Bauer et al 2007[54]. Healthy control subjects were taking no known medications for cardiovascular disorders and had no known health conditions before the protocol was started but one healthy control subject (aged 35) did appear to have pre-hypertension. Both PAD patients were hypertensive but did not notify us as to any treatment medications such as vasodilators or diuretics. PAD Patient 1 was wearing a compression boot on his left (most claudicant) leg and reported resting pain in this leg, while the other patient had no pain at rest. This indicated that Patient 1 was in a more advanced disease state than Patient 2.

Preliminary clinical tests performed during assessment for treatment demonstrated notable differences between patients using similar continuous wave Doppler with segmental pressure exams, with the notable difference that one patient (patient 2) underwent a treadmill walking test (4 minutes, 2 mph, 12% incline). The ankle/brachial pressure index (ABI) is used to assess the degree of claudication in patients by determining the relative decrease in pressure in the lower limb as compared to the contra-lateral upper limb ($ABI = P_{ankel}/P_{brachial}$).

Generally, the scores greater than 0.95 to 1 indicate a healthy un-occluded limb while scores of less than 0.9 indicate increasing levels of claudication.

PAD patients were to be delivered to the test room via wheelchair to prevent claudicating symptoms and muscle fatigue before the protocol began. Subjects/patients were then asked to sit in an adjustable chair with their feet in a dependent (declined) position, as opposed to elevated, in order to increase perfusion pressure in the lower legs (comparing Figures 22 and 30)[90]. The instrumentation, optical probe, and data collection/processing were the same as those used to assess healthy control hemodynamics during the translation study detailed in Chapter 4.1, as were the baseline absolute hemodynamic calibrations (Chapter 4.1.2) and exercise protocols (Chapter 4.1.3) used for inducing hemodynamic challenge in this study. The entire protocol set up is illustrated in Figure 29.

Resting relative blood flow during calibration occlusions was not saved for healthy subjects, online data was used to evaluate successful occlusions for these 3 healthy subjects but was later recorded for PAD patients to better evaluate occlusion success and is now standard practice for all protocols.

a) 

b) 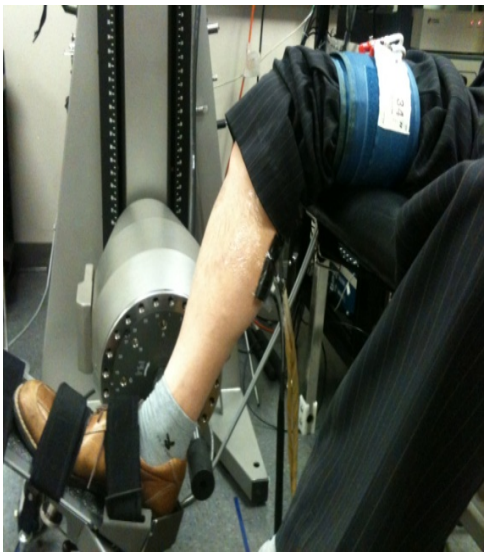

Figure 29. PAD Pilot Measurement Set-up and Probe/Leg Position

Figure 29a shows a full protocol set up during calibration phase. After calibration and MVIC test a finger plethysmograph is placed on the right hand middle digit to record systemic parameters. The device can cause bluing of the finger and mild discomfort over time and so is not used during calibration. 1) shows the placement of the optical probe (viewed more closely in figure 20) over the medial gastrocnemius muscle belly. ATT are taken from this same location. 2) Shows the hybrid FD-NIRS/DCS optical system. The operating systems for both devices are on separate computers and are controlled separately except for TTL signaling during data collection. 3) This is the dynamometer head and footplate which controls the subject work output during exercise, just off-screen is the dynamometer operation screen (at patient's eye level) which contains the visual metronome and protocol control settings. 4) The occlusion thigh cuff is shown here in its typical placement, again in a closer view in Figure 29b, as is the optical probe.

5.2 PAD Pilot Protocol Results

5.2.1 Hemodynamic Profiles During Calibration Occlusion Protocols

Resting ABIs were within normal limits with patient 1 having a 1.23 (left) and 1.2 (right) score while patient 2 had a 1.0 (left) and 0.92 (right) score. Patients were deemed by this examination to be lacking evidence of significant arterial occlusive disease at rest. The treadmill test revealed patient 2 to have non-recovering scores of 0.3 (severely occlusive) for both legs and indicated

significant arterial occlusive disease and substantial insufficiency with exercise. Given the patient histories of diabetes and high blood pressure the high normal scores for patient 1 are indicative of arterial hardening and incompressible vasculature typical of diffusive PAD. Thus the resting ABI test should always be accompanied by an exercise test for PAD examination to rule out false positives caused by such contributing disease states.

Table 11. Subject Demographics and Resting Optical Baseline Values

Subject Demographics and Key Protocol Values	Healthy Control	PAD Patients
Age (yrs)	**35, 54, 26**	**62, 65**
Skin Fold Thickness (mm)	**6.5, 6, 7.5**	**8, 7.5**
MVIC (N·m)	**91, 53, 72**	**19, 45**
Mean Power (W)	**13.7, 8.0, 10.7**	**2.9, 6.8**
Baseline StO_2 (%)	**70, 65, 68**	**55, 60**
Baseline Optical BF (ml/100g/min)	**0.43, 0.74, 0.51**	**0.07, 0.36**

With only 3 controls and 2 patients' data, not age matched, conclusions are based on and emphasize observed trends; this data is not definitive and should only be considered from the perspective of showing the potential of hybrid diffuse spectroscopy to observe the healthy and patient population trends. MVIC for healthy subjects was generally greater than patients, with corresponding powers of exercise being higher. This suggests that there is a strength gap between healthy subjects and PAD patients but without more subjects this is a highly preliminary assessment.

The calibration protocol for healthy controls proceeded normally and was consistent in trend for all subjects (illustrated in Figure 30). Individual values for initial blood flow and oxygen consumption rate varied widely but were within ranges of previous studies, at 0.43 to 0.74 ml/100ml tissue/min for blood flow and 0.015 to 0.11 mlO_2/100g /min for oxygen consumption rate and no artifact was noted during the occlusions/fitting estimates (Figures 30 and 31, Table 12). Note that rBF for healthy controls during calibration were not recorded. The success of the occlusions is demonstrated by normal increases in THC during VO, and mostly stable THC during AO accompanied by divergent Hb (increase) and HbO_2 (decrease) as seen in Figure 30.

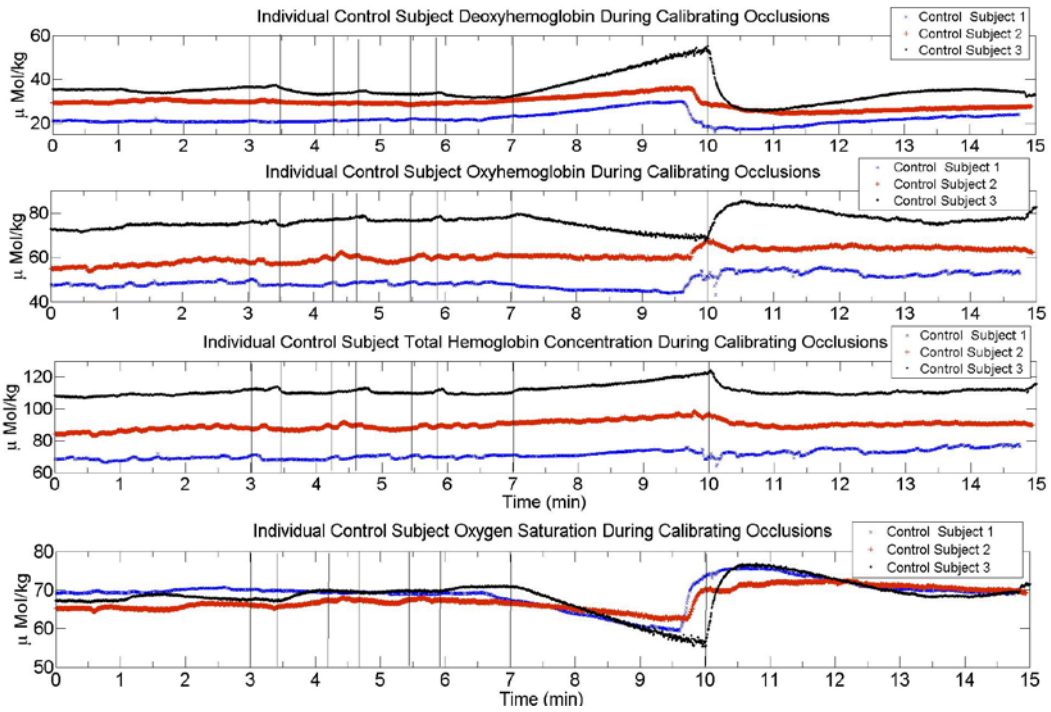

Figure 30. Calibration Hemoglobin Time Courses for Healthy Control Subjects

Descending order: Deoxy, Oxy, and THC, and StO_2. Occlusion periods are shown by arrows (to account for slight differences in occlusion time periods) with small arrows representing VO, and large arrows the AO.

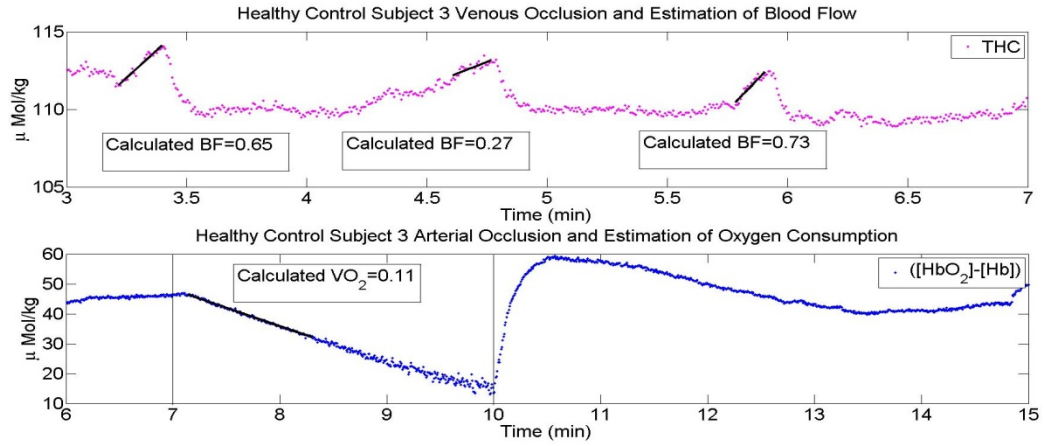

Figure 31. Sample Healthy Control Subject Occlusions with Calculated Resting Blood Flow and Oxygen Consumption Rate

VOs (top panel) were largely consistent and produce a physiologically normal resting muscle blood flow. Success of the arterial occlusion is observed in the immediate decrease in $[HbO_2]$ compared to [Hb] and the typical oxygen consumption rate value calculated.

PAD patient calibrations were met with mixed success. While venous occlusions and initial blood flow measurements seemed to be successful, no absolute $\dot{V}O_2$ values are available for PAD subjects. This is due to arterial occlusions being unsuccessful in these subjects, as can be observed both by the hemoglobin concentration (non diverging [Hb] and [HbO_2]) and by the additional observation of non zero relative blood flow during occlusion (Figures 32 and 33,).

Initial oxygen saturation values for healthy subjects ranged from 65 to 70% compared to PAD patients who had saturations of 60% and 55% at rest (Figure 30 and Figure 32, Table 11). PAD patient resting blood oxygen saturations were lower than all healthy controls. The resting oxygen saturation of PAD patients are comparable to the end arterial occlusion values of the healthy controls, suggesting that resting patient muscle is in a substantially hypoxic environment (Figure 30 and Figure 32). Neither patients' hemoglobin nor oxygen saturation values returned to rest within 5 minute recovery periods, indicating an observable lack of recovery in PAD patients compared to healthy controls. Calibration BF values for healthy subjects ranged from 0.74 to 0.43 ml/100ml tissue/min, while patients had widely different values of 0.07 and 0.36 ml/100ml tissue/min, both of which were values lower than even the smallest of the healthy control values.

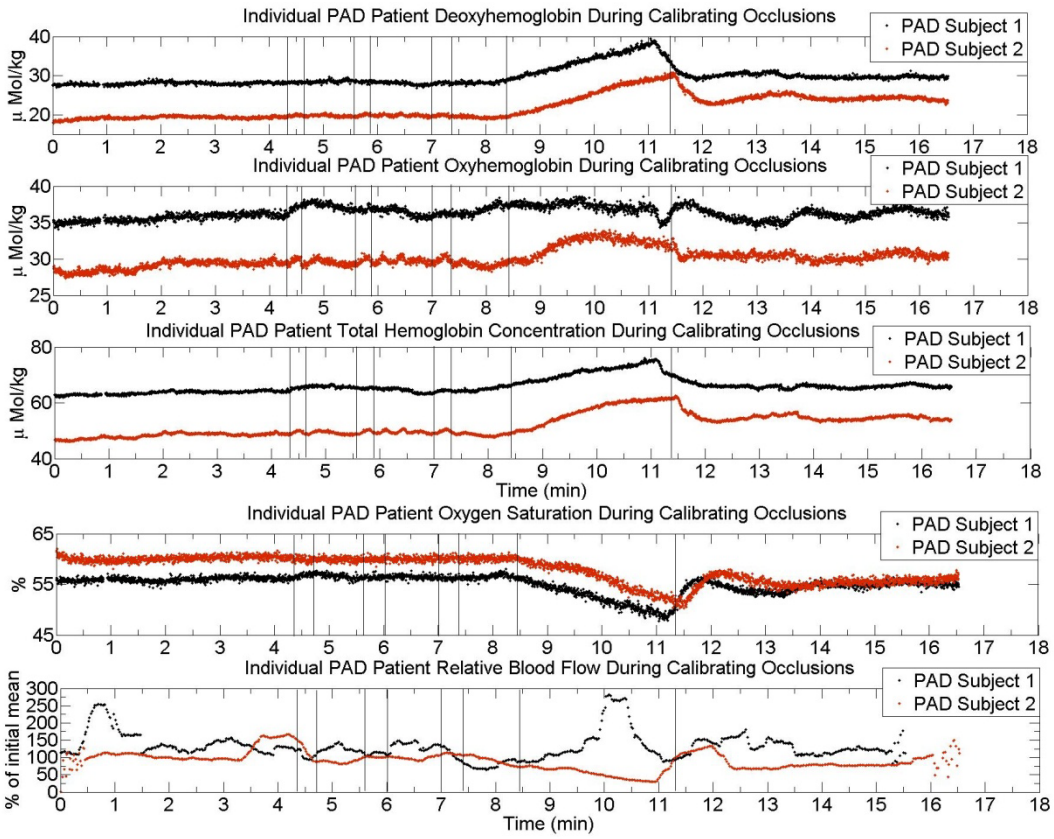

Figure 32. Calibration Hemoglobin Time Course for PAD Patients

Descending Order: [Hb], [HbO_2], and THC, StO_2, and rBF. Vertical lines denote three VOs, followed by a single AO time period. Subjects' responses to occlusion were markedly different, with Subject 1 possessing a highly muted blood flow and lower resting oxygen saturation than Subject 2. Neither subject could produce a successful arterial occlusion, as indicated by the oxygenated and total hemoglobin responses (second and third panel from the top). 250 mmHg pressure was used in Subject 2 AO but Subject 1 could not withstand this pressure (due to pain). rBF data show that rBF in Subject 1 is not greatly affected by this pressure (250 mmHg).

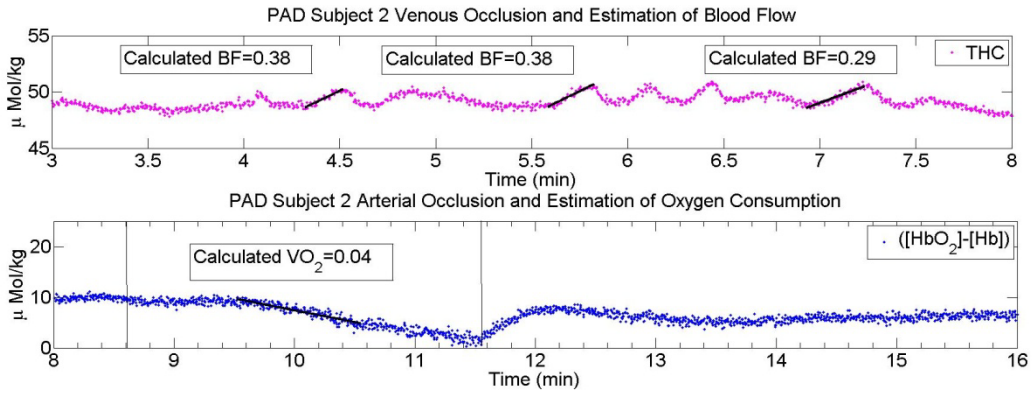

Figure 33. Sample PAD Patient Occlusions with Calculated Resting Blood Flow and Oxygen consumption rate

VOs (top panel) were successfully performed and with reasonable outcome. The AO (marked by vertical lines) displays a notable delay from onset of occlusion to apparent decrease in difference between HbO_2 and Hb. This is evidently due to the inability to fully restrict arterial inflow (see Figure 33) which causes a large underestimate of oxygen consumption rate despite relatively normal (low) blood flow. This calculated oxygen consumption rate value is not deemed to be acceptable for use in estimating resting tissue metabolism.

5.2.2 Hemodynamic Profile During 30% MVIC Plantar Flexion Protocols

Lacking a robust statistical relevance in this data set, individual data are presented and time series trends/mean values are presented, for the sake of this pilot study. A note on results from the first PAD patient should be made in that the subject was unable to maintain the correct rhythm initially and thus data were initially unstable during exercise (as indicated by large deviations) until coached into the correct rhythm for the appropriate duration of exercise at the 0.5Hz frequency.

Hemoglobin concentration changes differ between the groups with PAD patients exhibiting a muted change in all hemoglobin concentrations compared to healthy control subjects. All subjects exhibited an initial increase in oxygen saturation at the onset of exercise and this is observable to be related to the initial

clearance of [Hb] compared to desaturation of [HbO_2] (Figures 34 and 35). This trend has been observed in other studies under similar conditions[31, 54]. The observed hemoglobin time course is consistent with previous results for plantar flexion exercise (Chapter 4).

Exercise values (see Table 12) for healthy controls were generally robust, increasing a mean (787.4%, 609.5%, and 219.9% respectively from baseline. These healthy profiles followed the same trend observed in Chapter 4 healthy control exercise of rapid initial increase, plateau, and rapid decrease following the end of exercise (see Figure 34). PAD patients demonstrated sharply different responses from one another with the claudicant patient rBF increasing by a mean 216% while the less severe patient rBF increased to a mean 710% (Figure 35, Table 13). $r\dot{V}O_2$ values were different in trend between healthy and patient populations, with mean exercise $r\dot{V}O_2$ being typically lower than mean exercise rBF (89.8% higher, 125.9% lower, and 51.5% lower) for control subjects 1 through 3 respectively (Table 12). PAD patients had mean exercise $r\dot{V}O_2$ values that were only 5.0% lower (in the resting claudicant patient 1) and 26.4% lower (in the mild PAD patient 2) than end exercise rBF (Table 13). This suggested a larger increase in oxygen extraction for those PAD subjects with a lesser blood flow. Absolute blood flow seemed to be greater in most of healthy controls (3.88, 5.34, and 1.69 ml/100ml tissue/min) than in patients (0.14 and 2.56 ml/100ml tissue/min). Particularly notable was the difference between the claudicant PAD patient profile and the rest of the subjects (Figures 34 and 35, Tables 12 and 13). Oxygen saturation trends were greatly divergent however with healthy subjects

exhibiting desaturation during exercise while patients possessed very little change, even increasing during exercise (Figure 34 and 35).

Recovery was incomplete for most subjects in all parameters except pulse rate, which tended to not be significantly different from baseline (Table 12 and 13). The 1st minute and 15 minute recovery values were calculated and indicated rapid recovery but a sustained super baseline level for both local parameters and systemic MAP persists, similarly to the results of chapter 4 protocols.

The systemic data (pulse rate and MAP) for both populations show a response with a trend of increase during exercise. MAP data is, however, notably unstable (see Figure 35) for both patients, which may indicate some plethysmograph instrumentation errors. The two patients are clinically hypertensive as is one of the control subjects (as defined by a resting MAP >105). These data are not stable or consistent enough on which to base any sound conclusions, given the instability in the instrument for observation of the PAD patients.

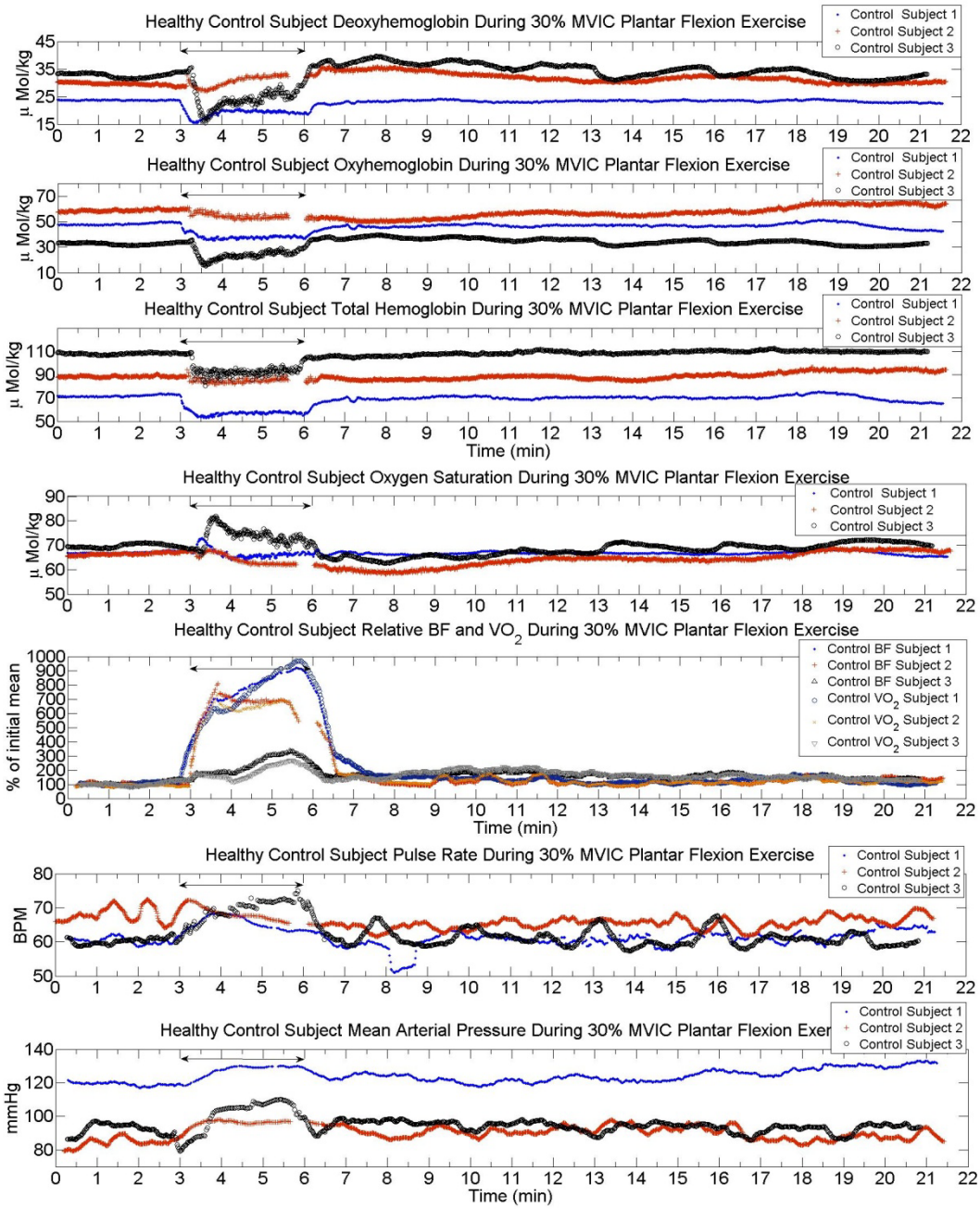

Figure 34. Healthy Control Subject Hemodynamic Profiles During Dynamic Exercise

Descending order: [Hb], [HbO_2], and THC, StO_2, rBF and $r\dot{V}O_2$ coaxially, pulse rate, and MAP. Exercise periods are denoted with a black arrow. Note here that the oxy saturation increases at onset of exercise before decreasing, in contrast to the slight increase followed by plateau of PAD subjects.

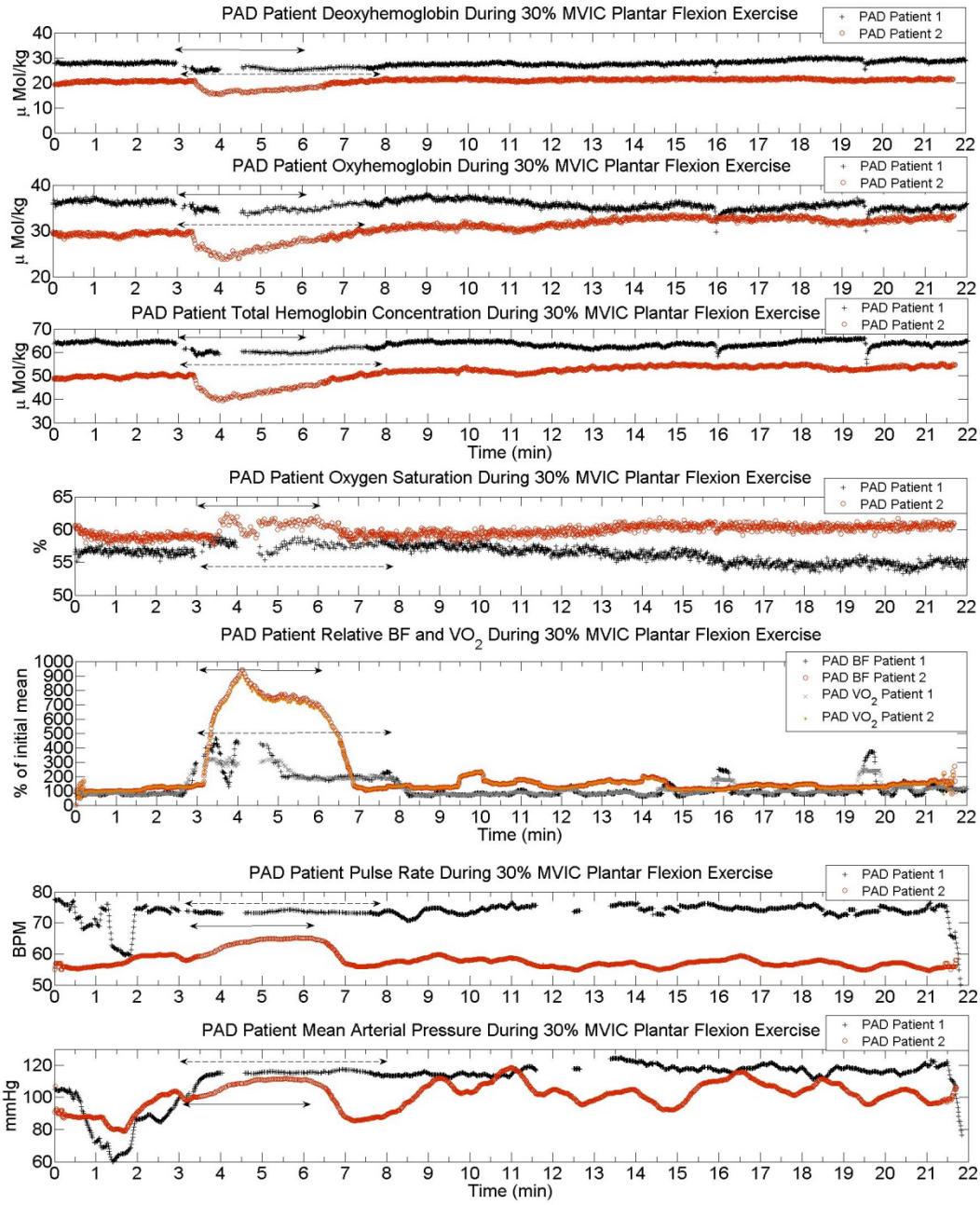

Figure 35. PAD Subject Hemodynamic Profiles During Dynamic Exercise

Descending order: [Hb], [HbO_2], and THC, StO_2, rBF and $r\dot{V}O_2$ coaxially, pulse rate, and MAP. Exercise periods are denoted with a dotted black arrow for subject 1(due to inability to retain correct rhythm, initially) and solid for the second patient. Data shown are the filtered individual time series, filtration is done as previously described. Of note is the apparent lack of decrease in oxygen saturation and lack of separation between relative blood flow and oxygen consumption rate curves.

Table 12. Summary for Healthy Control Subject Hemodynamic Values

Time Period Mean	Control 1	Control 2	Control 3
Baseline rBF (%)	106.3±30.8	99.9±33.8	106.7±49.7
Baseline BF (ml/100ml/min)	0.46±0.13	0.75±0.25	0.55±0.26
Baseline r$\dot{V}O_2$ (%)	111.9±32.0	75.0±25.3	108.6±51.2
Baseline $\dot{V}O_2$ (mlO_2/100g/min)	0.045±0.013	0.015±0.005	0.098±0.046
Baseline MAP (mmHg)	119.2±1.0	84.6±2.6	92.0±3.8
Baseline Pulse (BPM)	60.4±0.9	68.0±2.2	60.2±0.9
End Exercise rBF (%)	893.7±121.8*	709.4±201.9*	326.6±102.1*
End Exercise BF (ml/100ml/min)	3.88±0.53*	5.34±1.52*	1.69±0.53*
End Exercise r$\dot{V}O_2$ (%)	983.5±146.6*	583.5±165.3*	275.4±86.5*
End Exercise $\dot{V}O_2$ (mlO_2/100g/min)	0.393±0.059*	0.117±0.033*	0.248±0.078*
End Exercise MAP (mmHg)	129.6±0.4*	96.8±0.3*	106.5±4.0*
End Exercise Pulse (BPM)	63.7±0.5*	66.3±0.6*	72.2±0.8*
Recovery 1 min rBF (%)	398.7±260.7*#	239.7±177.4*#	160.5±62.0*#
Recovery 1 min BF (ml/100ml/min)	1.73±1.13*#	1.80±1.34*#	0.83±0.30*#
Recovery 1 min r$\dot{V}O_2$ (%)	444.0±293.9*#	201.8±147.8*#	143.3±58.3*#
Recovery 1 min $\dot{V}O_2$ (mlO_2/100g/min)	0.178±0.118*#	0.040±0.030*#	0.129±0.053*#
Recovery 1 min MAP (mmHg)	123.9±1.97*#	95.1±0.7*#	94.2±3.6*#
Recovery 1 min Pulse (BPM)	61.1±1.9*#	65.2±0.2*#	64.0±3.9*#
End Recovery rBF (%)	101.5±37.1#	145.3±46.3*#	134.9±50.9*#
End Recovery BF (ml/100ml/min)	0.44±0.16#	1.09±0.35*#	0.70±0.26*#
End Recovery r$\dot{V}O_2$ (%)	107.2±39.1#	103.6±32.9*#	136.1±51.1*#
End Recovery $\dot{V}O_2$ (mlO_2/100g/min)	0.042±0.016#	0.021±0.007*#	0.123±0.046*#
End Recovery MAP (mmHg)	131.0±1.5*#	88.0±2.4*#	94.3±0.9*#
End Recovery Pulse (BPM)	64.2±0.4*#	67.1±2.0*	59.2±0.4*#

Data presented as mean ± std for each individual. These were calculated from 3 mins baseline data (150 frames), the final minute of exercise data (20-30frames), the first minute of recovery data (50 frames), and the final minute of recovery data (50 frames). Significance ($p < 0.05$) is represented by * for comparing against baseline, and # for significance from end exercise. Raw time series data were selected according to data frame time stamps to ensure accurate time points.

Table 13. Summary for PAD Patient Hemodynamic Values

Time Period Mean	PAD 1	PAD 2
Baseline rBF (%)	112.4±50.7	106.4±37.3
Baseline BF (ml/100ml/min)	0.07±0.03	0.38±0.13
Baseline r$\dot{V}O_2$ (%)	111.2±49.9	107.5.0±37.9
Baseline MAP (mmHg)	97.9±5.2	88.7±5.9
Baseline Pulse (BPM)	74.3±2.0	57.0±1.6
End Exercise rBF (%	215.7±143.3*	709.7±219.7*
End Exercise BF (ml/100ml/min)	0.14±0.09*	2.56±0.79*
End Exercise r$\dot{V}O_2$ (%)	210.7±144.0*	683.3±208.3*
End Exercise MAP (mmHg)	115.9±0.7*	110.2±1.6*
End Exercise Pulse (BPM)	73.5±0.3*	64.9±0.3*
Recovery 1 min rBF (%)	136.5.7±132.9*#	165.0±155.5*#
Recovery1min BF (ml/100ml/min)	0.09±0.09*#	0.60±0.56*#
Recovery 1 min r$\dot{V}O_2$ (%)	132.7±128.6*#	165.5±155.0*#
Recovery 1 min MAP (mmHg)	113.9±0.6*#	91.6±6.8*#
Recovery 1 min Pulse (BPM)	72.8±1.0*#	58.4±2.7*#
End Recovery rBF (%)	98.6±37.1#	151.0±74.9*#
End Recovery BF (ml/100ml/min)	0.06±0.04#	0.54±0.27*#
End Recovery r$\dot{V}O_2$ (%)	103.5±69.7#	146.8±72.8*#
End Recovery MAP (mmHg)	116.0±1.1*	102.6±2.1*#
End Recovery Pulse (BPM)	74.0±0.8#	56.4±0.8*#

Data are presented as mean ± std for each individual. These were calculated from 3-minute baseline data, the final minute of exercise data, the first minute of recovery data, and the final minute of recovery data. Significance ($p < 0.05$) is represented by * for comparing against baseline, and # for significance from end exercise. Raw time series data were selected according to data frame time stamps to ensure accurate time points. Due to failure to adequately occlude the limb $\dot{V}O_2$ could not be determined for these patients.

5.3 PAD Pilot Protocol Discussion

5.3.1 Calibration Protocol

The results of this pilot indicate that there seems to be a combination of factors involved with PAD. The most obvious parameter is the reduced resting oxygen saturation. The baseline oxygen saturation measured in these two subjects was below or near those reached during the end of 3 minutes arterial occlusion or at the end of exercise for healthy control subjects (see Table 11, Figure 30 and Figure 32). This disparity clearly indicates that PAD is an ischemic condition, which is supported by most PAD literature [3, 13, 55, 93]. The ability of NIRS instrumentation to observe difference in baseline oxygen saturation is a positive sign for future studies being able to discern possible PAD tissue perfusion effects at rest.

Optical venous occlusion measurements were able to calibrate initial blood flow for the DCS instrument in both healthy and patient subjects. The patients, particularly the resting claudicant, had lower baseline BF than healthy subjects. We were unable to calibrate our $r\dot{V}O_2$ measurements in PAD patients since we could not successfully induce a total AO in either subject. The claudicant patient was unable to tolerate arterial occlusion pressures due to claudication pain. The second patient, even at 250 mmHg, could not sufficiently be occluded (see Figure 32) as to be able to assume an isolated compartment. As a result, both patients exhibited marked arterial leakage (Figures 32 and 33) which invalidated the calibration occlusion. Given the sensitive nature of later stage PAD patients and

the likelihood that some future studies may attempt comparisons between pre and post operative patients to assess successful reperfusion surgery, AO calibration may not be feasible within this subject population. However, our recent studies have shown that using a VO protocol can also estimate oxygen consumption rate, which will be explored in PAD patients in the future[94, 95].

Baseline and calibration occlusion trends for absolute hemoglobin and relative blood flow were observable for all subjects using the methods outlined in 4.1.2 and these were similar to those results found in chapter 4.2.1. Despite observable indications that there may be a different StO_2 trend during recovery from AO we cannot say that such difference is positively confirmed, nevertheless the trends for oxygen saturation between the two PAD subjects were consistent between each other and are suggestive of tissue oxygenation effects due to PAD being possibly quantifiable by NIRS spectroscopy.

Depressed tissue saturation and muscle strength is indicative of compromised function in the gastrocnemius microvasculature for these patients. The PAD patients we measured, especially the resting claudicant, were substantially weaker than controls. Without more subjects no generalizations may be made about control and patient populations strength however, and some literature indicates that there may be no difference in strength for mild PAD[54]. It should be noted that since healthy controls were not age matched the effect of age on all these parameters cannot be evaluated and age matching would be paramount to establish in a full scale study with MVIC used as a possible regression parameter for predicting $BF/\dot{V}O_2$ response to exercise.

5.3.2 Exercise Protocol

Following trends in previous studies, individual responses varied widely between individuals but in the case of this protocol the responses were much more robust for healthy controls. The large increases in rBF found in these subjects (including both healthy subjects and a patient) compared to Chapter 4 responses may indicate that postural perfusion pressure may be more potent than previously assumed. As expected, the resting claudicant subject was unable to greatly increase flow and appeared to fatigue before the end of the protocol as the exercise flow response could not be maintained throughout the protocol. While this exercise intensity may be applicable in the seated position, it would likely prove too strenuous for severely claudicant patients or for patients measured in supine.

The apparent increase in oxygen saturation at the onset of exercise is likely attributable to a fluid shift since THC, HbO_2, and Hb decrease initially but Hb is preferentially removed indicating venous clearance by the muscle contraction, a similar trend is observed in forearm data reported by our lab[20]. The lack of desaturation and overall hemoglobin profile in these subjects is different from that observed in Chapter 4 protocols and requires more data to be conclusive but does demonstrate potential for observing differential responses to exercise onset.

Relative oxygen consumption rate trends closely follow those of relative blood flow for healthy controls indicating that these subjects have a flow dominated increase in oxygen consumption rate as opposed to an extraction dominated one.

These responses, at least for healthy control subjects, are in contrast to the Chapter 4 protocol results in that $\dot{V}O_2$ nearly uniformly increased much more than BF as would be expected of a metabolically challenging protocol. These responses were consistent among patients with most subjects having an $r\dot{V}O_2$ unexpectedly close to rBF, but more data is required before this observation can be assumed to apply to the general population. The ability to monitor both flow and oxygen metabolism in comparison to one another may prove to be a potent tool in determination of possible PAD effects on muscle oxygen utilization.

Pressure responses were similar to previous protocols in that there was a distinct increase in MAP during the protocol and a decrease to a super baseline pressure throughout the recovery period. Pulse rates are also consistent with previous protocol results, recovering completely. Systemic parameters were not greatly different compared to healthy controls, indeed the blood pressure profiles were more similar than initially assumed and would not explain the differences in exercise responses observed. Pulse rate and MAP were clearly elevated for all subjects during exercise, except the claudicant who could not generate enough effort to stimulate pulse rate response.

5.4 PAD Pilot Protocol Conclusions

Important for the purposes of this pilot, all subjects could complete the majority of the protocols with the exception of arterial occlusions which require re-evaluation for employment/stability in patient populations and may possibly be

replaced by a venous occlusion protocol to calibrate resting oxygen consumption rate.

Systemic and local hemodynamic profiles were generally in line with those observed in supine healthy control exercise protocols sharing rapid changes at onset/end of exercise with sustained hemodynamic elevation persisting throughout the 15-minute recovery period, with the exception of the oxygenation data discussed above. Of particular interest, it was found that there seemed to be a different trend of response in healthy control hemodynamics while sitting compared to supine. This might be due to the difference in hemodynamic environments from supine to sitting posture and so much more data is required to be able to draw meaningful comparisons between healthy control responses in sitting vs. supine subjects let alone disease populations against healthy ones. With such a small subject size we cannot verify the generality of these responses but the overall similarity with previous studies and broadness of the hemodynamic data that we were able to obtain is promising.

Overall, this pilot was successful in demonstrating the potential of a hybrid flow/oximeter in observing and quantifying local muscle hemodynamics. The protocol methodology proved mostly sound and was repeatable for 5 subjects. While some questions pertaining to calibration, postural effects, and finger plethysmograph reliability must be resolved the hybrid diffuse optical methods and overall protocol design are ready for refinement to begin a broader set of experiments. Future studies, with greater numbers of subjects may more rigorously assess PAD hemodynamic responses based on these findings. Lastly,

the normal range of ABI test values for the patients at rest clearly indicates need for alternative means of detecting claudication and determining patient muscular microvascular health. For the purposes of more clearly defining disease status in future patient populations it would be preferable to use walking tests for all patients to better ascertain the level of claudication of each patient. These may then be used, in conjunction with our local measurements and exercise protocol, to better quantify disease progression and regress data on the basis of hemodynamic response versus clinical predictors.

CHAPTER 6: LIMITATIONS, SUMMARY, AND PERSPECTIVES

6.1 Limitations of Optical Spectroscopy and Measurement Methodology

The limitations of diffuse optical techniques, particularly DCS, are predominantly related to the light penetration depth into the tissue. Low power NIR light sources and single mode detection fibers make for a maximal tissue penetration depth of ~1.5 cm for DCS, depending on tissue absorbance and power delivery to the tissue[31, 44, 96]. NIRS allows for the use of larger multimode detector fibers and can collect oxygenation data in tissues up to ~3 cm deep[13, 31, 59, 64, 65]. The current penetration depth of DCS allows for examination of the superficial skin and muscles but not deeper muscles and organs. The use of bundled detector fibers greatly improves what signal we may obtain from these tissues, even at greater depths[31-33, 41, 59].

Related to penetration depth is the inability of (especially DCS) optical signal to reliably escape from large vessels. The high absorber concentration (blood volume) of the veins and arteries means that optical probes positioned with large vessels in the photon diffusion path length experience greatly reduced signal amplitude resulting in the inability to correlate flow or determine tissue oxygenation through these vessels. Probes should be positioned carefully to avoid optical paths through such vessels. This disadvantage compensates by strictly limiting our observations to microvascular flow.

Temporal resolution is dependent on correlation time, which is itself dependent on signal strength. While each individual correlation curve calculation is very rapid (~20 Hz or 50 ms per curve), these curves must be averaged to

reduce noise[20, 33]. With low absorbance tissues (female muscle e.g., typically exhibits a much greater signal to noise ratio as compared to male muscle tissue) correlation averaging times may be decreased, increasing the ultimate sampling frequency. Experimentally, it was general practice here for leg muscles to use sampling rates of 1-2 Hz, which when coupled with oximetry, resulted in an overall sampling rate of 1 Hz for every hemodynamic parameters (MAP, pulse rate, BF, [Hb], [HbO_2], THC, StO_2, $\dot{V}O_2$).

The use of an optical probe secured directly to the tissue surface has its own problems. Contact measurements are subject to introducing curvature errors due to the flattening of soft tissue underneath the optical probe[96]. Sharply curving surfaces, such as small limbs, alters the geometry of the probe/tissue interface and, in the case of small tissue volumes, may induce spatial violations of the semi-infinite boundary condition[96]. Contact probe pressure can also generate substantial hemodynamic response in resting baselines and during exercise. The reasons for this are explored in detail in Chapter 3.

Previously, a major limitation was that of motion artifacts. Changes caused by motion may be observed in both NIRS oximetry and DCS, but DCS is influenced in a particular way that makes it more susceptible to artifact. The ratio of dynamic to static scatterers (α) is assumed to remain constant during measurements reflecting at least short term stability in hematocrit. It is this assumption that can lead to motion artifacts during measurements however. When non-blood related cells move, light is scattered by these additional dynamic scatterers e.g., muscle fibers and α is substantially increased. This causes a

greatly overestimated flow index and its effects are noted in literature using DCS methodology to observe muscle systems[16, 20, 44, 83]. Much of this artifact can be avoided by careful protocol control and subject training. The restriction of data collection to static phases of exercise allows a very near approximation to continuous observation without loss of important data.

An exercise protocol specific problem was that it proved difficult for patients and new subjects to adjust to the exercise timing. The pacing for contraction and rest are crucial to collecting stable data and difficulties in proper timing result in erratic data points (see PAD subject 1 exercise data, chapter 5.2.2). Also, some questions arise as to how much MVIC tests and the familiarization period may impact baselines. Extended responses to exercise indicate potential for elevation between calibrating occlusions and exercise baselines, thus it may be preferential to separate this procedure either by moving it to the start of the protocol and requiring 25 to 30 minutes before calibrating occlusions, or doing it on a separate day.

One of the challenges of measuring exercise hemodynamics is the large (and widely documented) range of inter-patient variation. We noted substantial differences in hemodynamic response even with strength normalization and age matching, and this indicates that large populations will be required to assess the diagnostic quality of these measurements. Statistical analyses demonstrate that the results are more robust with 10 subjects providing a power of greater than 80% for baseline mean comparisons, rest vs. end-exercise comparisons, and end-recovery vs. baseline comparisons. rBF was used as a test variable for these

studies and the results of power analysis extrapolated onto the remaining variables, given the comparably large responses in these parameters with lesser variance.

6.2 Summary of Research and Perspectives

Initial research aims of my study were to adapt the hybrid diffuse optical techniques developed during previous examinations of forearm flexor muscles to the lower leg muscles (gastrocnemius) during dynamic exercise. The intent for this was to open a line of research into diseases of the vasculature and assessing lower limb muscle tissue performance via hemodynamic and metabolic parameter profiles during exercise.

Preliminary examinations and prior research indicated an unexpected baseline shift during contact measurements and these had to be rectified before satisfactory post exercise data collection or long duration protocols could be considered. Baseline evaluation studies confirmed and characterized the baseline shift and subsequent probe/protocol redesigns greatly stabilized the contact measurements. In addition to greatly decreasing the measurement effect on the muscle tissue the baseline studies confirmed the sensitivity of muscle microvasculature to circumferential applied pressure. The baseline flow increase agreed in trend with clinical assessments of the effectiveness of elastic bandaging for increasing perfusion in the limb, a common treatment for vascular insufficiency related disorders like PAD[69, 72, 73, 82]. By confirming the effectiveness of protocol

redesigns in both the forearm muscles and gastrocnemius we were able to proceed with lower limb studies.

Translating hybrid NIRS/DCS exercise measurement methods to the lower limb involved first identifying accepted dynamic exercise protocols which could be used in conjunction with our equipment and which could be controlled for reproducibility. Dynamometer based plantar flexion exercises were decided upon as was previously the case in forearm studies, for their commonality and for the great control over exercise motions and associated data collection via the dynamometer signaled positional gating algorithm developed previously. We finally determined a comparable protocol which was in agreement with standard practices in physiological journals, applicable to patient populations, and allowed for optimal use of our NIRS spectroscopy[13, 18, 54, 61, 83, 84, 97].

Using a concurrent strain gauge measurement, we cross-validated our absolute BF calibration by the optical technique during repeated VOs, finding correlation between the two measurements of baseline BF. Healthy control subjects produced hemodynamic profiles during exercise which agreed with those in literature and against which we can compare future vascular/muscle disease studies[13,17,54,55,83].

Lastly, a pilot study was performed to explore the feasibility of using the calibrated hybrid spectroscopy and gated exercise protocol methodology for PAD patient studies. The small population size, as mentioned previously, limits the amount of empirical conclusion that may be made based on this data but results

were promising. The measurement methodology proved no more difficult to apply to patients than to healthy subjects and did not incur any medical risks towards the patients. One flaw in the calibration protocol was that the arterial occlusion (but not venous) was unable to apply sufficient pressure, or such pressures induced pain and could not be applied, such that baseline absolute $\dot{V}O_2$ could not be calibrated and only the relative change in this parameter could be observed during exercise. Subsequent research by other lab members applied a similar method of calibrating both flow and oxygen consumption parameters with venous occlusions that remedies this shortcoming[94, 95].

Exercise protocols produced continuous hemodynamic/metabolic profiles for both healthy control and patient groups and the results thereof indicate a promising line of research for investigation of PAD effects on muscle tissue. By making use of the noninvasiveness, rapid sampling time, and continuous collection properties of hybrid diffuse optical flow-oximetry in muscle tissue during exercise the ability of the muscle to adapt/respond to metabolic stress can be assessed for long periods of time and during dynamic protocols. Application of these methods to future full-scale studies is likely to produce a unique investigation of muscle physiology and disease pathophysiology, but many more patients and healthy control subjects will be required to reach statistical and diagnostic relevance.

In conclusion, the overall objectives of this research were successfully met in that we were able to refine our measurement stability for contact probe DCS-Imagent hybrid spectroscopy on *in-vivo* muscle tissue and to extend the range of

calibrated, standard unit, absolute measurements to the lower limb musculature. We then obtained a consistent set of healthy control subject exercise responses, for a variety of measured parameters (and subsequent derived parameters), which could be used to monitor tissue hemodynamics/metabolic response to exercise stress. Using such measurements as a basis of comparison, the initial steps were taken to begin investigation of muscular disease states and their effects on muscle tissue microvascular hemodynamics and metabolism at rest and during exercise.

Appendix

Notes on Strain Gauge Plethysmography

Strain gauge plethysmography has many documented faults as an approach to dynamic measurements since it can be greatly affected by fluid shifts typical of working limbs (bone flow, interstitial fluids etc.) but this group found that more than these theoretical flaws, implementing the strain gauge was difficult during exercise due to the need to precisely apply a low pressure to the limb to get a venous occlusion. Despite limiting the movement of the limbs complete lack of motion is impossible and even small motions can loosen the pressure cuff (which must be applied so as to not induce enough passive pressure to cause baseline shift). This means that achieving venous occlusion without disturbing the hemodynamics of the limb is difficult at best (and may explain the underestimate of our venous occlusion values) if done properly.

Reasons for the possible underestimates in our strain gauge data are not certainly known but are suspected to lay elsewhere than the strain gauge itself and the recorded data as the sensitivity of the strain gauge to volume changes was very high and the variability between individual BF measurements during calibration quite low (mean standard deviation of 0.086). Pressure considerations being what they were, we erred on the side of conservatism in applying the cuff and this could have produced incomplete venous occlusions which (due to rapid changes in hemoglobin post exercise) would be difficult to confirm using local NIRS measurements. Post exercise VO can be observed in some subjects NIRS

data via data frame time stamps (as in Figure 27) but were not observable in enough cases to be correlated, and cannot be verified with the strain gauge itself. Literature reporting resting muscle blood flows as low as 0.9 to 1.1 ml/100ml tissue/min and as high 5 as have been observed using strain gauge plethysmography[98]. The large degree of variability in blood flows reported in literature from one study to the next suggests that there is a methodological or equipment induced variation between groups that introduces substantial difference in observed blood flow despite the procedure for strain gauge plethysmography being tested and accepted as reliable and individual groups reporting low variance within their respective studies. Given that our blood flow values are within physiologically accepted ranges for resting blood flow and ranges reported by other groups we may assume that our strain gauge data are reliable at rest. Overall, strain gauge venous plethysmography can be considered a useful tool to assess blood flow in resting conditions but is, in this author's experience, not trustworthy in dynamic measurements or for patient populations including elevated blood pressure conditions, which encompasses the PAD patient population, due to the increased mean pressures and often sclerotic vessels making occlusions very difficult to reliably achieve, without applying pressures in excess of those known to restrict vessel diameters[27].

REFERENCES

1. Scott K. Powers, Edward Howley, as presented by Brian B. Parr, Ph.D of University of South Carolina Aiken, *Skeletal Muscle: Structure and Function* in *Exercise Physiology: Theory and Application to Fitness and Performance*, 2009, The McGraw-Hill Companies, Inc.

2. Wolfe, R.R., *The underappreciated role of muscle in health and disease.* Clinical Nutrition, 2006. **84**: p. 475-82.

3. National Center for Chronic Disease Prevention and Health Promotion, D.f.H.D.a.S.P. *Peripheral Arterial Disease (PAD) Fact Sheet*. Fact Sheets, 2011.

4. National Center for Chronic Disease Prevention and Health Promotion, D.f.H.D.a.S.P. *Muscular Dystrophy*. Data and Statistics, 2012.

5. W. Wiedemair, M.A.Weber., A. Kroll, P. Kindl, and L. R. Schad, *Measurement of skeletal muscle perfusion at rest and its change after exercise using Arterial Spin-Labelling.* Proceedings of the International Society of Magnetic Resonance Medicine, 2007. **15**: p. 2666.

6. Stanley P. Brown, Wayne C. Miller, Jane M. Eason, Ph.D., *Exercise Physiology: Basis of Human Movement in Health and Disease* 2006: Lippincott, Williams, and Wilikins. 652.

7. Marc-André Weber, Martin Krix, Uta Jappe, Hagen B. Huttner, Marius Hartmann, Uta Meyding-Lamadé, Marco Essig, Christoph Fiehn, Hans-Ulrich Kauczor, Stefan Delorme, *Pathologic Skeletal Muscle Perfusion in Patients with Myositis: Detection with Quantitative Contrast-enhanced US—Initial Results.* Radiology, 2005. **238**: p. 640-49.

8. Hermansen, L., Ekblom B., *Cardiac output in athletes.* Journal Applied Physiology, 1968. **25**(5): p. 619-25.

9. Robert Zelis, John Longhurst, Robert J. Capone, Dean T. Mason, Robert Kleckner, , *A Comparison of Regional Blood Flow and Oxygen Utilization During Dynamic Forearm Exercise in Normal Subjects and Patients with Congestive Heart Failure* Circulation, 1974. **50**: p. 137-43.

10. Haacke EM, Lai S., Reichenbach JR, Kuppusamy K., Hoogenraad F.G., Takeichi H., Lin W., *In vivo measurement of blood oxygen saturation using magnetic resonance imaging: a direct validation of the blood oxygen level-dependent concept in functional brain imaging.* Human Brain Mapping, 1997. **5**(5): p. 341-6.

11. Peter Jezzard, Paul M. Matthews, Stephen M. Smith, *Functional MRI: An Introduction to Methods,* 2001, Great Clarendon Street, Oxford Oxford University Press.

12. Deblasi, R.A., Ferrari M., Natali A., Conti G., Mega A., Gasparetto A., *Noninvasive Measurement of Human Forearm Oxygen-Consumption by near-Infrared Spectroscopy.* European Journal of Applied Physiology, 1994. **67**(1): p. 20-25.

13. H.M. Koojiman, M.T. Hopman, W.N. Colier, N.J. J.A. van der Vliet, and B. Oeseburg, *"Near Infrared Spectroscopy for Noninvasive Assessment of Claudication".* Journal of Surgical Research 1997: p. Vol.72:1-7.

14. Casavola C., Paunescu L.A., Fantini S., Gratton E., *"Blood Flow and oxygen consumption with near-infrared spectroscopy and veneous occlusion: spatial maps and the effect of time and pressure of inflation".* Journal of Biomedical Optics, 2000: p. Vol.5(3): 269-76.

15. Durduran, T., *Non-invasive measurements of tissue hemodynamics with hybrid diffuse optical methods*, in *Physics and Astronomy*2004, University of Pennsylvania: University of Pennsylvania. p. 266.

16. Guoqiang Yu, Tergut Derderan, Gwen Lech, Chao Zhou, Britton Chance, Emile R. Mohler III, and Arjun G Yodh., *"Time-dependent blood flow and oxygenation in human skeletal muscles measured with noninvasive near-infrared diffuse optical spectroscopies", .* Journal of Biomedical Optics, 2005: p. Vol.10(2): Art. 024027;1-13.

17. Nioka S., Kime R., Sunar U., Im J., Izzetoglu M., Zhang J., Alacam B., Chance B., *"A novel method to measure regional muscle blood flow continuously using NIRS kinetics information".* Dynamic Medicine 2006: p. Vol.5 Iss.5: pg 1-13.

18. Harel, F., Denault A., Ngo Q., Dupuis, J., and Khairy, P., *Near-infrared spectroscopy to monitor peripheral blood flow perfusion.* J Clin Monit Comput, 2008. **22**(1): p. 37-43.

19. Ferrari, M., Muthalib, M., and Quaresima, V., *The use of near-infrared spectroscopy in understanding skeletal muscle physiology: recent developments.* . Philosophical Transactions of the Royal Society a-Mathematical Physical and Engineering Sciences, 2011. **369**(1955): p. 4577-90.

20. Gurley, K., Use of Hybrid Diffuse Optical Spectroscopies in Continuous Monitoring of Blood Flow, Blood Oxygenation, and Oxygen Consumption Rate in Exercising Skeletal Muscle, in *Center for Biomedical Engineering*2012, University of Kentucky.

21. Liu H., Song Y., Worden K.L., Jiang X., Constantinescu A., and Mason R.P., *"Noninvasive investigation of blood oxygenation dynamics of tumors by near-infrared spectroscopy".* Applied Optics, 2000: p. Vol. 39 No. 28:5231-43.

22. Boas, D.A., *Diffuse Photon Probes of Structural and Dynamical Properties of Turbid Media: Theory and Biomedical Applications*, in *Physics and Astronomy*1994, University of Pennsylvania. p. 244.

23. Cooper, C.E., Matcher S.J., *Absolute quantification of deoxyhaemoglobin concentration in tissue near infrared spectroscopy.* Physics of Medicine and Biology, 1994. **39**: p. 1295-1312.

24. Sergio Fantini, Maria-Angela Franceschini, John S. Maier, and Scott A. Walker, *Frequency-domain multichannel optical detector for noninvasive tissue spectroscopy and oximetry.* Optical Engineering, 1995. **34**(1): p. 32-42.

25. Diamond, S.G., Giacometti P., *Types of NIRS Systems*, in *Optical Methods and Instrumentation in Brain Imaging and Therapy*, S.J. Madsen, Editor 2012, Springer. p. 61-62.

26. Radegran, G., *Limb and skeletal muscle blood flow measurements at rest and during exercise in human subjects.* Proceedings of the Nutrition Society, 1999. **58**(4): p. 887-898.

27. Hiatt W.R., Huang S.Y., Regensteiner J.G., Micco A.J., Ishimoto G., Manco-Johnson M., Drose J., Reeves J.T., *"Venous occlusion plethysmography reduces arterial diameter and flow velocity"* Journal of Applied Physiology, 1980: p. Vol.89:2239-44.

28. G. Yu, T.F., Floyd, T. Durduran, C. Zhou, J. Wang, J.A. Detre, and A.G. Yodh, *"Validation of diffuse correlation spectroscopy for muscle blood flow with concurrent arterial spinlabeled perfusion MRI".* Optics Express, 2007: p. Vol. 15, Issue 3: 1064-1075

29. Gosseries O., Demertzi A., Noirhomme Q., Tshibanda J., Boly M., Op de Beeck M., Hustinx R., Maguet P., Salmon E., Moonen G., Luxen A., Larureys S., and De Tiege X., *Functional neuroimaging (fMRI, PET, and MEG): what do we measure?* Revue Medical le Liege, 2008. **63**(5-6): p. 231-7.

30. Boas, D., *"Diffuse photon probes of structural and dynamical properties of turbid media: theory and biomedical applications".* Dissertation, University of Pennsylvania, Dept. of Physics and Astronomy, 1996.

31. Katelyn Gurley, Yu Shang., and Yu Guoqiang, *Noninvasive Optical Quantification of Absolute Blood Flow, Blood Oxygenation, and Oxygen Consumption Rate in Exercising Skeletal Muscle.* 2012.

32. Shang, Y., Zhao Y., Cheng R., Dong L., Irwin D., Yu G., *Portable optical tissue flow oximeter based on diffuse correlation spectroscopy.* Optical Letters, 2009. **34**(22): p. 3556-8.

33. Irwin, D., *" Influence of tissue absorption and scattering on diffuse correlation spectroscopy blood flow "* Masters Thesis, University of Kentucky, 2011: p. Paper 136: 68pgs.

34. Li J.,Dietsche G., Iftime D., Skipetrov S. E., Maret G., Elbert T., Rockstroh B., and Gisler T., *Noninvasive detection of functional brain activity with near-infrared diffusing-wave spectroscopy.* Journal of Biomedical Optics, 2005. **10**(4): p. 44002.

35. Durduran T., Yu G., Burnett M.G., Detre J.A., Greenberg J.H., Wang J., Zhou C., Yodh A.G., *Diffuse optical measurement of blood flow, blood oxygenation, and metabolism in a human brain during sensorimotor cortex activation.* Optical Letters 2004. **29**(15): p. 1766-68.

36. Buckley, E.M., et al., *Cerebral hemodynamics in preterm infants during positional intervention measured with diffuse correlation spectroscopy and transcranial Doppler ultrasound.* Optical Express, 2009. **17**(15): p. 12571-81.

37. Roche-Labarbe, N., et al., *Noninvasive optical measures of CBV, StO(2), CBF index, and rCMRO(2) in human premature neonates' brains in the first six weeks of life.* Human Brain Mapping, 2010. **31**(3): p. 341-52.

38. Menon, C., et al., *An integrated approach to measuring tumor oxygen status using human melanoma xenografts as a model.* Cancer Research, 2003. **63**(21): p. 7232-40.

39. Kim, M.N., et al., *Noninvasive measurement of cerebral blood flow and blood oxygenation using near-infrared and diffuse correlation spectroscopies in critically brain-injured adults.* Neurocritical Care, 2010. **12**(2): p. 173-80.

40. Zhou, C., et al., *Diffuse optical monitoring of hemodynamic changes in piglet brain with closed head injury.* Journal of Biomedical Optics, 2009. **14**(3): p. p.034015.

41. R. Cheng, Y. Shang, D. Hayes, S. Saha, and G. Yu, *Noninvasive optical evaluation of spontaneous low frequency oscillations in cerebral hemodynamics.* NeuroImage, 2012. **62**(3): p. 1445-54.

42. Zhou, C., Choe, R., Shah, N., Durduran, T., Yu, G., Durkin, A., Hsiang, D., Mehta, R., Butler, J., Cerussi, A., Tromberg, B.J., and Yodh, A.G., *Diffuse optical monitoring of blood flow and oxygenation in human breast cancer during early stages of neoadjuvant chemotherapy.* Journal of Biomedical Optics, 2007. **12**(5).

43. Durduran, T., Choe, R., Yu, G., Zhou, C., Tchou, J.C., Czerniecki, B.J., and Yodh, A.G., *Diffuse optical measurement of blood flow in breast tumors.* Optics Letters, 2005. **30**(21): p. 2915-17.

44. Yu Shang, Brock T. Symons., Turgut Durduran, Arjun G. Yodh, and Guoqiang Yu, *"Effects of Muscle Fiber Motion on Diffuse Correlation Spectroscopy Blood Flow Measurements During Exercise".* Optical Society of America, 2010: p. Vol. 1,Iss. 2: 500-511.

45. Mesquita, R.C., et al., *Direct measurement of tissue blood flow and metabolism with diffuse optics.* Philosophical Transactions of the Royal Society a-Mathematical Physical and Engineering Sciences, 2011. **369**(1955): p. 4390-4406.

46. N. Munk, B. Symons., Y. Shang, R. Cheng, and G. Yu, *Noninvasively measuring the hemodynamic effects of massage on skeletal muscle: a novel hybrid near-Infrared diffuse optical instrument.* Journal of Bodywork and Movement Therapies, 2012. **16**(1): p. 22-8.

47. Yu, G., *Near-infrared diffuse correlation spectroscopy (DCS) in cancer diagnosis and therapy monitoring.* Journal of Biomedical Optics, 2012. **17**(2): p. 010901.

48. L. Chen, Y.Shang., E. Sipos, K. E. Saatman, G. Yu, and M. Toborek, *Novel experimental model for repeated forebrain ischemia-reperfusion.* Journal of experimental stroke and translational medicine, 2012. **5**(1): p. 1-10.

49. A. L. Maas, S.L. Carter , E. P. Wileyto, J. Miller, M. Yuan, G. Yu, A. Durham, and T. M. Busch, *The tumor vascular microenvironment determines responsiveness to photodynamic therapy.* Cancer Research, 2012. **72**(8): p. 2079-88.

50. Y. Shang, L. Chen, M. Toborek, and G. Yu, *Diffuse optical monitoring of repeated cerebral ischemia in mice.* Optics Express, 2011. **19**: p. 20301-15.

51. Y. Shang, R. Cheng, L. Dong, S. J. Ryan, S. P. Saha, and G. Yu, *Cerebral monitoring during carotid endarterectomy using near-infrared diffuse optical spectroscopies and electroencephalogram.* Physics in Medicine and Biology, 2011. **56**(3015-32).

52. G. Yu, Y.Shang, Y. Zhao, R. Cheng, L. Dong, and S. P. Saha, *Intraoperative Evaluation of Revascularization Effect on Ischemic Muscle Hemodynamics Using Near-infrared Diffuse Optical Spectroscopies.* Journal of Biomedical Optics, 2011. **16**(2): p. 027004.

53. Yu Shang, Katelyn Gurley, Brock Symons, Douglas Long, Ratchakrit Srikuea, Leslie J. Crofford, Charlotte Peterson, and Guoqiang Yu, *Noninvasive optical characterization of muscle blood flow, oxygenation, and metabolism in women with fibromyalgia.* Arthritis Research and Therapy, 2012. **14**(R236): p. 1-12.

54. Timothy A. Bauer, E.P. Brass, Thomas J. Barstow, and William R. Hiatt, *"Skeletal muscle StO2 kinetics are slowed during low work rate calf exercise in peripheral arterial disease".* European Journal of Applied Physiology, 2007: p. Vol.100:143-51.

55. Don J. Wallace, Brent Michener, Devasmita Choudhury, Moshe Levi, Padraic Fennelly, Dennis M. Hueber, Beniamino Barbieri, *"Summary of the results of a 95 subject human clinical trial for the diagnosis of peripheral vascular disease using a near infrared frequency domain hemoglobin spectrometer.".* SPIE Conference on Optical Tomography and Spectroscopy of Tissue II, 1999: p. Vol.3597:300-316.

56. Paul S. van Bemmelen, M., PhD, Mark A. Mattos, MD, William E. Faught, MD,M. Ashraf Mansour, Lynne D. Barkmeier, MD, Kim J. Hodgson, MD, Don E. Ramsey, MD, and David S. Sumner, MD, *Augmentation of blood flow in limbs with occlusive arterial disease by intermittent calf compression.* The Society for Vascular Surgery and International Society for Cardiovascular Surgery, North American Chapter, 1994: p. Vol.19:1052–8.

57. Konstantinos T. Delis, M., PhD, Marc J. W. Husmann, MD, Nick J. Cheshire, MD, FRCS, and Andrew and M. N. Nicolaides, FRCS,, *Effects of intermittent pneumatic compression of the calf and thigh on arterial calf inflow: A study of normals, claudicants, and grafted arteriopaths.* Surgery 2001. **129**(2): p. 188-95.

58. Hueber, D., Fantini, S., Cerussi, A., and Barbieria, B, *New Optical Probe Designs for Absolute (Self-calibrating) NIR Tissue Hemoglobin Measurements. .* SPIE Proceedings, 1999. **3597**: p. 618-631.

59. L. He, Y.Lin, Y. Shang, B. Shelton, and G. Yu, *Using optical fibers with different modes to improve the signal-to-noise ratio of diffuse correlation spectroscopy flow-oximeter measurments.* Journal of Biomedical Optics, 2013. **18**(3): p. p. 037001.

60. Higgins, J.M., Eddington D.T., Bhatia S.N., Mahadevan L., *Statistical Dynamics of Flowing Red Blood Cells by Morphological Image Processing.* Plos Computational Biology, 2009. **5**(2).

61. Lelia P. Pauneseu, Claudia Casavola, Maria A. Franceschini, Sergio Fantini, Lew Winter, Jin Kim, Debra Wood, and Enrico Gratton, *"Calf muscle blood flow and oxygen consumption measured with near-infrared spectroscopy during venous occlusion".* SPIE Conference on Optical Tomography and Spectroscopy of Tissue III, 1999: p. Vol. 3597:317-23.

62. L. Dong, L. He, Y. Lin, Y. Shang, and G. Yu, *Simultaneously extracting multiple parameters via fitting one single autocorrelation function curve in diffuse correlation spectroscopy.* IEEE Transactions on Biomedical Engineering, 2013. **60**(2): p. 361.

63. Sergio Fantini, Matthew L. Hoimes, Claudia Casavola, and Maria A. Franceschini, *"Spatial mapping of blood flow and oxygen consumption in the human calf muscle using near-infrared spectroscopy.* Proceedings of SPIE, 2001: p. Vol.4241:69-76.

64. R. Boushel, H. Langberg, S. Green, D. Skovgaard, J. Bulow, and M. Kjaer, *"Blood Flow and oxygenation in peritendinous tissue and calf muscle during dynamic exercise in humans."* Journal of Physiology, 2000: p. Vol.524.1:305-13.

65. Van Beekvelt M.C., Colier W.N., Wevers R.A., and Van Engelen B.G., *"Performance of near-infrared spectroscopy in measuring local O2 consumption and blood flow in skeletal muscle".* Journal of Applied Physiology, 2001: p. Vol.90:511-19.

66. Heinonen I., Brothers R.M., Kemppainen J., KnuutiJ., Kalliokoski K.K.,, and Crandall C.G., *"Local heating, but not indirect whole-body heating increases human skeletal muscle blood flow".* Journal of Appl Physiology, 2011: p. Vol 111:818-24.

67. Pearson J., Low D.A., , Stohr E., Kalsi K., Ali L., Barker H., and Gonzalez-Alonso J., *"Hemodynamic responses to heat stress in the resting and exercising human leg: insight into the effect of temperature on skeletal muscle blood flow".* American Journal of Physiology-Regulatory Integrative, and Comparative Physiology, 2010: p. Vol.300:663-73.

68. Louhevaara J., Louhevaara V., *Effect of heat stress on muscle blood flow during dynamic handgrip exercise.* European Journal of Applied Physiology, 1992 **65**: p. 215-220.

69. Mosti, G. and Partsch H., *Inelastic bandages maintain their hemodynamic effectiveness over time despite significant pressure loss.* Journal of Vascular Surgery, 2010. **52**(4): p. 925-931.

70. A. H. Chen, S.G. Frangos, S. Kilaru and B. E. Sumpio, *Intermittent Pneumatic Compression Devices –Physiological Mechanisms of Action.* European Journal of Vascular Endovascular Surgery, 2001. **21**: p. 383-392.

71. Delis K.T., Husmann M.J., Cheshire N.J., Nicolaides A.N., *Effects of intermittent pneumatic compression of the calf and thigh on arterial calf inflow: A study of normals, claudicants, and grafted arteriopaths.* Surgery, 2000: p. Vol.129(2):188-95.

72. Mayrovitz, H.N., *Compression-induced pulsatile blood flow changes in human legs.* Clinical Physiology, 1997: p. Vol.18(2):117-24.

73. Mayrovitz H.N., Larsen P.B., *Effects of compression bandaging on leg pulsatile blood flow.* Clinical Physiology, 1997: p. Vol.17:105-17.

74. Krupa, D. *Expecting an Afternoon Nap Can Reduce Blood Pressure*. APS, 2007.

75. Elsenbruch S., Harnish M.J., and Orr W.C., *Heart Rate Variability During Waking and Sleep in Healthy Males and Females.* SLEEP, 1999. **22**(8): p. 1067-71.

76. Lew, M., *Good statistical practice in pharmacology Problem 2.* British Journal of Pharmacology, 2007. **152**: p. 299-303.

77. J.W. Williamson, J.H.Mithcell., H.L. Olesen, P.B. Raven and N.H. Secher, *Reflex increase in blood pressure induced by leg compression in man.* Journal of Physiology, 1994. **475**(2): p. 351-7.

78. Chen G.Y., Kuo C.D., Yang M.J., Lo H.M., and Tsai Y.S., *Comparison of supine and upright positions on autonomic nervous activity in late pregnancy: the role of aortocaval compression.* Anaesthesia, 1999. **54**: p. 215-9.

79. Nobuhiro Watanabe, James Reece, and Barbara I. Polus, *Effects of body posture on autonomic regulation of cardiovascular function in young, healthy adults.* Chiropractic & Osteopathy, 2007. **15**(19): p. 8.

80. Pump B., Talleruphuus U., Christensen N. J., Warberg J., and Norsk P., *Effects of supine, prone, and lateral positions on cardiovascular and renal variables in humans.* American Journal of Physiology - Regulatory, Integrative and Comparative Physiology, 2002. **283**(1): p. R174-80.

81. Buckwalter J.B., Clifford P.S., *Autonomic control of skeletal muscle blood flow at the onset of exercise.* American Journal of Physiology - Heart and Circulatory Physiology, 1999. **277**: p. H1872-7.

82. Rolf P. Bochmann, W.S., Elke Haase, Volker Hietschold, Hartmut Rödel and Andreas Deussen, *External compression increases forearm perfusion.* Journal Applied Physiology, 2005: p. Vol.99:2337-2344.

83. R.C. Mesquita, M. Putt, M. Chandra, G. Yu, X. Xing, S. W. Han, G. Lech, Y. Shang, T. Durduran, C. Zhou, A. G. Yodh, and E.R.Mohler III, *Diffuse optical characterization of an exercising patient group with peripheral artery disease.* Journal of Biomedical Optics, 2013. **18**(5): p. 057007.

84. V. Quaresima, S. Homma, K. Azuma, S. Shimizu, F. Chiarotti, M. Ferrari, and A. Kagaya, *"Calf and shin muscle oxygenation patterns and femoral artery blood flow during dynamic plantar flexion exercise in humans."* European Journal of Applied Physiology, 2001: p. Vol.81:387-94.

85. Green, S., et al., *Venous occlusion plethysmography versus Doppler ultrasound in the assessment of leg blood flow during calf exercise.* European Journal of Applied Physiology, 2011. **111**(8): p. 1889-1900.

86. Boushel, R., et al., *Regional blood flow during exercise in humans measured by near-infrared spectroscopy and indocyanine green.* Journal of Applied Physiology, 2000. **89**(5): p. 1868-1878.

87. Bangsbo J., Hellsten Y., *Muscle blood flow and oxygen uptake in recovery from exercise.* Acta Physiologica Scandinavica, 1998. **162**(3): p. 305:12.

88. Van Beekvelt M.C., Shoemaker J.K, Tchakovksy M.E., Hopman M.T., Hughson R.L., *Blood flow and muscle oxygen uptake at the onset and end of moderate and heavy dynamic forearm exercise.* American Journal of Physiology - Regulatory, Integrative and Comparative Physiology, 2001. **280**: p. R1741-47.

89. Egana M., Green S., *Effect of body tilt on calf muscle performance and blood flow in humans.* Journal of Applied Physiology, 2005. **98**: p. 2249-58.

90. B.E. Van Leeuwen, G.J. Barendsen, J. Lubbers, and L. De Pater, *"Calf blood flow and posture: Doppler ultrasound measurements during and after exercise".* Journal of Applied Physiology 1992: p. Vol.72(5):1675-80.

91. Sjegaard G., Savard G., Juel C., *Muscle blood flow during isometric activity and its relation to muscle fatigue.* European Journal of Applied Physiology, 1988. **57**: p. 327-35.

92. Binzoni, T., V. Quaresima, G. Barattelli, E. Hiltbrand, L. Gurke, F. Terrier, P. Cerretelli, and M. Ferrari, *Energy metabolism and interstitial fluid displacement in human gastrocnemius during short ischemic cycles.* Journal of Applied Physiology, 1998. **85**: p. 1244-1251.

93. Oscar U. Scremin, M., PhD Stephen F. Figoni, PhD, RKT, Keith Norman, BSc A.M. Erika Scremin, MD, Charles F. Kunkel, MD, MS, Dorene Opava-Rutter, MD, Eric D. Schmitter, MD, Alberto Bert, PhD, Mark Mandelkern, MD, PhD, *Preamputation Evaluation of Lower-Limb Skeletal Muscle Perfusion with H2 15O Positron Emission Tomography.* American Journal of Physical Medicine & Rehabilitation, 2010. **89**(6).

94. Mingjun Zhao, Yu Shang, Brad Henry, Tim L. Uhl, and Guoqiang Yu, *Tissue Metabolic Rate of Oxygen Consumption in Calf Muscle Measured by Arterial and Venous Occlusion Protocols*, in *Medical Optics Instrumentation: Spectroscopy, Tissue Diagnostics* 2014: University of Kentucky, Lexington, KY, 40506.

95. Mireille C.P. van Beekvelt, Willy N. Colier, Bazieal G. M. van Engelen, Maria T. E. Hopman, Ron A. Wevers, and Berend Oeseburg *Validation of measurement protocols to assess oxgyen consumption and blood flow in the human forearm by near infrared spectroscopy*. SPIE Conference on Optical Tomography and Spectroscopy of Tissue 1998. **3194**, 133-44.

96. T. Li, Y. Lin, Y. Shang, L. He, C. Huang, M. Szabunio, G. Yu, *Simultaneous measurement of deep tissue blood flow and oxygenation using noncontact diffuse correlation spectroscopy flow-oximeter.* Scientific Reports, 2013. **3**(1358).

97. Richardson, D., *"Blood flow response of human calf muscles to static contraction at various percentages of MVC".* Journal of Applied Physiology, 1981: p. Vol.51:929-33.

98. Saito M., Mano T., and Iwase S., *Changes in muscle sympathetic nerve activity and calf blood flow during static handgrip exercise.* European Journal of Applied Physiology, 1990. **60**: p. 277-81.

Vita

Brad Henry

Previous Positions

8/20/2011-present Masters Graduate Student, Biophotonics Laboratory, Biomedical Engineering, University of Kentucky, Lexington, KY

8/20/2011-6/14/2012 Research Assistant, Biophotonics Laboratory, Biomedical Engineering, University of Kentucky, Lexington, KY

7/15/2011-8/20/2011 Adjunct Math Faculty, Maysville Community College, Morehead, KY

Education

2005-2010 B.S. Physics (minor in Biology), Morehead State University, Morehead, KY

Honors

2005-2010 Honors Graduate, Morehead State University, Morehead, KY

2005-2009 Presidential Scholarship, Morehead State University, Morehead, KY

Professional Memberships

2012-2014 *Member,* American College of Sports Medicine

Publications (Peer Reviewed)

1) Brad Henry, Y.Shang, M. Zhao, K. Gurley, G. Yu, "Hybrid Diffuse Optical Techniques for Continuous Hemodynamic Measurement in Gastrocnemius during Plantar Flexion Exercise", manuscript under revision

2) Y. Shang, Y. Lin, B. Henry, R. Cheng, L. Chen, B.J. Shelton, K.R. Swartz, S.S. Salles, G. Yu, "Noninvasive evaluation of electrical stimulation impacts on muscle hemodynamics via integrating diffuse optical spectroscopies with muscle stimulator." Journal of Biomedical Optics, 2013, 18(10) 105002